POLITECNICO
MILANO 1863

Scoula di Ingegneria Industriale e dell'Informazione
Master of Science in Automation and control engineering

Modelling, simulation and predictive control of the medium temperature Solar Cooling Plant

Thesis by

Niraj Rathod

Matricola: 834168

Supervisor: **Prof. Riccardo Scattolini**

Co-supervisor: **Eng. Andrea Rossetti** & **Eng. Alessio La Bella**

Academic year 2015-2016

Abstract

This thesis focuses on the modelling, simulation and predictive control of the medium temperature solar cooling plant. The economic advantage of the solar cooling plant is mostly influenced due to the electric power consumed by it. The aim is to use the thermal energy from solar radiation for most of the process work while keeping the electric power consumption as low as possible using predictive control.

The work was conducted on the plant built by RSE in Milan, Italy. After careful study of the plant's equipment and operating conditions, models for the individual equipment were developed using first principles and model identification techniques and validated with the real data from the plant. The simulator of the plant was designed from these models and further validated. For the predictive control design of the plant, a two layer architecture was proposed both in the fixed and hybrid configuration mode. For the fixed configuration mode, the Real time optimizer (RTO) was designed as a higher level whereas, the fast linear MPC with explicit integral action serves at lower layer. The RTO and MPC were employed to the simulator of the plant to check their operation. For the hybrid configuration, the development of the Mixed logical dynamical model was carried out that serves as a predictive model for the higher level MPC. The higher level MPC was implemented and simulated with the plant simulator. The lower level for this configuration will be a fast linear MPC.

The results from the simulator indicate the satisfactory design of the plant model. The RTO and MPC operation on the simulator of the plant shows the successful tracking of the optimal setpoint calculated by RTO with the help of linear MPC with integral action, given the prediction of the disturbances acting on the plant. For hybrid configuration, the higher level MPC simulation results confirm its operation to find the optimal input and define the configuration of the plant. The lower level MPC for this configuration should be implemented and tested on the simulator as a part of the future work.

Sommario

Questa Tesi riguarda la modellistica, la simulazione e il controllo di un impianto di raffreddamento operante a media temperatura e basato sull'energia solare (solar cooling plant). I vantaggi di tipo economico relativi all'utilizzo di questi impianti sono dovuti al ridotto impiego di energia elettrica, sostituita quando possibile dall'energia radiante del sole. Il lavoro descritto nella Tesi è stato condotto con riferimento all'impianto disponibile presso RSE (Ricerca sul Sistema Energetico) nella sua sede di Milano.

Dopo una fase di studio preliminare dell'impianto e delle sue principali condizioni operative, sono stati sviluppati i modelli dinamici dei suoi elementi costitutivi, sia basati su equazioni fisiche di bilancio di massa ed energia, sia sviluppati con tecniche di identificazione a partire da dati sperimentali appositamente raccolti sul sistema. A partire da questi modelli è stato poi realizzato e validato il modello complessivo dell'impianto.

Lo schema di controllo del sistema è stato sviluppato secondo una struttura gerarchica a due livelli. Ipotizzando una configurazione specifica dell'impianto, dapprima è stato progettato un sistema di alto livello, basato sulla cosiddetta Real Time Optimization (RTO), in grado di calcolare le migliori condizioni statiche di funzionamento, e conseguentemente i valori di regime delle variabili di processo, minimizzando un opportuno funzionale di costo. Successivamente è stato progettato un regolatore lineare dinamico di tipo MPC, o Model Predictive Control, per il mantenimento di tali condizioni anche a fronte di disturbi o limitate variazioni delle condizioni operative. Lo schema di controllo, implementato nel simulatore, ha dimostrato la sua validità consentendo di mantenere i valori di riferimento calcolati da RTO.

Successivamente è stato impostato il problema relativo all'ottimizzazione anche della configurazione dell'impianto a fronte di variazioni significative delle condizioni operative, per esempio a causa di una variata intensità della radiazione solare. Per far ciò, si è dovuto modellizzare l'impianto come un sistema ibrido descritto da un modello MLD, o Mixed Logical Dynamical. Tale modello ha consentito di formulare un problema di ottimizzazione Mixed Integer, relativo al livello più alto della struttura gerarchica del controllo, per la determinazione della configurazione ottima del sistema a fronte di diverse condizioni ambientali. A più basso livello un regolatore MPC lineare può ancora essere utilizzato per il controllo dinamico del sistema.

I risultati di simulazione hanno evidenziato l'affidabilità del modello sviluppato dell'impianto e l'efficacia dell'utilizzo della procedura RTO per la determinazione del punto di lavoro ottimo assumendo una configurazione fissa del sistema. A fronte delle diverse condizioni ambientali in cui il sistema può lavorare, l'approccio basato su modelli ibridi e ancora sull'ottimizzazione ha consentito di pervenire a una procedura per la scelta della configurazione ottima dell'impianto. Questo risultato è ritenuto di notevole interesse al fine di minimizzare i consumi del sistema mantenendo alti livelli di efficienza.

To my family

Truth is ever to be found in the simplicity,
and not in the multiplicity and confusion of things.

Isaac Newton.

Acknowledgements

First and foremost, I would like to express my deepest gratitude to my supervisor Prof. Riccardo Scattolini for such a rewarding thesis experience. I shall always be thankful for your guidance, caring, patience and support throughout the thesis work. I could have never hoped for the better supervisor than you.

Besides my supervisor, I would like to thank my co-supervisor Eng. Andrea Rossetti from RSE for awarding me the internship, allowing me to work on the plant and helping me with the modelling part of my thesis. I would also like to thank a lot to Eng. Alessio La Bella for all the efforts he put to help me with the control design part of the thesis and motivating me during the downfalls of my work.

I also take this opportunity to thanks my friends from the automation and control department, Andrea, Renzo, Enrico and Farzan for always keeping the positive and uplifting environment in the lab during my thesis work tenure. I can never thank enough to my friends Prasad, Nikita, Akshay, Pooja, Priyanka, Stefano, Giacomo, Mauro, Katarina, Ines, Silvia, Ricardo, Toshi, Paolo, Luca, Matteo and Vedad. You all have been nothing but source of love, joy and energy ever since I know you. Special thanks to my friend and roommate Vignesh for all his support and company during master studies that I shall cherish forever.

From the bottom of my heart, I wish thank my sister Vidya for financially supporting me during my master studies without which, this journey would have never happened. Last but not least, I would like to thank my family, especially my mother and father for your unconditional love, belief in me and supporting throughout my life. Words are never enough to express my gratitude to you for the sacrifices you made to get me where I am today.

Contents

List of Figures

List of Tables

Chapter 1

Introduction

Air conditioning is the process of removing heat from confined space, thus cooling the air and removing humidity that can be used for domestic and commercial environment. The reason for the growing use of air condition is twofold. First, the comfort demand from consumer have increased due to high standard of living. Second, the electricity prices are comparatively low and it is not in the order of magnitude to influence the consumer behavior significantly. The obvious consequence of this growing air-conditioning demand has increased the power consumption. Recently, Europe has seen several power grid breakdowns in summer caused by a seasonal peak use of air-conditioners in combination with reduced power plant output. This brings a need to move towards the air-conditioning that uses renewable sources.

Any air cooling system that uses solar energy can be referred as Solar cooling system. Solar cooling system is more desirable because cooling is needed when solar energy is most available. Over past few years lots of methods have been researched and developed in this field for commercial uses apart from research work. However, despite of their ecological advantages the Solar cooling system should have an economic advantage to consumer. The installation cost of solar cooling system on the other hand is more expensive than the traditional ones, since the full potential of this technology is still far from being realized.

The economic advantage of solar cooling systems results from much lower operation costs which include the costs for power, water and maintenance. Especially the electrical power consumption of a solar cooling system influences the economics strongly. The main idea of such a system is to use thermal energy for most of the process work, thus the remaining power consumption should be kept as low as possible. The power consuming components of a solar cooling system include pumps, fans and control units. The latter can usually be neglected, but pumps and especially cooling tower fans can have a power consumption in the range of few hundred Watts. Their operation time and speed are relevant parameters for the total power consumption of the system.

However, operating this type of system brings certain additional challenges that must be addressed through control system. Firstly, the primary source (the Solar radiation) of energy cannot be manipulated. Secondly, presence of disturbances mainly due to changing environmental conditions. Finally, the user demand is a

variable that depends upon the aim and requirement of the user. To maximize the use of thermal energy from solar radiation with reduced power consumption becomes the main objective for the control system designed for these systems.

As the system is prone to external disturbances related to the environment conditions and user demand, it needs a control system that can account for these disturbances while optimizing the functionality to pursue the main objective. One of the features of the solar cooling system is that it is flexible to adapt the changes due to environmental condition allowing the control system put it in the best operational configuration to achieve the primary energy saving.

Even though several control strategies have been tested for Solar cooling plant, predictive control seems to be effective one due to its capability to use the predictive model and to calculate the sequence of future control signals that minimizes the cost function related to primary energy savings. The fact that predictive control uses the predictive model allows it to account for the changing disturbances acting on the system. Obviously, the prediction of the disturbances is desired for this control strategy which in many cases is available.

1.1 Objectives

This thesis work was carried out in collaboration with "Ricerca sul Sistema Energetico" (RSE) on the medium temperature Solar cooling plant built at their facility located in Milan headquarters, Italy. The objectives of the thesis can be broadly expressed in the following bullets.

- The modelling, validation and simulation of the Solar cooling plant.
- To design and develop a two layer predictive control strategy for the Solar cooling plant to optimize its energy efficiency in a *fixed configuration* mode.
- To design and develop a two layer predictive control strategy for the Solar cooling plant to optimize its energy efficiency in a *Hybrid configuration* mode.

1.2 Thesis overview

Beginning with the introductory part in this chapter, this thesis involves the study of the general functionalities and modes of operation of the plant apart from the modelling and control design. The thesis content is arranged in the following fashion.

Chapter 2

This chapter describes the function of the Solar cooling plant under study. It involves the specification of equipment of the plant and their functionalities. The control system and strategies related to the plant are also covered briefly. At the end of this chapter the parameters to evaluate the plant performance are mentioned.

Chapter 3

The models for all the components of the plant is detailed in the first part of this chapter. Implementation of these models and their validation results are reported in the following section. The chapter also includes the plant simulator that is built from its components and the validation results from it is documented at the end of this chapter.

Chapter 4

This chapter introduces the idea of two layer control architecture for the Solar cooling plant and its benefits. It presents the development of this architecture for a *fixed configuration* operation of the plant. It involves the Real time optimizer (RTO) and linear MPC formulation and implementation.

Chapter 5

In this chapter two layer architecture for the Solar cooling plant is described for a *hybrid configuration*. The required Hybrid model of the system is developed starting from the model developed in chapters 3 and 4. The optimization problem definition for the higher layer MPC, its implementation and simulation results are reported at the end of this chapter.

Chapter 2

The experimental plant of RSE

The experimental plant for the medium temperature solar cooling was built by RSE in 2014 in the Milan headquarters. The location for the installation is the building 848 (Laboratorio Caratterizzazione Membrane), whose dimensions are 40.67 m in length and 20.90 m wide as pictured in figure 2.1.

The design and sizing of the system components have been made based on a simulation environment model [1]. This model was aimed to identify the combination of the characteristic parameters of the various elements that maximize the PER (Primary Energy Ratio) index considering different operating conditions for laboratory 848 cooling, through parametric analysis.

Figure 2.1: Solar cooling plant installed at building 848 in RSE

The dimensioning of the plant covered important characteristic parameters, namely:

- Area of the solar collector
- Ratio of the volume of the hot storage tank and solar collector area
- Nominal power of an absorption chiller

- Cold storage tank volume

The results obtained from the simulations are reported in Table 2.1. On the basis of these values, the plant has been designed and implemented for medium temperature experimentation.

Table 2.1: Main parameters of the RSE experimental plant

Name of parameter	Value	Units
Nominal refrigeration power of a chiller	23	kW
Surface area of parabolic solar collector	50	m^2
Volume of hot storage tank	0.75	m^3
Volume of cold storage tank	1.5	m^3

The experimental plant consists of two water circuits, a high temperature that connects the solar collectors to the chiller, and a low temperature, which connects the cooling unit to the air handling unit (AHU). Both the circuits have been provided with appropriate storage tanks.

During summer, as shown in 2.2, the solar circuit is maintained at a pressure of $10 - 15\,bar$ and the solar energy received by the collectors is used to heat the hot storage tank or fed to the absorption chiller. The operating temperature varies between $160 - 190°C$, while the distribution circuit is maintained at the temperature range of $5 - 14°C$.

The switching On/Off of the absorption chiller is adjusted as per the temperature control and depends on the thermal load, whether it is from real user or simulated.

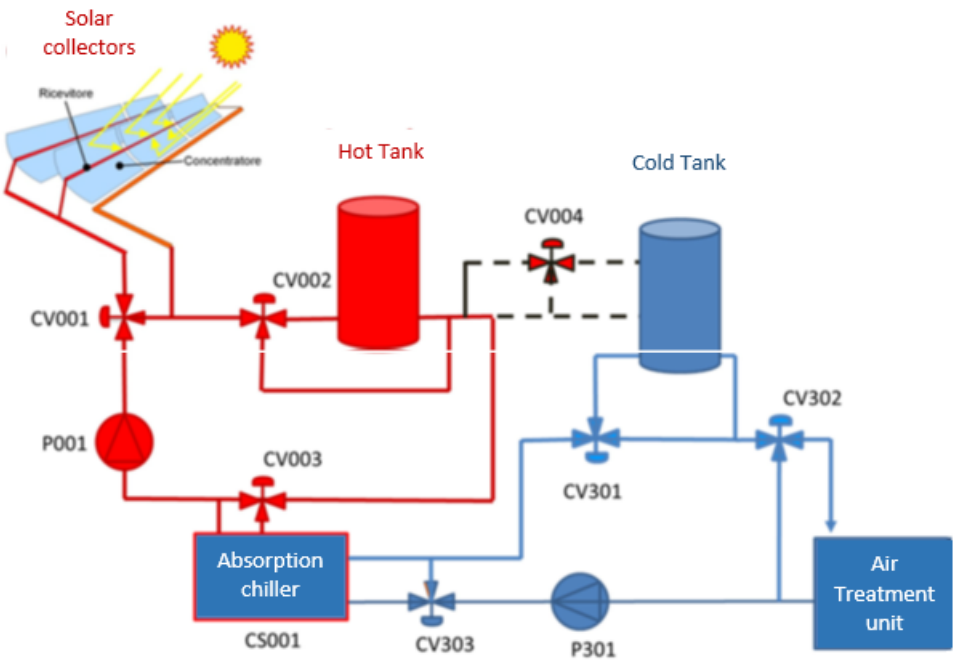

Figure 2.2: Solar cooling plant during summer configuration

During winter, the solar circuit is directly coupled with the distribution circuit, as shown in figure 2.3. The solar energy is used to heat the water for two hot storage tanks connected in series with an operating temperature of the solar field between $50 - 90°C$. In this case, the absorption chiller is utilized as heater and fed with natural gas to heat the water of the distribution circuit, if the heat from the solar field is not sufficient. The distribution circuit is maintained at a suitable temperature for heating of the building between $50 - 70°C$.

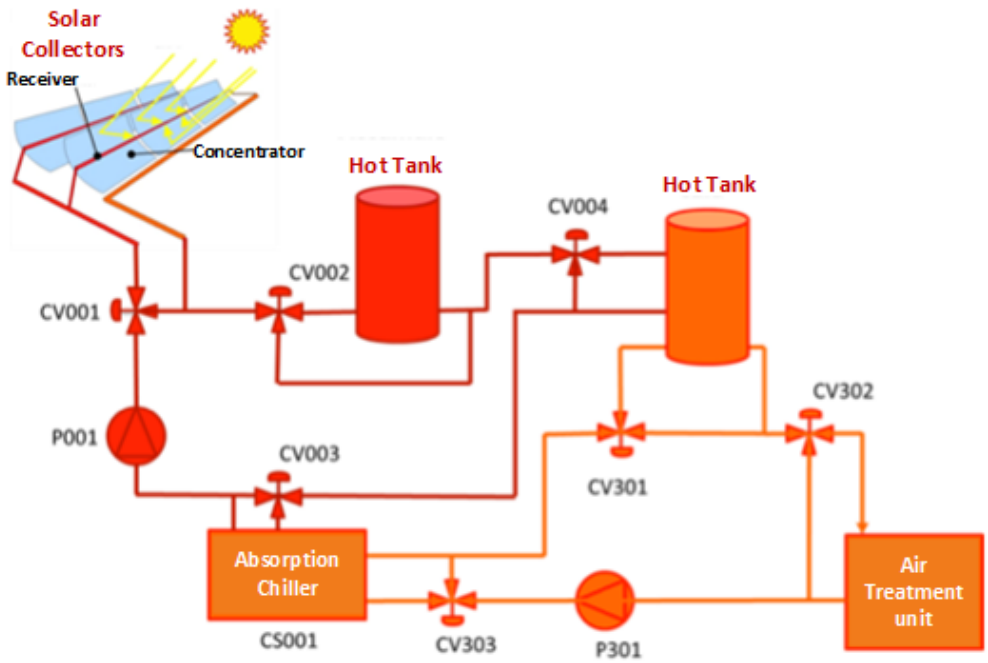

Figure 2.3: Solar cooling plant during winter configuration

The hot water/solar circuit is placed outside of the building to be conditioned and it includes the chiller, heat storage tank, hot water pump and pipes for connection. The proper positions of the different components have been chosen to minimize the length of the pipes and the thermal losses. The distribution circuit (the cold storage tank, circulation distribution pump and AHU connection pipes) is located inside the building to be conditioned.

2.1 Solar collector

The Solar collector is provided by RONDA HIGHTECH which is a parabolic linear type with tracking on a single axis as pictured in figure 2.4. The collector axis is north-south oriented, with the aim of increasing the thermal energy collected during the summer.

The field of solar collector installed consists of five basic parabolic modules connected in series and moved by a single drive motor. Each module has a length of $4.1\,m$ and width of $2.3\,m$ approximately and is composed of two ground connection elements containing the rotation mechanisms of the mirrors.

Figure 2.4: Solar collector picture

The rotation of the collector takes place around the axis of the mirror focal length with the help of the circular guides. The mirrors have the peculiar reduced thickness of $1\,mm$ that is pasted on a printed panel in SMC (Sheet Moulding Compound), which ensures the accuracy of the parabolic shape and at the same time maintains adequate resistance in the mirror. The use of a thin glass has essentially two advantages, to reduce the effect of absorption of solar radiation and the effect of refraction (phenomena proportional to the glass thickness). This implies that the reflectance of the mirror RONDA HIGHTECH is equal to 96%, with a benefit that affects the performance of the entire solar field.

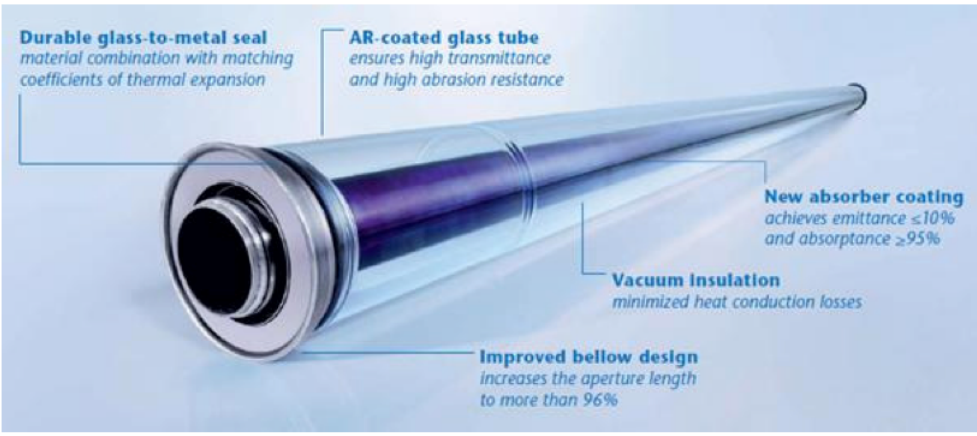

Figure 2.5: Receiver tube of the solar collector

The receiver tube installed on the collector is SCHOTT type, formed by five individual elements and produced by Archimede Solar Energy (HCE12 model). It consists of an inner tube (in which the heat transfer fluid flows) made of austenitic stainless steel coated by a thin multilayer film to maximize the solar energy absorbed. An external tube of borosilicate glass is maintained under vacuum that has a function

to minimize the convective losses. The receiver tube remains fixed in the center. This configuration minimizes the effect of wind and simplifies the handling of the entire structure during operation of the plant.

Working principle of the solar collector

As shown in Figure 2.6, in the linear or Parabolic Trough Collector (PTC), the reflective parabolic structure concentrates solar rays on an receiver tube. The heat transfer fluid flowing through the receiver tube is heated by the solar radiation. Its automated solar tracking system allows to receive the solar radiation efficiently.

The main parameters that characterize a PTC are the concentration factor (CR) and Incidence Angle Modifier (IAM), related to the geometry of the systems [3]. The concentration factor is defined as the ratio of the aperture area for the radiation to the surface area of the receiver tube. The Incidence Angle Modifier describes the losses of the collector according to the angle of incidence of the solar rays with respect to the normal to the plane of a mirror. When the rays are perpendicular to the surface of the parabola the losses are zero (IAM = 1), while increase in the incidence angle decreases the efficiency of the collectors.

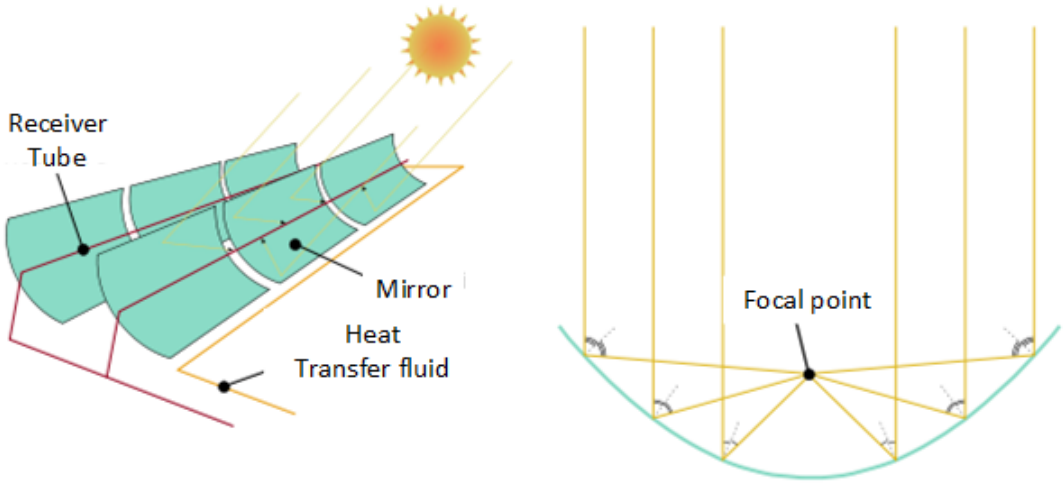

Figure 2.6: Working principle of the solar collector

2.2 Double-effect absorption chiller

For refrigeration unit, the machine made by SYSTEMA, model SYBCTZH (23 kW) was chosen. It is an integrated system which, in addition to the double effect absorption chiller (Li-Br), also includes the evaporative cooling tower to dissipate the heat to an environment.

This unit can be powered through hot water and is able to produce a 23 kW cooling power with COP_{ref} equal to 1. During winter operation, the unit can operate as a heater with rated heat output of 22kW and COP_{PdC} equal to 1. The unit is also equipped with an auxiliary burner, operated on natural gas that ensures the rated power of the machine. 2.7 shows the chiller used in the plant and its internal schematic.

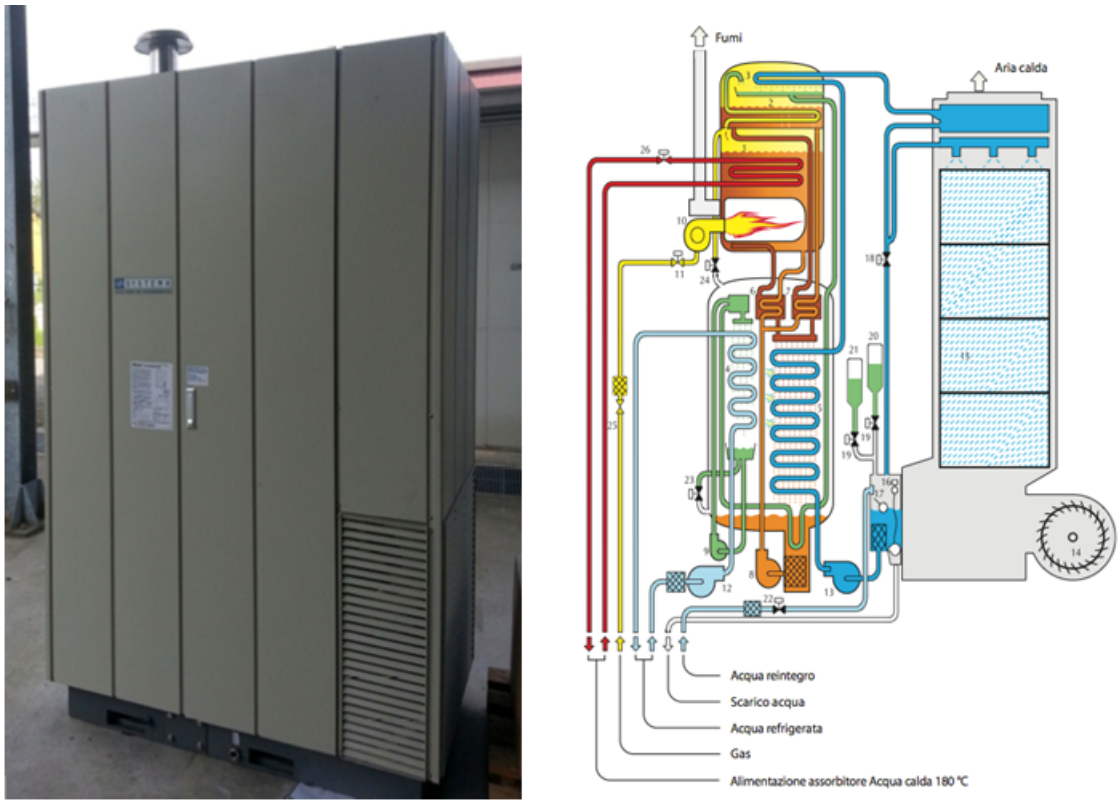

Figure 2.7: Double-effect absorption chiller model SYBCTZH 23 kW by SYSTEMA

The rated operating temperatures are as follows:

- Cold water outlet temperature: $7° C$
- Cold water inlet temperature: $14° C$
- Heating water outlet temperature: $57° C$
- Heating water inlet temperature: $50° C$
- Hot water inlet temperature: $180° C$
- Hot water output temperature: $165° C$

Working principle of the absorption chiller

In a hot water driven absorption chiller there is a main cycle and an auxiliary cycle. The chilled water is cooled down twice by the refrigerant from a double tray in the evaporator and the vaporized refrigerant is absorbed into concentrated solution which comes from the 2nd generator. The quantity of vapour that can be absorbed in absorber is increased by the double tray system. The concentrated solution becomes diluted solution and the heat is absorbed into the cooling water. The diluted solution in the absorber flows to the 1st generator through a low temperature heat exchanger and a high temperature. heat exchanger, and hot water heats up the diluted solution and the refrigerant is vaporized. The absorbent solution becomes an intermediate solution in the 1st generator and it flows to 2nd generator through the high temperature heat exchanger. The intermediate solution in the 2nd generator

is heated by the hot water and more refrigerant is vaporized in the 2nd generator. The vapour is absorbed into absorbent solution in the auxiliary absorber to become auxiliary diluted solution. The auxiliary diluted solution is delivered to auxiliary. generator through auxiliary heat exchanger, and the solution is heated by hot water coming from 1st generator and becomes auxiliary concentrated solution. The auxiliary concentrated solution is delivered to auxiliary absorber through auxiliary heat exchanger. The refrigerant vapours which are generated in the 1st generator and auxiliary generator are condensed in the condenser and then flow into evaporator. The heat in the condenser is absorbed by cooling water [4].

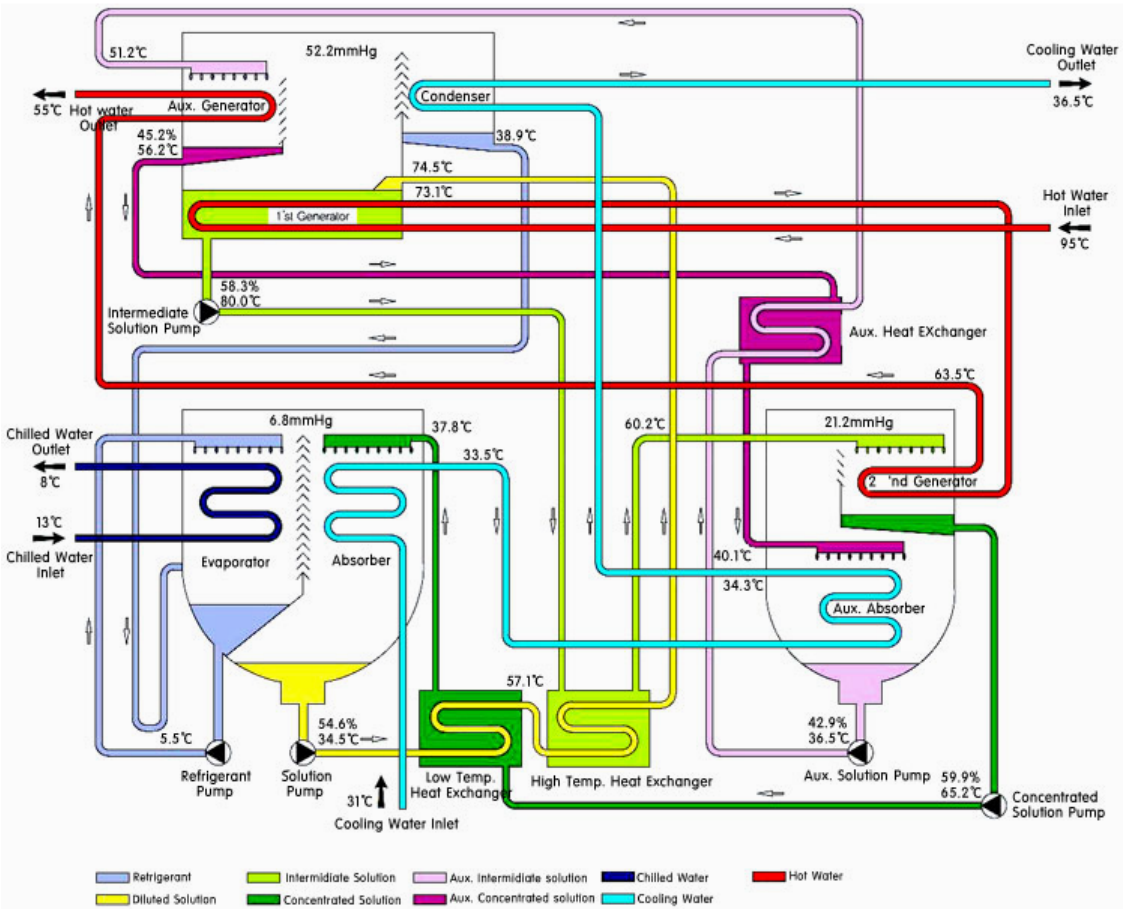

Figure 2.8: Working principle of the double effect chiller. (Source:[4])

2.3 Air distribution system and User simulator

The air distribution system is designed to create different types of user profiles by adjusting the three-way valve and AHU. It is also possible to simulate significantly different profiles of heating/cooling requirements. Specifically, it is possible to vary the amount of recirculation air and one can choose whether to send the treated air to conditioned environment (laboratory) or directly to the outside environment (functioning as a simple heat sink). The air handling system, the interior heat exchangers and the distribution channels are sized to provide the following cooling/heating capacities:

Figure 2.9: Air handling units and distribution system installed in the RSE laboratory.

- Maximum Cooling capacity: $30\,kW$
- Rated cold source temperature (Send/Return): $7 - 14°\,C$
- Minimum outside air temperature for the cooling season: $18°\,C$
- Maximum heating power: $50\,kW$.
- Nominal hot spring temperature (Send/Return): $50 - 70°\,C$
- Maximum temperature outside air for the heating season: $24°\,C$

2.4 Solar circuit water circulation pump

Given the requirement to have the high operating pressure and low flow rate ($0.5\,kg/s$), it was necessary to select a circulation pump of special design. The volumetric pump with magnetic drive (PUMPS CUCCHI NCX041X0KA0L000 model) was chosen, which meets the requirements.

The body, cover, shaft and gear of a pump are made of AISI 316L, the magnetic drive is made from AISI 316Ti, while the drive gear is of a plastic KK material. The bushings are made of graphite-antimony for high temperature. The electric motor has $1.1\,kW$ power. The pump can operate with the speed of $900 - 1450\,RPM$.

2.5 Hot storage and cold storage tanks

The hot storage tank was made by LONGONI Engineering; the total volume is about $750\,l$. The main features are listed below:

- Fluid: pressurized water
- Type: vertical with feet support

Figure 2.10: Solar circuit water circulation pump with magnetic drive

- Tank body material: AISI 316
- Maximum pressure: $25\,bar$
- Maximum operating pressure: $16\,bar$
- Maximum design temperature: $250°\,C$
- Maximum operating temperature: $220°\,C$

The distribution storage tank (cold) was provided by FIORINI INDUSTRIES. The volume is $1500\,l$ with an internal coil for connection to the solar circuit.

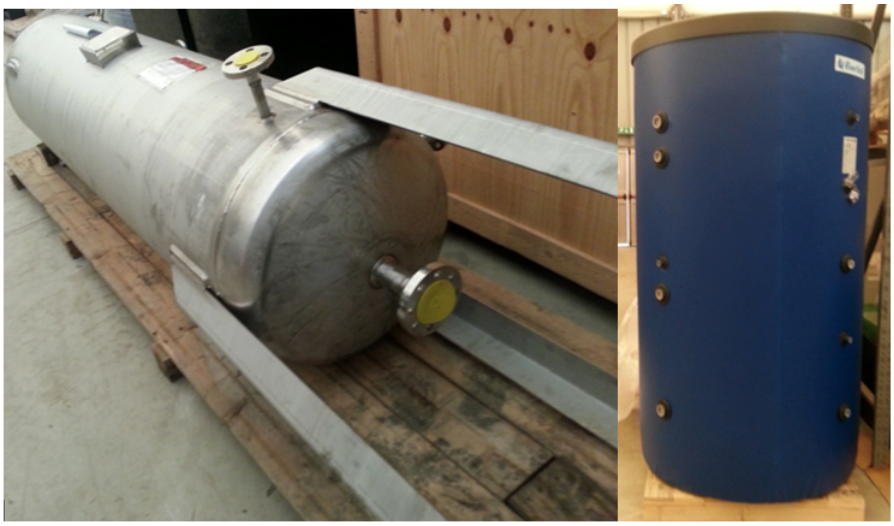

Figure 2.11: Hot storage tank (left) and cold storage (right) tank

2.6 Insulations

Different types of insulation for the pipes and tanks were considered for the hydraulic circuits depending on the operating conditions and the places where they were installed. It can be described as:

- Outer solar/hot water circuit (pipes and tank): $150\,mm$ rock wool ($0.05\,W/m^2K$ at $100°\,C$)
- Inner solar circuit (for winter): $50\,mm$ of elastomeric barrier ($0.04\,W/m^2K$) and $50\,mm$ rock wool
- Internal distribution circuit: $50\,mm$ of elastomeric barrier and $50\,mm$ rock wool.
- External distribution circuit: $100\,mm$ rock wool.

Such a solution should guarantee minimum thermal losses. It is estimated that the heat losses to environment is less than 10% of solar energy collected by the collectors.

2.7 Control valves

The three valves installed on the solar circuit has been provided by the WTO and the model is V250D with electric actuator. The main features are as follows:

- 3-way valve DN20 PN40 Body in Acc. Inox. Mod. V250D
- Bonnet finned for high temperatures (T> $200°\,C$) - Mat. ASTM A105 - Galvanized
- Stuffing box double Self-adjusting HTS300 for Temp $\leq 400°\,C$)
- Shutter in Acc. Steel (DEVIATR.), CV: 6 Linear Feature
- Electric actuator Mod. MC253 - $2.5kN$ Strength - Ratings $230V\ 50Hz$
- Electromechanical limit switch "SPDT"
- $4 - 20\,mA$ transmission

2.8 Data acquisition system and signal processing

The data acquisition of all the field signals and the plant control is done by a Siemens S7-300 PLC (Programmable Logic Controller). A typical PLC cycle provides in sequence:

- Acquisition of all field signals (analog and digital)
- Calculation of secondary variables
- Verification of the general safety

- Verification of specific safety (summer/winter)
- Specific range adjustments (summer/winter)

All processed values provided by the PLC are not instantaneous, but sampled over the time and this sampling time can be chosen. These values are calculated at an interval of 10 s of measured quantity (although the values read at every 10 s are not viewable on the screen). The sampling time was initially set to 30 s, but the volume of data collected was excessive hence, for test days the sampling time of 60 s was chosen.

2.9 User interface software

The user interface is developed in WinCC flexible environment that allows full system control. The main page consists of the synopsis as shown in figure 2.12, which displays the system diagram with all the components. The page also displays,

- All the signals acquired (temperature, flow and pressure).
- The status of chiller operation, AHU and solar collectors (On/Off and manual/automatic).
- Proportion opening of valves.

When the system is in manual mode, one can act on each component by adjusting the specific parameters through dedicated windows. On the other hand, when the system is in automatic mode, only operational status is displayed on the screen.

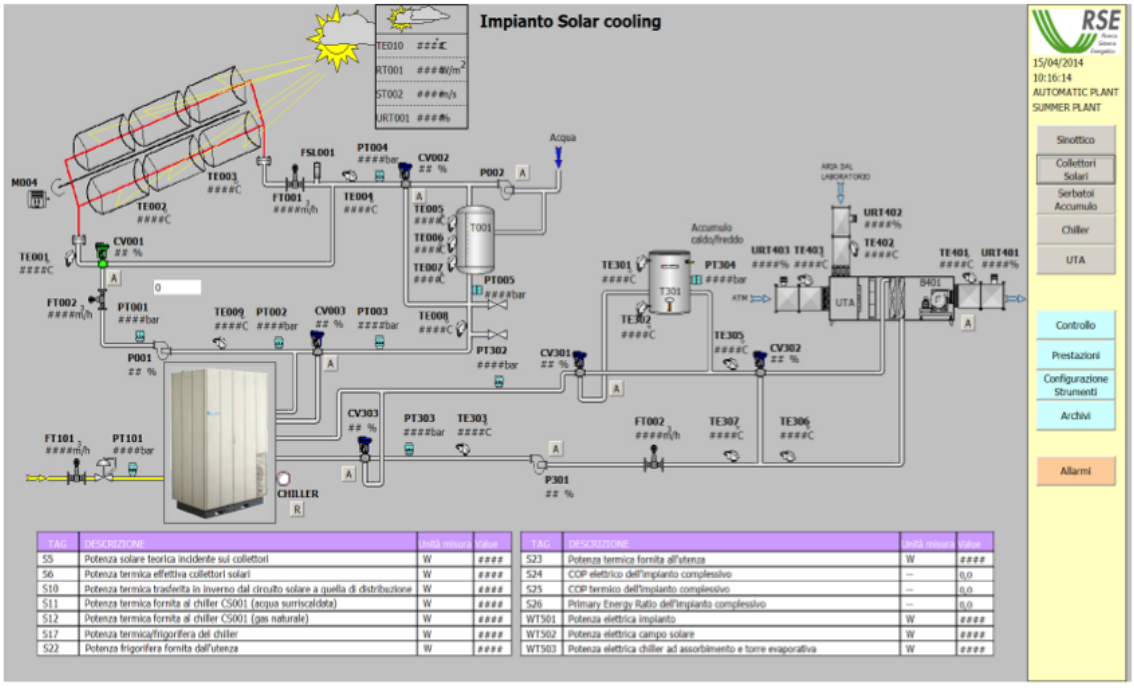

Figure 2.12: Main page of the control system software

2.10 Control Structure

The supervisory control system for the plant was designed and developed by RSE to meet the following main requirements:

- Operational Flexibility: different system configurations and operating modes have been implemented to effectively test the performances of the individual components and the whole plant.
- System operation for all the months of a year, to satisfy both the thermal and refrigeration loads by the typical user of a possible European/Mediterranean climates.
- Optimization of electricity consumption of the plant auxiliaries: logical fixed-flow and variable flow rate for pumps were considered to make a direct comparison between the two strategies.
- Measurement for the uncertainty of the main performance indices of the plant compared with the performance of conventional cooling systems.

Specifically, the control system allows the plant to operate in four operating modes mentioned below:

- **Manual mode for summer** : In this mode, all the system components are operated manually and general safety controls along with the summer safety controls are active.
- **Manual mode for winter**: In this mode, all the system components are operated manually and general safety control along with the winter safety control are active.
- **Automatic mode for summer**: The plant works independently and the PLC continues to run the operations and specific control logic for the summer. The general and specific safety controls are active.
- **Automatic mode for winter**: The system works independently and the PLC continues to run the operations and specific control logic for winter. The general and specific safety controls are active.

The signal acquisition occurs at a frequency of 1 Hz and the safety controls related either to hardware or software are always active in all the control modes.

For each component, different operational modes were considered. For example, the solar circuit can operate at a fixed storage temperature mode, always ensuring the constant heat supply to the chiller or it can operate in variable accumulation temperature mode maximizing the collection of solar energy. The air handling unit can operate to heat load imposed by the operator or according to the internal temperature of the laboratory.

The following paragraphs describe the main operational procedures implemented, detailing the logical safety and specific control actions for each component.

2.10.1 Control related to solar field

For the summer and winter seasons, two different control strategies of the solar field have been developed and implemented, *fixed storage temperature mode* and *variable accumulation temperature mode*.

During summer, in *fixed storage temperature mode*, when there is solar radiation, the flow of the solar water circuit is adjusted to keep constant temperature (or equal to the nominal value of the chiller) of the hot water storage tank. In this mode, the efficiency of the chiller is increased but the efficiency of the solar field is lost, while maintaining the hot circuit at required temperature (typically $180° C$).

There are three main components involved in the regulation:

- Absorption Chiller (CS001)
- Solar field Valve (CV001)
- Solar circulation pump (P001)

When the chiller is off, the solar pump and bypass valve of the solar water circuit are regulated to fill the hot storage tank with hot water. But when the cooling unit is switched on, the hot water is fed to the chiller to guarantee its operation at high efficiency. The solar field valve is controlled to fill the hot water tank.

In winter, the same operation is implemented but the heat is removed directly from the circuit through the hot storage tank by distribution circuit (CV004) instead of absorption chiller.

In the *variable accumulation temperature mode*, the thermal energy collected by the collectors is maximized. The solar pump is operated when the outlet temperature of the collectors is higher than the temperature of hot storage tank. The chiller is thus fed with water at variable temperature ($160 - 180° C$). In this mode natural gas backup heater is also used whenever necessary. This reduces thermal coefficient of performance (COP).

The control of a movement mechanism for the solar collector both in normal operation and in emergency, is carried by a dedicated controller that drives the motor. The tracking position is calculated by the software based on GPS coordinates and orientation of the collectors, while in case of emergency positions are established apriori.

Particularly, two modes are provided:

- **Automatic**: The collector provides a thermal power when required by the user and the solar tracking is activated. Otherwise the collector remains defocused.
- **Manual**: The collector position is fixed by the operator.

Moreover, four different emergency events have been implemented:

- **High temperature**: The temperature of the fluid inside the reciever tube is measured via two dedicated resistance thermometers, one installed at the inlet and another at outlet. If this value exceeds the preset limit ($95° C$ in winter and $180° C$ in summer), the collector is automatically defocused and placed in the 90° safety position.
- **Wind**: Adjacent to the walkway, a weather station is installed that measures all environmental parameters (wind, light, humidity, temperature). If the wind exceeds the speed limit of $15\,m/s$ for more than 10 seconds then the collector plate is positioned at 0°, in order to minimize the loads on the underlying structure and to guarantee the integrity of the mirrors.
- **Accidental focusing**: If there is no heat demand by the user or the plant is in maintenance mode, the collector stays stationary in a fixed position and it can happen that during a day that the collector is accidentally in focused position. In order to avoid damage to the solar tube in such a situation, the control software continuously checks the theoretical position of the Sun and current one and if necessary defocusses the collector by 10° with respect to the current position.
- **Blackout**: In the case of power failure, the solar collector is automatically defocalized from the current position by the motor operated on UPS unit.

2.10.2 Control related to cold water circuit

Similar to the solar field, two different modes of operation for the management of the distribution system have been implemented, *fixed opening mode* and *fixed temperature mode*. There are two main components involved in regulation:

- Chiller absorption (C001)
- Control valve for cold storage tank (CV301)

The switching of the chiller is operated depending on the supply water temperature of air handling unit (AHU), which works to maintain the user demand.

In the *fixed opening mode*, the regulating valve CV301 remains open at a fixed value towards the cold storage tank. The number of switching of the chiller is reduced but it works in the most demanding condition (lower temperature flow and higher load).

In the *fixed temperature mode*, the regulating valve CV301 maintains the value of the flow temperature of the AHU unit to the setpoint of the temperature required by the user. This setpoint could be different than the chiller setpoint. The switching of the chiller is higher but it works under less demanding condition (higher flow temperature and partial load).

2.10.3 Control related to air handling unit (AHU)

The air handling unit is used to simulate the thermal load or cooling required by the user. The control has been implemented by two possible management methods, that

are temperature adjustment of the laboratory and simulation of a pre-set thermal profile. There are two main components involved in regulation:

- Air handling units UTA (in particular its fan M401)
- control valve distribution (CV302)

In the *laboratory temperature tracking mode*, the fan of UTA unit is turned on or off depending on the temperature of the return air. The regulating valve (CV302) is adjusted in order to maintain the outlet temperature of the air inside the laboratory at a set point value.

In the *pre-set heat load mode*, the manual operator sets the single value or the time profile of the cooling load to simulate. When the refrigeration load is positive, the fan is switched on and the regulating valve (CV302) is actuated to maintain the amount of refrigeration required by AHU to the keep the setpoint value.

2.11 General safety control

Saftey system is designed to ensure the safe operation of a plant and to cope up with unwanted situations in case of malfunction or anomalies. Single alarm event at a time was generated and specific action related to each one of them was studied in order to secure plant safely in case of an emergency.

The events are divided into two types, the general events related to the anomalies of the individual components and the specific events related to summer and winter operation of the plant. The specific events are mostly related to the temperatures and pressures of the solar and distribution circuit. When an abnormality occurs, the particular component is turned off, the hydraulic circuit to which it belongs is deactivated.

2.11.1 Specific safety related to summer/winter operation

The specific safety controls for the summer and winter operations are listed below:

- **High temperature in solar circuit**: All the components are designed with a design temperature of $250° C$. Temperature rise beyond this value may increase the pressure of the circuit, consequently the safety valves get activated.
- **Low temperature in solar circuit**: This event typically occurs in winter when the outside temperature is low and the solar radiation is absent. In these condition, it is necessary to prevent the freezing of water in pipes.
- **Low pressure in solar circuit**: The pressure inside the solar circuit must remain above a certain threshold value to avoid the vaporization of water.
- **Lower pressure distribution circuit**: Minimum pressure of the circuit must be guaranteed to prevent cavitation of the circulation pump.

2.12 Measurement instruments

The instrument panel provides comprehensive monitoring of overall system performance and the individual components. In particular:

- Upstream and downstream measurement are provided for temperature and pressure of each main component (chiller, tank, collector,etc.) , available locally and remotely.
- Two flowmeters, one is intalled on the overall circuit and another on the branch of solar collectors.
- The pyranometer (LASTEM) is installed to detect the total incident radiation on the parabola of the solar collectors.
- For the measurement of electrical consumption a counter device is provided .

Table 2.2 shows the uncertainties on the main measurement devices as given on the datasheet provided by the manufacturers.

Table 2.2: Uncertainties in the measurements (as reported in the datasheet)

Parameter	Unit	Reading uncertainty	Scale uncertainty
Temeperature	$^\circ C$	0	0.1
Water flow	kg/s	0.65	0
Gas flow	Nm^3/hr	0.5	0.0027
Radiation	W/m^2	2	0
Electric power	W	1	0

2.13 Evaluation of plant performance

The evaluation of the plant performance and the sizing of the main components are carried out through the estimation of the primary energy consumption and the energy saving reachable in comparison with traditional systems [5].

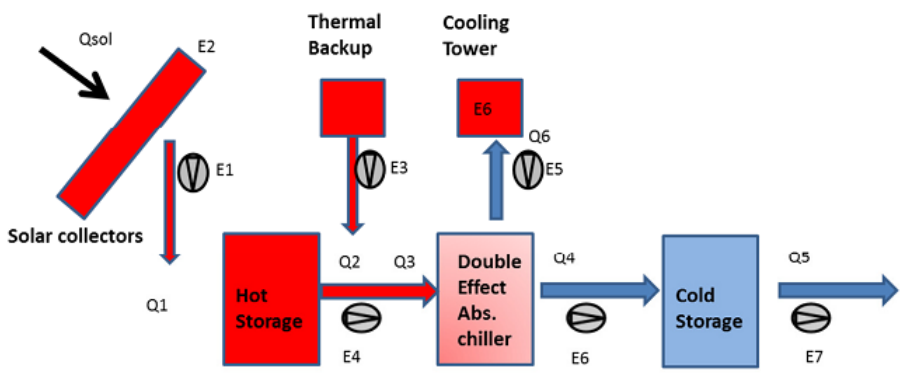

Figure 2.13: Closed loop solar cooling plant

During summer season, the produced chilled water sent to the distribution system is the only useful result i.e. the refrigeration power Q_5. The primary energy consumption is composed of two main parts: the natural gas used in the backup system providing power Q_2 and the auxiliary electrical power consumptions. In particular electrical power consumptions, the circulation pumps consume the electric power $E_1, E_3, E_4, E_5, E_6, E_7$, while the power consumed by the electric motor of the solar field and the cooling tower fan are E_2 and E_8 respectively.

The overall performance of a solar cooling plant is typically evaluated by the Primary Energy Ratio (PER), which represents the cooling effect produced using a single kWh of primary energy

$$PER = \frac{Q_5}{\frac{Q_2}{\eta_{boiler}\,\varepsilon_{fossil}} + \frac{\sum E_x}{\varepsilon_{elet}}} \tag{2.1}$$

where, η_{boiler}: 0.95 (boiler efficiency), ε_{fossil}: 0.9 (combustion efficiency), ε_{elet}: 0.4 (electrical conversion factor), $\sum E_x$ is the sum of the electric consumption by the circulation pumps, the electric motor of the solar field and the cooling tower fan.

Other parameters are also used to understand how the different kind of energy flows are used to get the desired results. Those are Solar Factor (SF), electric coefficient of performance COP_{elet} and thermal coefficient of performance $COP_{thermal}$ and given by,

$$SF = \frac{Q_1}{Q_1 + Q_2};\;\; COP_{elet} = \frac{Q_5}{\sum E_x};\;\; COP_{thermal} = \frac{Q_5}{Q_2} \tag{2.2}$$

2.14 Summary

In this chapter, the details about the solar cooling plant built by RSE was studied. The functionality and operation of the plant and its equipment explained in this chapter will be used to build the detail model, simulator and the predictive control of the plant in upcoming chapters.

Chapter 3

Modelling of Solar cooling Plant

In this chapter the development and implementation of the dynamic model in MATLAB/Simulink of the plant for control purpose is explained. All the components of the solar cooling plant have been considered namely, solar collector, pipes, storages and pumps are modelled with thermodynamic principles. The chiller is a complex system and a simple model for control purposes based on the physical equations is difficult to obtain. So, the chiller model has been developed by black-box identification techniques. At the end of this chapter, the simulator of the whole plant is described along with some simulation results.

3.1 Solar collector model

This plant uses a Parabolic Trough Collector type for Solar collector. This collector concentrates sunlight onto a receiver pipe located along the focal line. A heat transfer fluid (HTF), typically water or thermal oil is heated and flows in the receiver tube, then it is routed either to chiller or the hot storage tank. For this model the HTF is water. A simple view of a receiver tube of a generic parabolic collector with the indication of different heat fluxes is shown in figure 3.1.

The sun light is concentrated on the receiver pipe after it falls on a parabolic reflecting surface. This radiation passes through the glass tube and falls on the metal tube made of Austenitic stainless steel. The metal tube is heated and the energy contributed by solar radiation that heats up the metal tube is called solar energy Q_{solar}. Part of energy is lost to the environment through radiation and conduction from the metal tube denoted by $P_{rc}(t)$. The fluid flowing through the metal tube is also heated due to heat transfer from the heated metal to fluid. Hence the energy balance for the metal tube of the trough collector is given by equation 3.1. The rate of change of energy E_m of a metal tube is nothing but the sum of energy from the Sun Q_{solar}, heat loss to the environment $P_{rc}(t)$ and heat transfer to the fluid flowing inside the collector $Q_{tofluid}$.

$$\frac{\partial E_m}{\partial t}(t,x) = \dot{Q}_{solar} - P_{rc}(t) - \dot{Q}_{tofluid} \tag{3.1}$$

The solar energy can be expressed as,

$$\dot{Q}_{solar} = \eta_0 \, G \, I(t) \, \eta_{end} \tag{3.2}$$

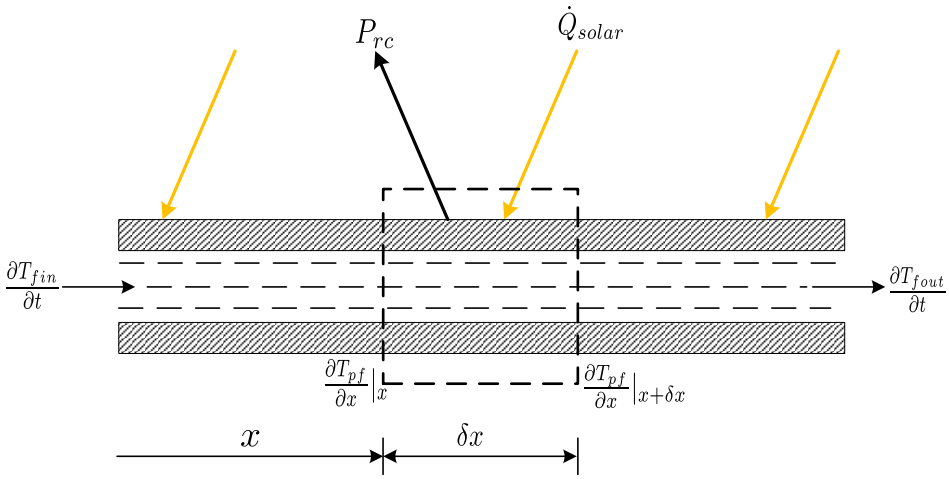

Figure 3.1: Energy balance of parabolic trough collector

where, η_0 is a Mirror optical efficiency, G is a Mirror optical aperture, $I(t)$ is a solar radiation and η_{end} is an end losses associated with the reciever tube. The sum of the thermal losses due to radiation and conduction is usually modelled as a linear conductive relation term [7].

$$P_{rc}(t) = H_1(T_m(t,x) - T_a(t)) \tag{3.3}$$

Here, H_1 is the global coefficient of thermal losses. Further, the rate of change of energy of the fluid is nothing but sum of the energy acquired from the metal tube and the energy transfer due to the flow of a fluid $\dot{Q}_{flow}$

$$\frac{\partial E_l}{\partial t}(t,x) = -\dot{Q}_{flow} - \dot{Q}_{tofluid} \tag{3.4}$$

The dynamics of the solar collector is expressed by equations 3.1 and 3.4. After expansion of individual terms in those equations, the following system of partial defferential equations can be obtained [7].

$$\begin{cases} \rho_m c_m A_m \dfrac{\partial T_m}{\partial t}(t,x) = \eta_0 G I(t) \eta_{end} - P_{rc}(t) - D_i \pi\, H_t(T_m(t,x) - T_f(t,x)) \\ \rho_f c_f A_f \dfrac{\partial T_f}{\partial t}(t,x) + \rho_f c_f q(t) \dfrac{\partial T_f}{\partial x}(t,x) = D_i \pi H_t(T_m(t,x) - T_f(t,x)) \end{cases} \tag{3.5}$$

where, subscripts m and f refer to the metal of collector and fluid flowing through the collector. The details of all other parameters and variables are described in Table 3.1. $T(t,x)$ is the fluid temperature at position x along the collector length, with boundary condition $T(t,0) = T_{in}(t)$, where T_{in} is the inlet water temperature to the solar collector.

The effective solar energy reached to the receiver tube of the solar collector depends on the peak optical efficiency of the collector, mirror reflection, effective reflecting surface and the effective irradiance onto the collector. The radiation $I(t)$ is measured by the sensor mounted on the panel and hence considered as an effective incident solar irradiance multiplied by an aperture area A_a of a collector which holds true only when the solar panel tracking is ON. However, the equation of the effective incident solar irradiance can be given as [8],

$$I_{eff}(t) = G_{DN}\, \rho (\tau\alpha\gamma)_n\, cos(\theta)\, \eta_{IAM}\, \eta_{end} \tag{3.6}$$

Table 3.1: Solar collector model variables and parameters

Symbol	Description	Value	Units
t	Time	-	s
x	Space	-	m
ρ_m	Density of metal	8000	$kg\,m^{-3}$
ρ_f	Density of fluid	1000	$kg\,m^{-3}$
c_m	Specific heat capacity of metal	500	$J\,kg^{-1}{}^{\circ}C^{-1}$
c_f	Specific heat capacity of water	4186	$J\,kg^{-1}{}^{\circ}C^{-1}$
A_m	Cross-sectional area of metal tube	0.000428	m^2
A_l	Cross-sectional area of fluid	0.0034	m^2
$T_m(t,x)$	Temperature of metal	-	$^{\circ}C$
$T_f(t,x)$	Temperature of fluid	-	$^{\circ}C$
$q(t)$	Volumetric flow rate of water pump	-	$m^3\,s^{-1}$
$I(t)$	Solar radiation	0-1000	$W\,m^{-2}$
η_0	Mirror optical efficiency	1	-
η_{end}	End loss efficiency	-	-
G	Mirror optical aperture	2.28	m
$T_a(t)$	Ambient temperature	-	$^{\circ}C$
H_1	Global coefficient of thermal losses	7.3	$W\,m^{-1}\,{}^{\circ}C^{-1}$
H_t	Coefficient of metal-fluid thermal transmission	600	$W\,m^{-2}\,{}^{\circ}C^{-1}$
D_i	Inner diameter of collector tube	0.066	m
L	Receiver tube length	21	m

The parameter G_{DN} is a direct normal solar irradiance; $\rho(\tau\alpha\gamma)_n$ is the peak optical efficiency when the direct solar rays are perpendicular to the collector aperture and refers to reflectance of a reflecting surface, the transmittance and absorption of the collector and intercept factor; θ is an incident angle between Sun's direct rays and the normal to the collector aperture plane; η_{IAM} is the incident angle modifier; η_{end} is the end loss efficiency caused by the off-normal incident angle as expressed in equation 3.7, f being a focal length of a collector.

$$\eta_{end} = 1 - \frac{f}{L} tan(\theta) \tag{3.7}$$

The end losses are due to the length l of receiver tube not illuminated by the sunlight. As shown in figure 3.2 the sun light falls on the parabola at an angle of θ which causes the part of the collector unexposed to the sunlight. To calculate the end losses of receiver tube it is necessary to know the incidence angle of the sun's rays from the normal to the plane of the collectors [8],[9],[10]. The incidence angle θ as shown in figure 3.3 is a variable parameter that changes at every day of all the months , so its value has to be calculated at every instance using an equation valid for collectors with tracking on a single axis [11]:

$$\theta = \frac{\pi}{2} - sin^{-1}(cos(\delta)cos(\omega)cos(\zeta)cos(\phi) - cos(\delta)sin(\omega)sin(\zeta) + sin(\delta)cos(\zeta)sin(\phi)) \tag{3.8}$$

As it can be visualized from figure 3.4, the meaning of each parameter is given by,

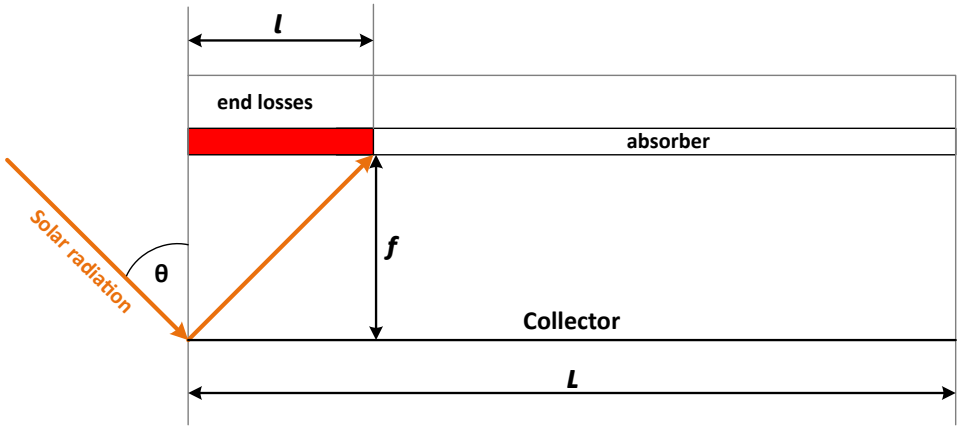

Figure 3.2: Schematic representation of the collector area not illuminated by the Sun light.(Source:[10])

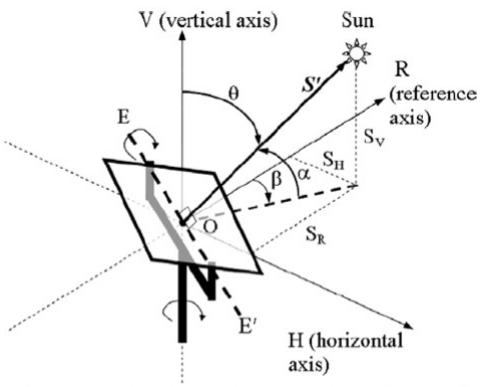

Figure 3.3: Incidence angle θ with respect to the normal to the plane of the collectors.(Source:[11])

- δ is a solar declination angle, that is the angle formed by sun's rays with the equatorial plane. It varies between $-23.27°$ (21 December) and $+23.27°$ (June 21).
- ω indicates the hour angle, i.e. the angular distance between the Sun and its position at mid-day along the apparent path in the sky.
- ϕ is the latitude (Milan $\phi = 45.476°$).
- ζ is inclination angle of the parabola with respect to the vertical axis (at each timestep value provided by the data acquisition system).

The values of angle δ and ω can be derived from the equation.

$$\begin{cases} \delta = 23.45 \cdot sin\left[\dfrac{360}{365} \cdot (N + 284)\right] \\ \omega = 15 \cdot h_{sol} - 180° \\ h_{sol} = h_{conv} + \left[\dfrac{E_t - 4 \cdot (\phi_{mr} - \phi_{oss})}{60}\right] \\ E_t = -10.1 \cdot sin\left[360\,\dfrac{2N + 31}{366}\right] - 6.9 \cdot sin\left[360\,\dfrac{N}{366}\right] \end{cases} \tag{3.9}$$

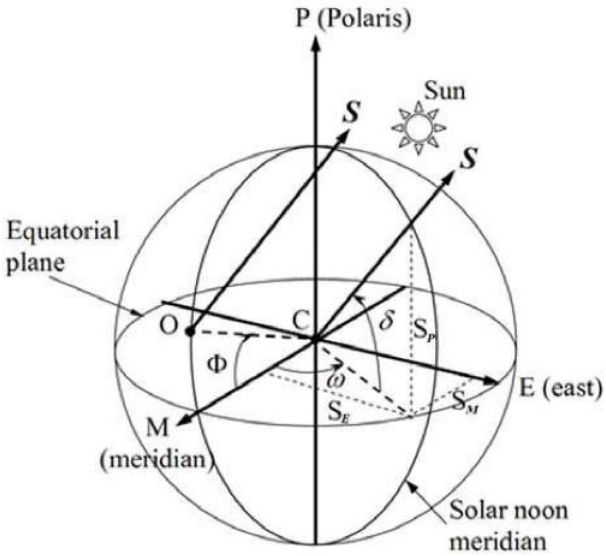

Figure 3.4: Graphical representation time angle ω, the latitude ϕ and solar declination δ with respect to the position of the sun.(Source:[11])

where [3],

- N indicates the sequence number of a day of a year (For example, December 30 belongs to N = 364)
- h_{sol} is the winter time, i.e. the time defined so that it signs always noon when the sun passes the meridian of the locality
- h_{conv} is the conventional marked time on the clock, which differs from standard as it is same for all locations in a time zone
- ϕ_{mr} is the longitude of the Prime Meridian (15° for Italy);
- ϕ_{oss} is the longitude of the meridian at the locations where there is the parabola (9.26° for Milan);
- E_t represents a correction factor for the solar time calculation. Due to Earth's revolution around the sun and therefore the speed variation of the Earth's revolution during the year, the meridian doesn't pass exactly in equal intervals of 24 hours, but shows delays or advances depending on the time of a day.

3.1.1 Simulation of the Solar collector

The model for the solar collector was developed using MATLAB/Simulink software. The parameters for the simulation were initialized in the MATLAB file whose values can be found in table 3.1. The function was written to implement the distributed parameter model of the receiver tube. In this type of a model, the receiver tube of the solar collector is formed of equisized small elements of pipes connected to each other along its length. The first element of receiver pipe with length δx is initialized with the inlet temperature of the receiver pipe. The proceeding element acquires the input temperature from the first element and its output temperature acts as the input temperature for next element. The process repeats for the number of such

elements defined over the total length of receiver tube. The output temperature of the final element is regarded as the outlet temperature of the receiver tube. For simplicity, the length of all these small element δx is considered as $1\,m$ size. The system of equations for such a spatial distribution for the metal and fluid can be written as,

$$\begin{cases} \rho_m c_m A_m \dfrac{\partial T_{m_1}}{\partial t}(t,x) = \eta_0 GI(t)\eta_{end} - H_1(T_{m_1}(t,x) - T_a(t)) - D_i \pi H_t(T_{m_1}(t,x) - T_{f_1}(t,x)) \\ \vdots \\ \rho_m c_m A_m \dfrac{\partial T_{m_N}}{\partial t}(t,x) = \eta_0 GI(t)\eta_{end} - H_1(T_{m_N}(t,x) - T_a(t)) - D_i \pi H_t(T_{m_N}(t,x) - T_{m_N}(t,x)) \end{cases} \tag{3.10}$$

$$\begin{cases} \rho_f c_f A_f \dfrac{\partial T_{f_1}}{\partial t}(t,x) + \rho_f c_f q(t) \dfrac{\partial T_{f_1}}{\partial x}(t,x) = D_i \pi H_t(T_{m_1}(t,x) - T_{f_1}(t,x)) \\ \vdots \\ \rho_f c_f A_f \dfrac{\partial T_{f_N}}{\partial t}(t,x) + \rho_f c_f q(t) \dfrac{\partial T_{f_N}}{\partial x}(t,x) = D_i \pi H_t(T_{m_N}(t,x) - T_{f_N}(t,x)) \end{cases} \tag{3.11}$$

T_{m_1} and T_{f_1} are the temperature of the first elements of metal and fluid spatial distribution. After being heated they act as the input temperature to next element and after successive N iteration the final elements T_{m_N} and T_{f_N} are regarded as output temperature of the solar collector.

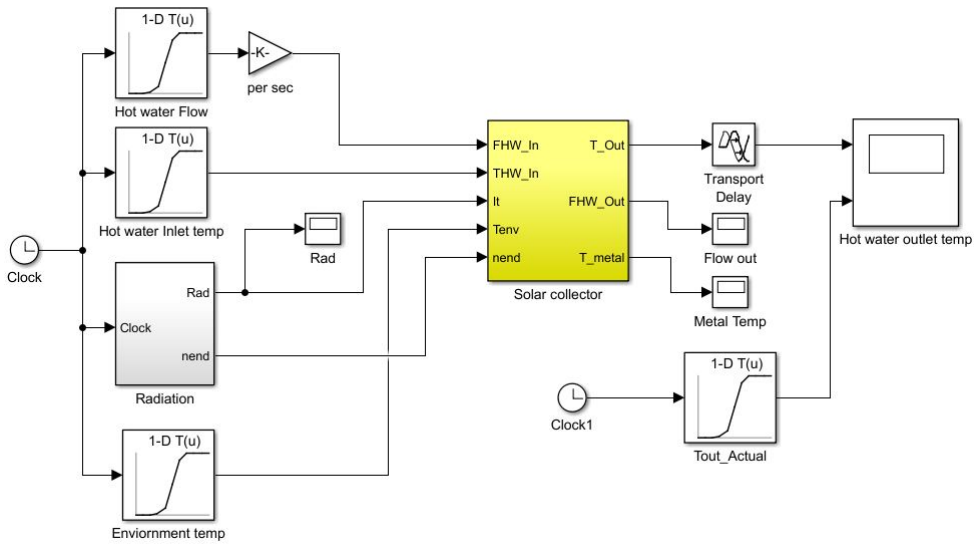

Figure 3.5: Simulink simulator for solar collector

As it can be seen from the figure 3.5 the solar collector (yellow block) is fed by five inputs that are *Hot water input flow and inlet temperature, Radiation, end losses of receiver tube and environment temperature.* The outputs are *Hot water outlet temperature and flow and temperature of the metal tube of the receiver.* The temperature of a metal can't be measured directly on the real system hence it was used for reference whereas, the Hot water outlet temperature could be validated using the real data collected from the solar collector.

The transportation delay was incorporated in the solar collector model caused due to the transportation of the fluid from inlet to outlet of receiver tube. It must be

noticed that the inlet temperature and outlet temperature measurement were not exactly at the inlet and outlet of the solar collector. The temperature sensors are mounted at a distance of $2\,m$ before inlet and $8\,m$ after the outlet of a solar collector with different diameter size. As the heat losses due to these pipes are insignificant, only the transportation delays related to them were considered. The total transportation delay was calculated to be $145\,sec$ to travel receiver tube of length $21\,m$ and $10\,m$ pipe (total pipe length before and after the tube where the temperature sensors are mounted) considering an average speed of fluid to be 0.1535 and $1.0695\,m/s$ for the collector tube and the pipe respectively.

Many simulations were performed by feeding the data of several days from operational period of a plant during the years 2015 and 2016 to the model to take into account the dynamic behaviour of the solar collector in varying environmental conditions. The initial value of Global coefficient of thermal losses $H_1 = 9.72\,W\,m^{-1}\,{}^{\circ}C^{-1}$ was taken from calculated value by [3] with the TRNSYS model of the collector. After many simulations, it was realized that the values for these coefficients were not good enough for the MATLAB model as these values can't be always calculated correctly as they are function of the fluid speed. Therefore they had to be estimated to fit the real data. The estimated values found to be $H_t = 600\,W\,m^{-2}\,{}^{\circ}C^{-1}$ and $H_1 = 7.3\,W\,m^{-1}\,{}^{\circ}C^{-1}$.

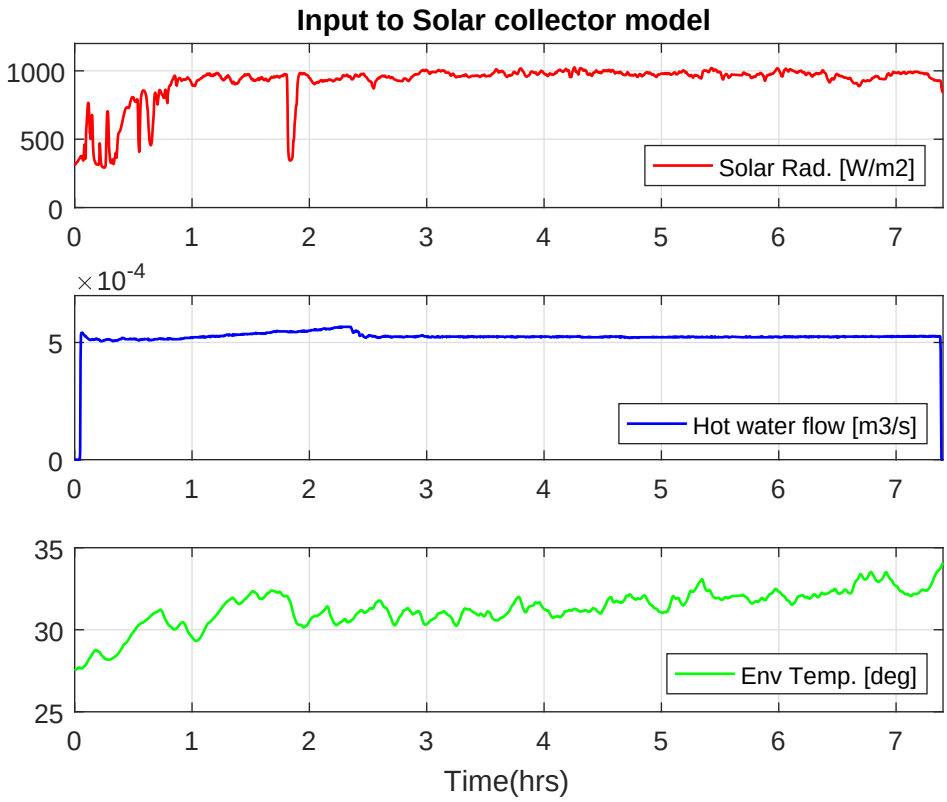

Figure 3.6: Inputs to the solar collector model for validation

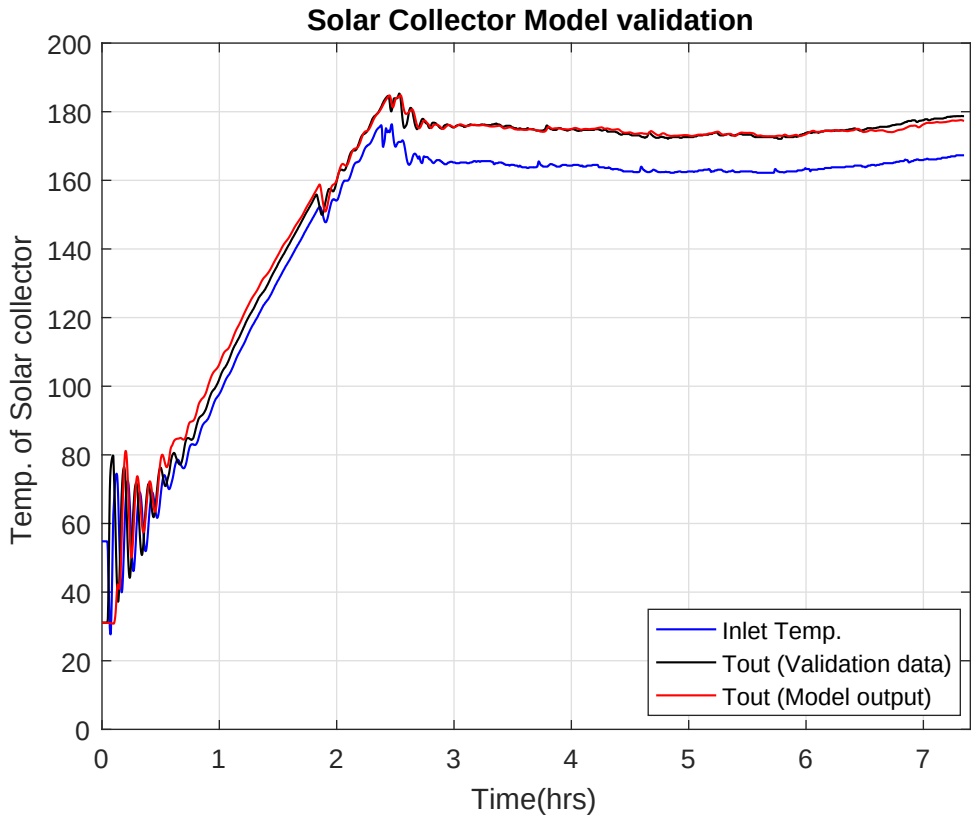

Figure 3.7: Model validation

The model was then validated with the data referred to 5-7 days that was gathered during the days of summer 2016 while the normal operation of the solar plant. Figure 3.6 and 3.7 show the inputs to the model and the validation result of one of these days respectively. The solar radiation during this day is quite good and the input flow of the hot water stays almost constant to maximum value throughout the operation.

It can be seen from Figure 3.7 that the model produces very good results with the fitness of 99.97 % by MSE (Mean square error) for transient as well as steady state. The model could reconstruct even the oscillation exhibited by the system quite well. The data used were acquired from the plant at sampling time of 12 *sec*. The time required to heat the solar circuit temperature above 165° is more than 2 hrs and this is the time when the hot water chiller starts working. With the chiller ON the outlet temperature has equilibrium around 175° with almost constant radiation from the Sun.

3.2 Storage tank model

The hot water and cold water storage tanks in the plant act as buffers to store hot and cold water obtained from the solar collector and chiller respectively. When the amount of solar energy available during the day is high, the hot storage tank can be heated with hot water to store more energy from sun and used mostly when there is no sunlight and the user demand exists. The cold storage tank can also be cooled

when the chiller produces more refrigeration power which depends on the flow rate that is fixed in the distribution circuit. The cooled water from cold storage can be used as per user requirement.

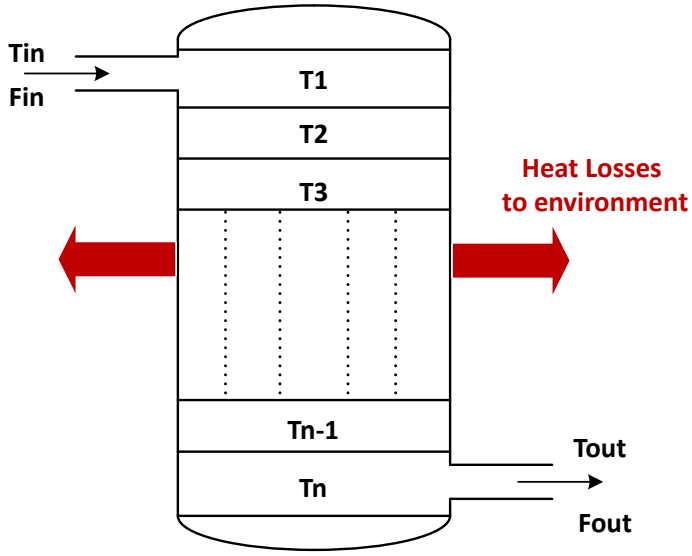

Figure 3.8: Storage tank scheme

The temperature distribution in a storage tank is typically 3 dimensional. For the purpose of this work, it was enough to approximate the system in one dimension with a variable temperature along the height of a tank. This is because the heat losses in a day are really low in comparision to other terms in the energy balance i.e. around 10 % [3]. As shown in the figure 3.8, the fluid in a tank has different level of the temperature as it flows from inlet down to the outlet. The tank temperature is considered as the average of all these temperatures.

The Energy balance of a tank can be written as stated by equation 3.12. The rate of change of the energy of a tank is equal to the energy input from hot water Q_{in} minus the heat losses to the environment Q_{toenv}.

$$\frac{\partial E_t}{\partial t}(t,x) = \dot{Q}_{in} - \dot{Q}_{toenv} \tag{3.12}$$

Both the lumped and distributed parameter model can be obtained from the expanded form of the former equation and given by,

$$c_f M_f \frac{\partial T_t(t)}{\partial t} = c_f F_{in}(t)(T_{in}(t) - T_t(t)) - H_{tank} A_{ext}(T_t(t) - T_a(t)) \tag{3.13}$$

Table 3.2 describes all the parameter used in this equation. The hot and cold storages can be modelled using the same energy balance equation 3.12, but the coefficient for heat losses H_{tank} is different for both of them as the insulation and physical size of these tanks are different.

Table 3.2: Model variables and parameters for the hot and cold storage

Symbol	Description	Value	Units
t	Time	-	s
c_f	Specific heat capacity of water	4186	$J\,kg^{-1}{}^{\circ}C^{-1}$
M_{fh}	Fluid mass of hot storage	750	kg
M_{fc}	Fluid mass of cold storage	1500	kg
$T_t(t)$	Temperature of a tank	-	$^{\circ}C$
$F_{in}(t)$	Volumetric flow rate of water pump	-	$m^3\,s^{-1}$
$T_{in}(t)$	Input temperature of a tank	-	$^{\circ}C$
$T_a(t)$	Ambient temperature	-	$^{\circ}C$
H_{tank_h}	Coefficient of thermal losses of hot storage	0.006	$W\,m^{-2}\,^{\circ}C^{-1}$
H_{tank_c}	Coefficient of thermal losses of cold storage	0.0028	$W\,m^{-2}\,^{\circ}C^{-1}$
A_{ext_h}	External surface area of hot storage	6	m^2
A_{ext_c}	External surface area of cold storage	19	m^2

3.2.1 Simulation of Hot storage tank

The tank simulator was developed in Simulink. The model has three inputs, *hot water input temperature, hot water flow and environment temperature.* A MATLAB function was developed to model the tank as a single element instead of the distributed parameter to obtain simple but a sufficiently accurate model.

To estimate the heat loss coefficient for the hot storage, experiments were conducted to cool down the tank by itself overnight with no hot water flow after it had been heated by hot water from the solar collector during the day. The model was initialized with the average temperature measurement of a tank after it had been finished heating by hot water in the evening. The coefficient of thermal losses of a tank was then estimated to fit the real measurement. The estimated value turned out to be $H_{tank\_h} = 6 \times 10^{-3}\,W\,m^{-2}\,^{\circ}C^{-1}$. The model was then validated with an-

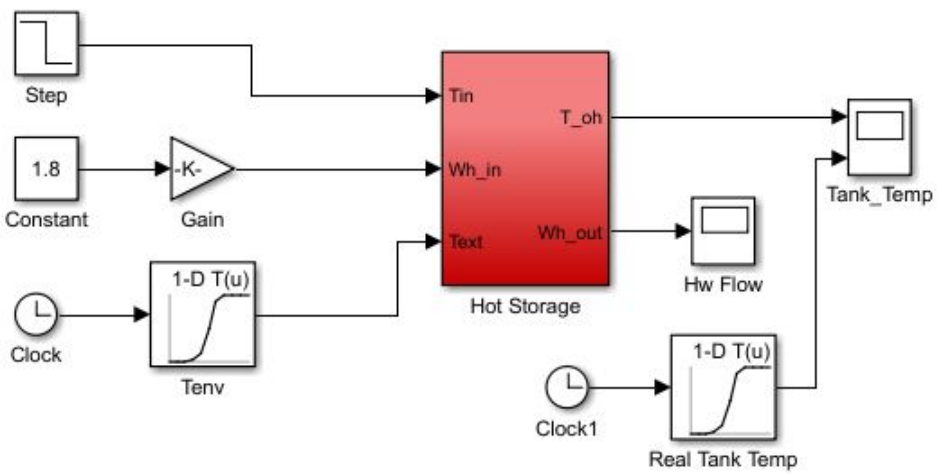

Figure 3.9: Simulator for the hot storage

other set of data gathered during different days. The validation result for one of these days is shown in figure 3.10, it can be seen that the temperature output of this model fits satisfactorily to the measured data.

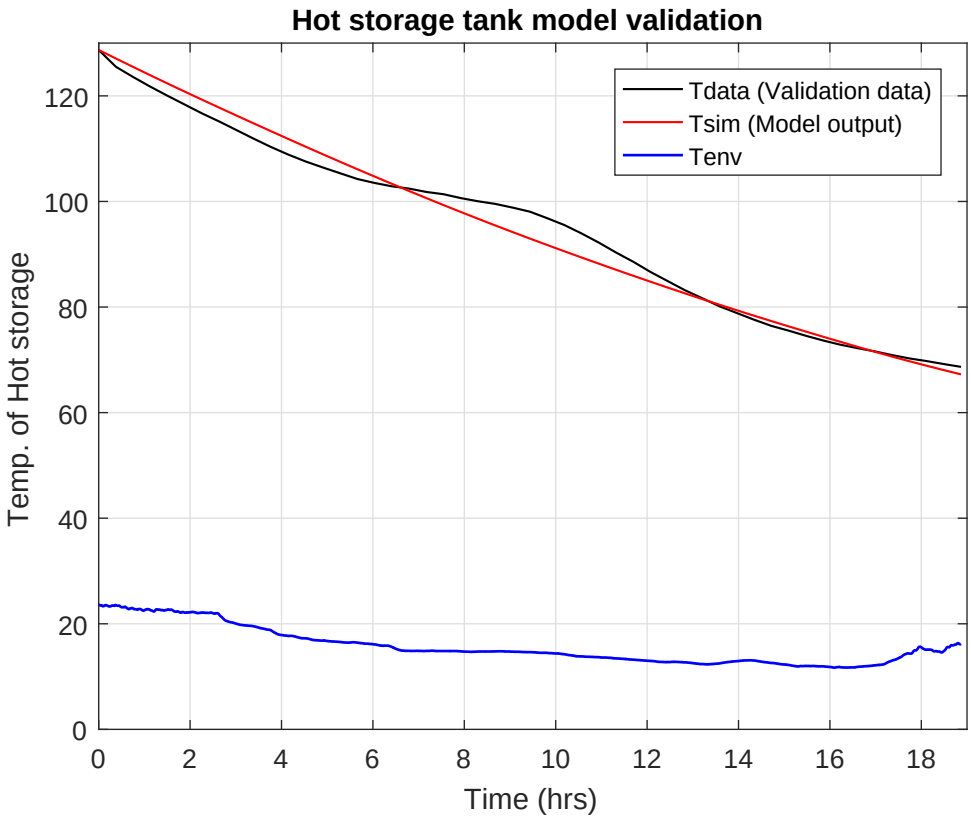

Figure 3.10: Model Validation of hot water storage with the envoirnmental temperature input (in blue)

3.2.2 Simulation of Cold storage tank

Since in the case of the cold storage tank, the cooling range is low i.e. $7 - 14°$, instead of estimating the value of the coefficient of heat losses from the real data, it was decided to consider the value for H_{tank_c} found during system testing and reported in [2].

$$H_{tank\_c} = 2.8 \times 10^{-3}\, W\, m^{-2}\, {}^{\circ}C^{-1}$$

3.3 Pipe model

The plant has around $90\, m$ and $110\, m$ of pipes for the hot water circuit and cold water circuit respectively. These pipes are utilized to connect the various equipment of the plant. The pipes on solar circuit has the insulation to prevent the heat losses to environment. Regardless of the insulation on the pipes, there are heat losses associated to them that must be modelled. Figure 3.11 shows the energy associated to the single element of the pipe.

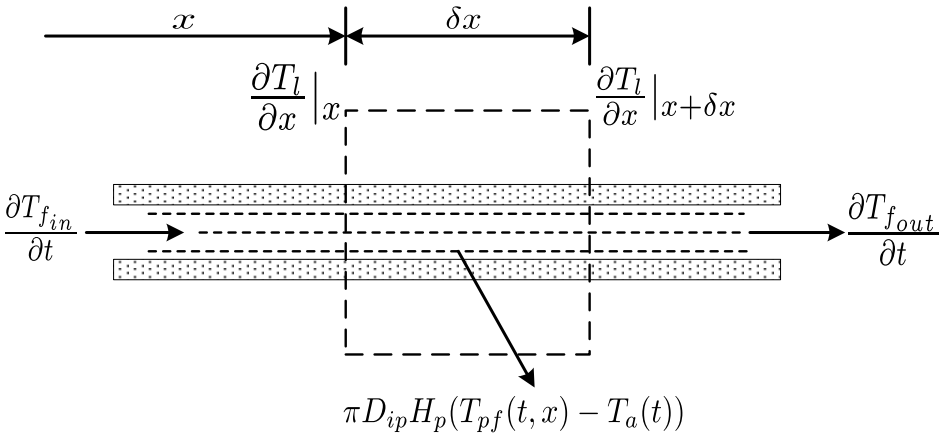

Figure 3.11: Pipe model scheme

The whole pipe is modelled as the distributed parameter model like the solar collector model. The rate of change of energy of a pipe is equal to the energy transfer due to the flow $\dot{Q}_{flow}$ and the thermal losses to the environment $\dot{Q}_{toenv}$.

$$\frac{\partial E_{pf}}{\partial t}(t,x) = -\dot{Q}_{flow} - \dot{Q}_{toenv} \tag{3.14}$$

After expanding the terms of the energy balance equation, the dynamics of the pipe can be formulated by the partial differential equation 3.15.

$$\rho_f c_f A_f \frac{\partial T_{pf}}{\partial t}(t,x) = -\rho_f c_f q(t) \frac{\partial T_{pf}}{\partial x}(t,x) - \pi D_{ip} H_p (T_{pf}(t,x) - T_a(t)) \tag{3.15}$$

All the parameters have the meaning explained in the Table 3.3. The pipes in the distribution circuit and hot water circuit have different heat loss coefficients because they have different kinds of insulations.

Table 3.3: Pipe model variables and parameters

Symbol	Description	Value	Units
t	Time	-	s
x	Space	-	m
ρ_f	Density of fluid	1000	$kg\,m^{-3}$
c_f	Specific heat capacity of fluid	4186	$J\,kg^{-1}{}^{\circ}C^{-1}$
D_{ip_h}	Inner diameter of the hot pipe	0.025	m
D_{ip_c}	Inner diameter of the cold pipe	0.03	m
A_{f_h}	Cross-sectional area of hot fluid	0.0005	m^2
A_{f_c}	Cross-sectional area of cold fluid	0.0007	m^2
$T_{pf}(t,x)$	Temperature of fluid	-	$^{\circ}C$
$q(t)$	Volumetric flow rate of water pump	-	$m^3\,s^{-1}$
$T_a(t)$	Ambient temperature	-	$^{\circ}C$
H_{phot}	Coefficient of thermal losses of a pipe	7.2	$W\,m^{-1}\,{}^{\circ}C^{-1}$
H_{pcold}	Coefficient of thermal losses of a pipe	0.5	$W\,m^{-1}\,{}^{\circ}C^{-1}$

3.3.1 Simulation of the hot water circuit pipe

The pipe model was developed as a distributed parameter system using a function build in the MATLAB/Simulink. As showed in figure 3.12 the model has three inputs *Hot water input flow, Hot water input temperature and environment temperature.* The transportation delay is almost 1 sec to pass one meter of the pipe and it was calculated considering the average speed of 1.07 m/s.

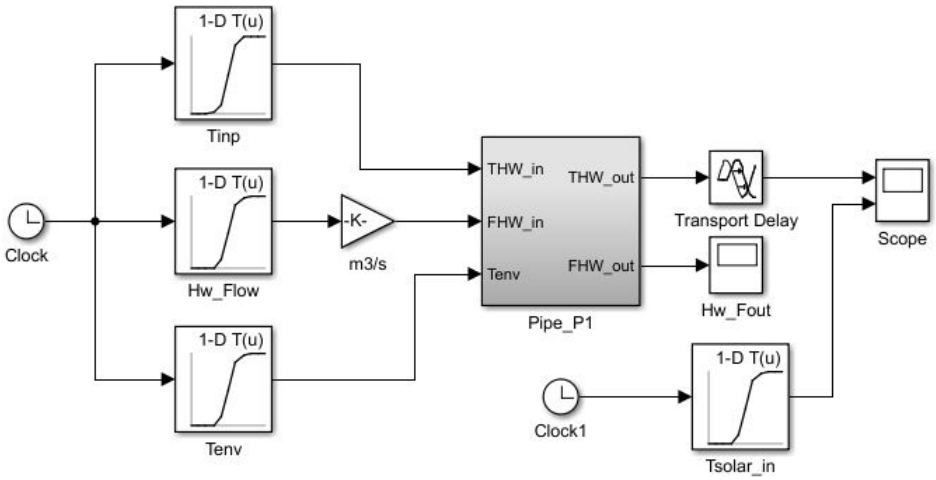

Figure 3.12: Simulator of hot water circuit pipe model

To estimate the coefficient of thermal losses H_{phot}, the reading between input and output temperature sensor of the pipe of the plant is recorded. Note that the readings were taken when the water was flowing through the pipe at nominal flow. This data was then used to estimate the H_{phot} by performing the curve fitting of the output temperature of the model with the output temperature of a pipe data measured during experimentation on real the plant. The estimated value for the coefficient was $H_{phot} = 7.2\,W\,m^{-1}\,°C^{-1}$. This value was then validated with another set of experimental data.

Figure 3.13 and 3.14 show the input data to the pipe model and validation result for a specific set of data respectively. The validation was carried on the 45 m of pipe connecting the hot water outlet of a chiller to the inlet of the solar collector. From validation result, it can be noticed that using the estimated coefficient of thermal losses, the model reproduces very good fit to real output.

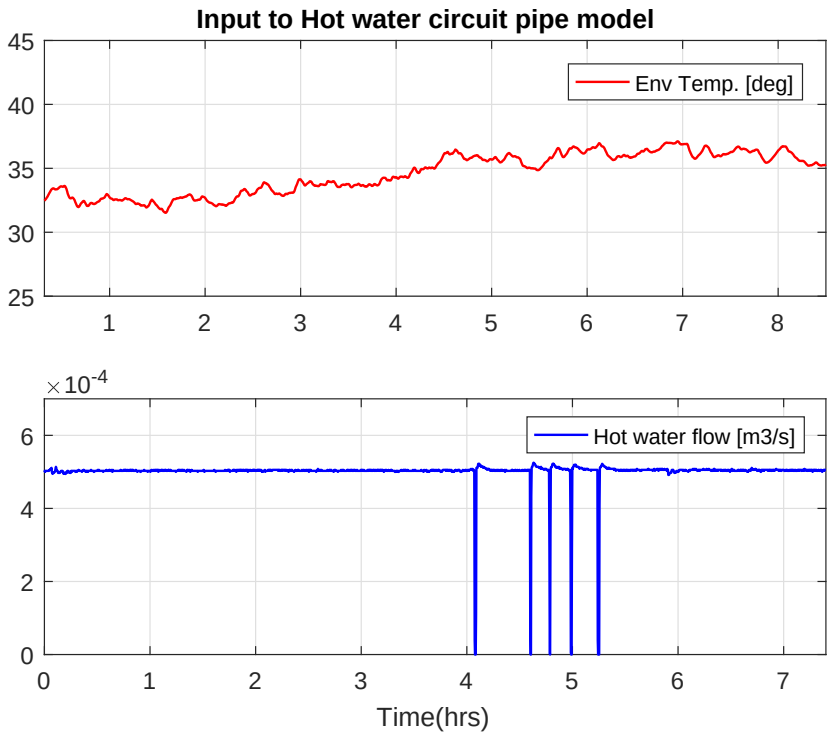

Figure 3.13: Inputs to the hot water circuit pipe model for validation

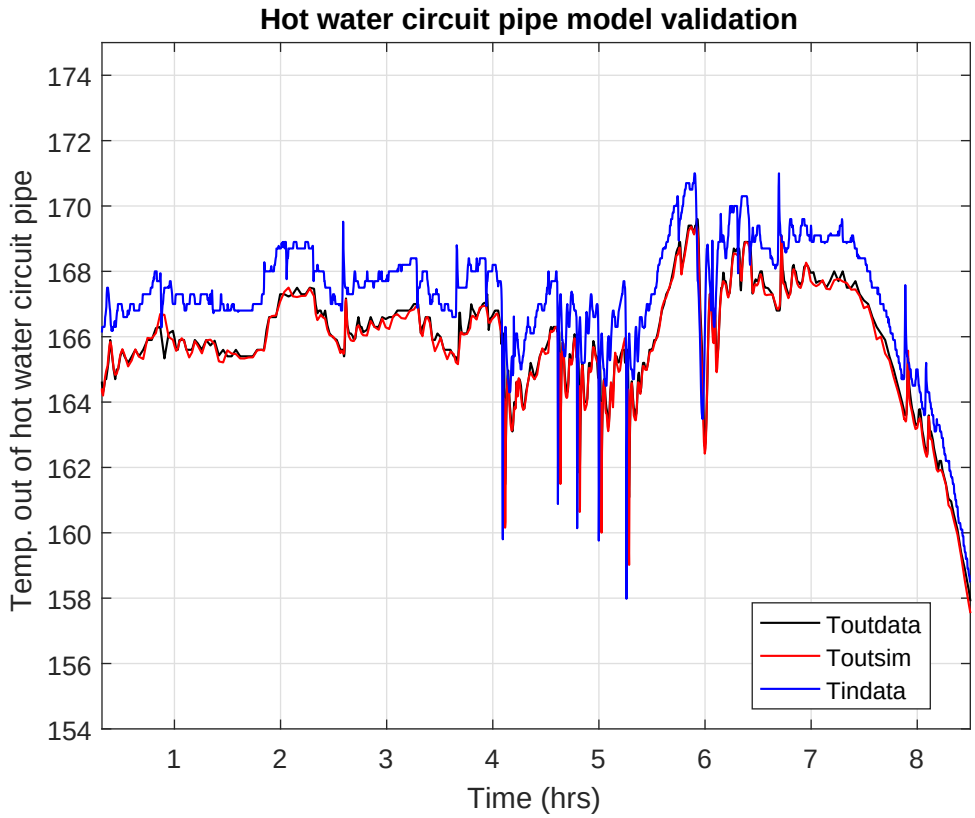

Figure 3.14: Validation of the hot water circuit pipe model

3.3.2 Simulation of cold water circuit pipe

Since in the case of cold water circuit pipe, the cooling range is low i.e. $7 - 14°$, instead of estimating the value of coefficient of heat losses from the real data, it was decided to consider the value for H_{pcold} found during system testing and reported in [2]. More simplified form was adopted to calculate the coefficient of thermal losses considering the thermal exchange with the environment. This approach is reasonable as the heat losses are really low because, the pipes are in the room to be air conditioned.

$$H_{pcold} = 0.5\, W\, m^{-2}\, °C^{-1}$$

3.4 Chiller Model

The chiller is a machine that removes heat from a liquid via a vapor-compression or absorption refrigeration cycle. This liquid can then be circulated through a heat exchanger to cool equipment or user.

The chiller present in this plant is double effect type which improves the performance of the system. A double-effect absorption system has two stages of generation to separate the refrigerant from the absorbent. The overall efficiency of the absorption system is increased by indirectly using the input heat a second time. In [13] the modelling of an absorption chiller is discussed. Also [14] presents a detailed mathematical model for absorption double-effect cycle parallel flow. But these models are quite complicated and too detailed for the purpose of this work. So, it was decided to develop the dynamic model of a chiller by black-box identification techniques.

The chiller used in the plant has an inbuilt regulator which controls the cold water output temperature by manipulating the electric power and input gas flow (when hot water is not present). The nature of the controller present in the chiller was unknown as it was designed by the manufacturer and it's proprietary. Hence, a Closed-loop identification problem of MIMO systems was considered starting from the measurements of the inputs to the chiller. Figure 3.15 depicts the schematic of the chiller system.

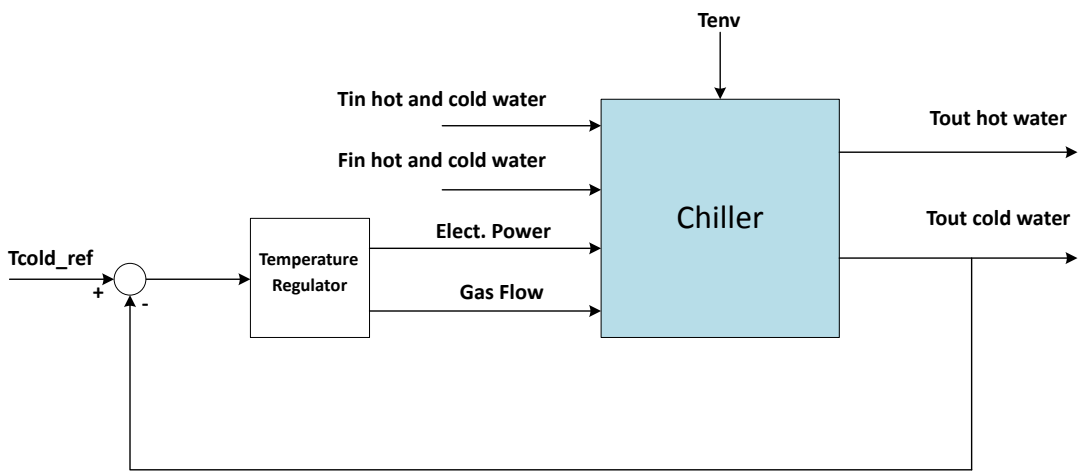

Figure 3.15: The schematic of the closed loop chiller system

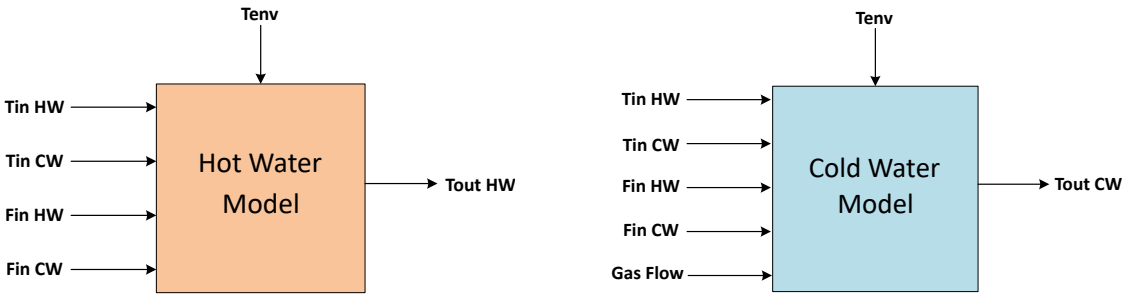

(a) Hot water input-output model (b) Cold water input-output model

Figure 3.16: Chiller black box models

The chiller has two modes of operation, *hot water mode* and *gas mode*. The switching between these modes was solely controlled by the temperature regulator present in the chiller and couldn't be manipulated externally. However, a signal indicating the current mode of operation was available for our disposal. Two seperate models for these modes could have been developed, but the nature of regulator is unknown. Hence, it was decided to develop two separate models for the chiller representing hot water output and cold water output temperature.

As shown in figure 3.16 input-output black-box models for the chiller Hot Water and Cold Water output temperature models are represented. The Hot Water model has inlet temperature and input flow of hot water (Tin/Fin_HW) and cold water (Tin/Fin_CW) as inputs whereas, in case Cold Water model Gas Flow is an additional input. The reason for considering Gas Flow as input to the Cold Water model is that, it can act as a manipulated variable for a simple proportional controller. This proportional controller is nothing but a temperature regulator showed in figure 3.15 which comes into action when the input hot water temperature to the chiller is less than some threshold and regulates the gas flow accordingly. The environment temperature acts as a measured disturbance to both the models. The hot water and cold output temperature are the outputs of Hot water model and Cold Water model respectively. It should be noticed that even though as per figure 3.15, electric power is an input to the chiller, for the electic power model it becomes the output because, to optimize the functionality of a plant electric power, and gas flow must be minimized. A simple linear model of electric power is developed that will be explained in section 3.4.4

3.4.1 Identification of the Chiller system

As the identification of a chiller system has a form of a closed-loop identification problem of MIMO systems , it was necessary to check if it was appropriate to use the existing open loop identification techniques to identify the models. Historically, there has been a substantial interest in both special identification techniques for closed-loop data and for analysis of existing methods when applied to such a data. The fundamental problem with closed-loop data is the correlation between the unmeasured noise and the input. The simple description would be: if the measurement of signals are right at the input-output ports of a plant, it indeed takes care of the effect of change in input at the plant's output. However, the input signal contains

the portion of the past output because of a feedback. This by itself is not a problem. However, you are not only feeding back the previous outputs, but also any disturbances that might have affected those previous output values. It is clear that, whenever the feedback controller is not identically zero, the input and the noise will be correlated. This is the reason why several methods that work in open loop fail when applied to closed-loop data.

In "Closed-loop identification revisited" by Forssell and Ljung (1999) [15] the problem of closed loop identification has been addressed and put some of the new results and method to perspective. The approaches are namely *the direct approach*, *the indirect approach* and *the joint of input-output approach. The direct approach* and the accuracy of estimates calculated by it could be the main advantage in comparison with the joint input-output approach if not for one problem: with an increase of intensity of additive noise, the estimates of the parameter in the denominator of the open-loop system transfer function take the values outside of the stability area of parameters [16]. For the identification of a MIMO system based on closed-loop data collected with a time invariant controller, it is not necessary to excite all reference inputs (in our case the Tcold_ref)[17]. So it was decided to work with inputs as shown in figure 3.16 to proceed with the identification.

After having done a careful survey on this topic, the experiments were conducted on chiller by changing the input flows (hot and cold water). It was difficult to manipulate the input temperatures (hot and cold water) due to limitation of the experimentation on the plant. To compensate this the experimental data collected during these tests were combined with the data of the several other days obtained from the plant during its normal operation and known operating conditions. The data were collected at sampling time of 12 *sec*.

3.4.2 Identification of Hot Water model

For the identification of Hot water chiller experiments were carried by putting chiller on hot water operation mode. The input flows of both hot water and cold water were changed one by one keeping all other inputs at constant value. The system is 5 inputs & 1 output as shown in figure 3.16a.

The training data set used for the identification is shown in figure 3.17. Using the MATLAB System Identification Toolbox, the identification was performed on the training data. Sequentially, the input to output delay was estimated first, then the model order was selected to begin with model estimation. Various models such as transfer function, state-space, polynomial models (ARX, ARMAX, OE, BJ, etc.) were tried on the training data.

The *Discrete-time Output Error* (oe141) had a very good fit of 80.54% as compared to *Discrete-time ARX* (arx240) 77.97% and *Discrete time ARMAX* (amx2221) 72.15% models. Hence, the *Output Error* model was chosen due to its good fitting and simplicity. The *Output Error* models can be described by equation 3.16.

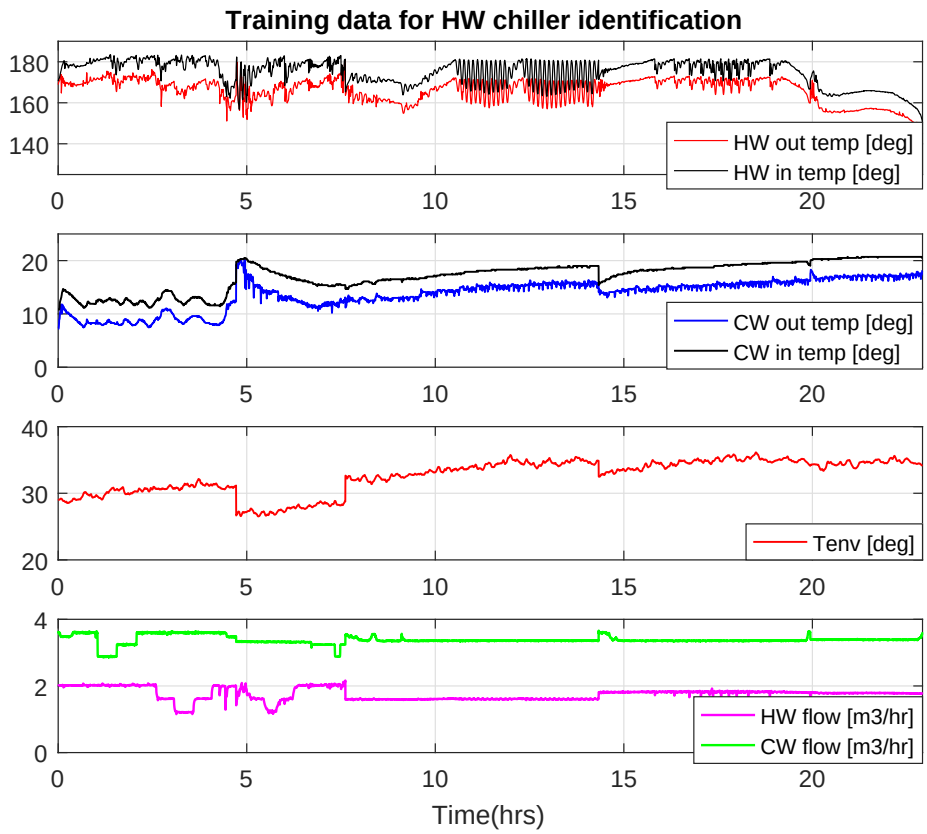

Figure 3.17: Training data set used for the hot water model

$$y(k) = \frac{B(z)}{F(z)}\, u(k-n) + e(k) \tag{3.16}$$

where,

$y(k)$ is the system output

$u(k)$ is the system input

n is the system delay

$e(k)$ is the system disturbance

$B(z) = b_0 + b_1\, z^{-1} + ... + b_{k_b}\, z^{k_b - 1}$

$F(z) = 1 + f_1\, z^{-1} + ... + f_{k_f}\, z^{k_f - 1}$

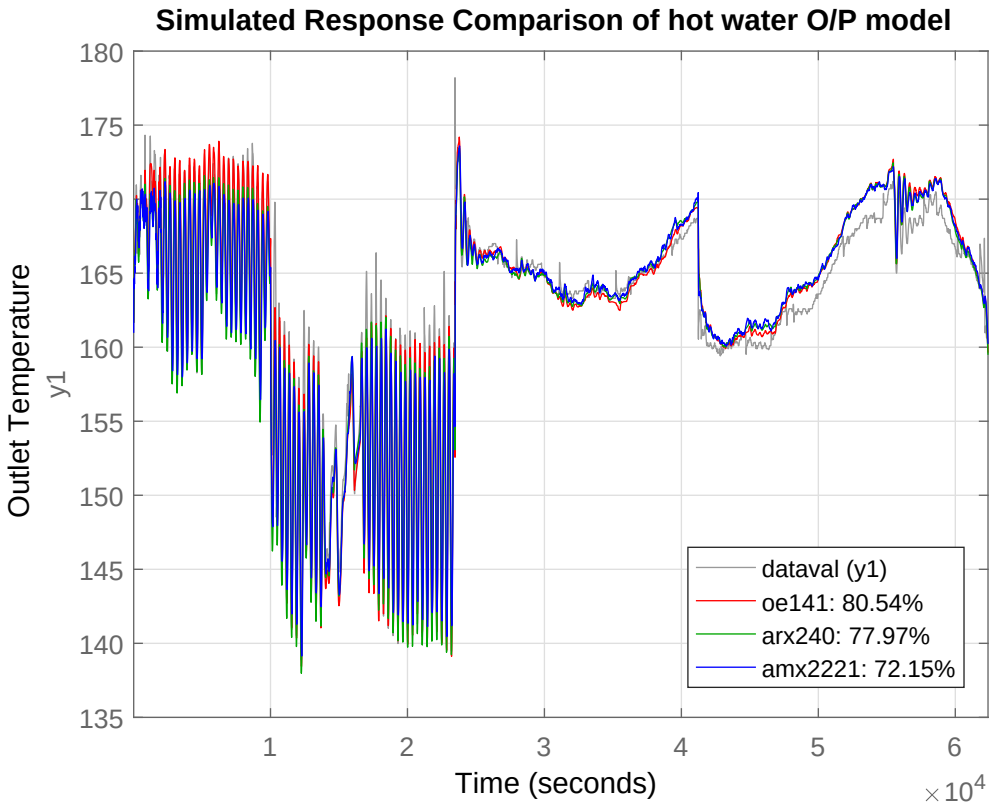

Figure 3.18: Simulated response comparison of different models for hot water out temperature

The chosen Output Error model has the order n_b = [1 1 1 1 1];n_f = [4 4 4 4 4]; n_k = [1 1 1 1 1] for $B(z)$, $F(z)$ and n respectively. The model is defined by following set of polynomials.

$$
\begin{aligned}
B1(z) &= 0.4759z^{-1}; & F1(z) &= 1+0.01051z^{-1}-0.3793z^{-2}-0.2571z^{-3}+0.1341z^{-4};\\
B2(z) &= 0.00146z^{-1}; & F2(z) &= 1-1.483z^{-1}+0.2269z^{-2}+0.7621z^{-3}-0.5006z^{-4};\\
B3(z) &= 0.4024z^{-1}; & F3(z) &= 1-0.233z^{-1}-0.8849z^{-2}-0.2351z^{-3}+0.4236z^{-4};\\
B4(z) &= -0.0004776z^{-1}; & F4(z) &= 1-1.046z^{-1}-0.07912z^{-2}-0.6637z^{-3}+0.8039z^{-4};\\
B5(z) &= -0.001469z^{-1}; & F5(z) &= 1-1.729z^{-1}+1.119z^{-2}-0.9117z^{-3}+0.5217z^{-4};
\end{aligned}
$$

3.4.3 Identification of Cold Water model

The data showed in figure 3.19 was used to identify the Cold Water Output model. Here, the output of the model is cold water temperature. Same procedures were followed as mentioned for Hot Water Output model for identification of this model. Figure 3.20 shows the comparison of different types of models. The best model obtained was *Output error* (oe112) with almost 69 % fit whereas, the *Discret-time state space* (ss1) and *ARX* (arx251) models have fitting of 67.7 % and 66.3 %. Here, the *Discret-time state space* model was chosen as it is two state model and the difference in fitting from *Output error* is not much.

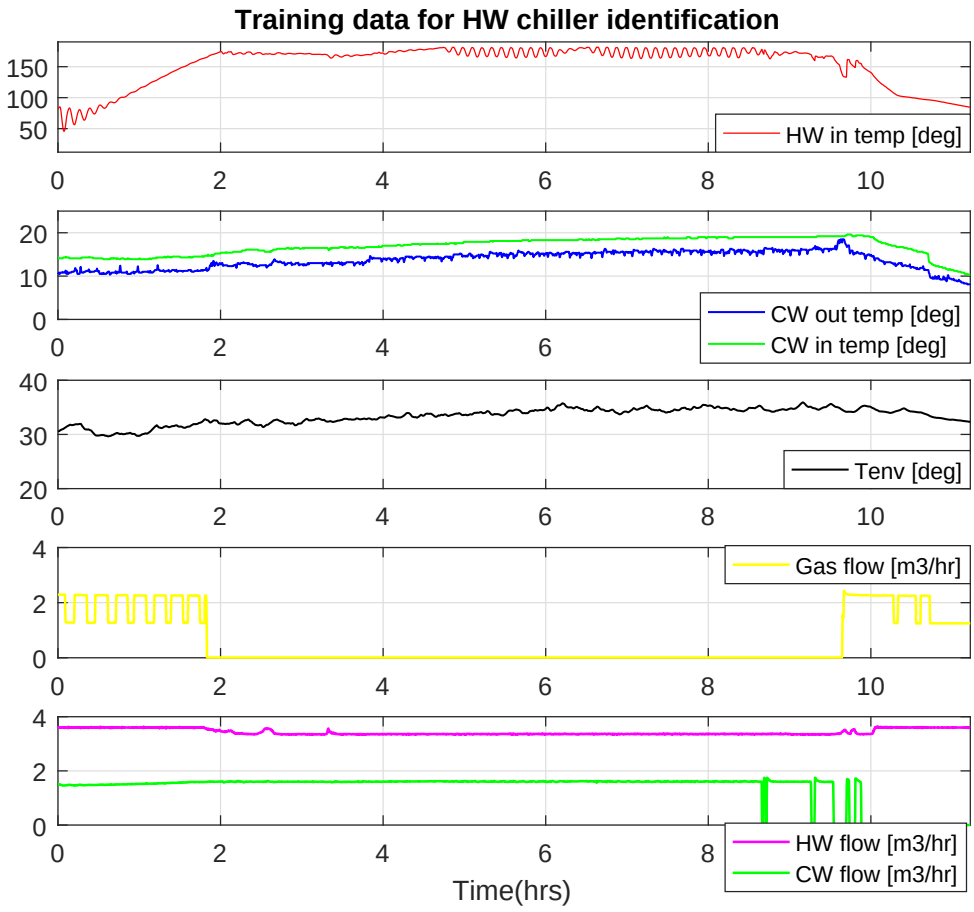

Figure 3.19: Training data set used for cold water model

The State-space model can be given by equation,

$$x(k+1) = Ax(k) + Bu(k) \tag{3.17}$$

$$y(k) = Cx(k) + Du(k)$$

where,

$$A = \begin{bmatrix} 0.9105 & 0.2802 \\ -0.02279 & 0.9121 \end{bmatrix}; B = \begin{bmatrix} 0.005802 & -0.0006591 & -0.002337 \\ -0.0001707 & 0.0002636 & 1.123e-05 \end{bmatrix}$$

$$C = \begin{bmatrix} 27.52 & 2.7 \end{bmatrix}; D = \begin{bmatrix} 0 & 0 & 0 & 0 & 0 & 0 \end{bmatrix}$$

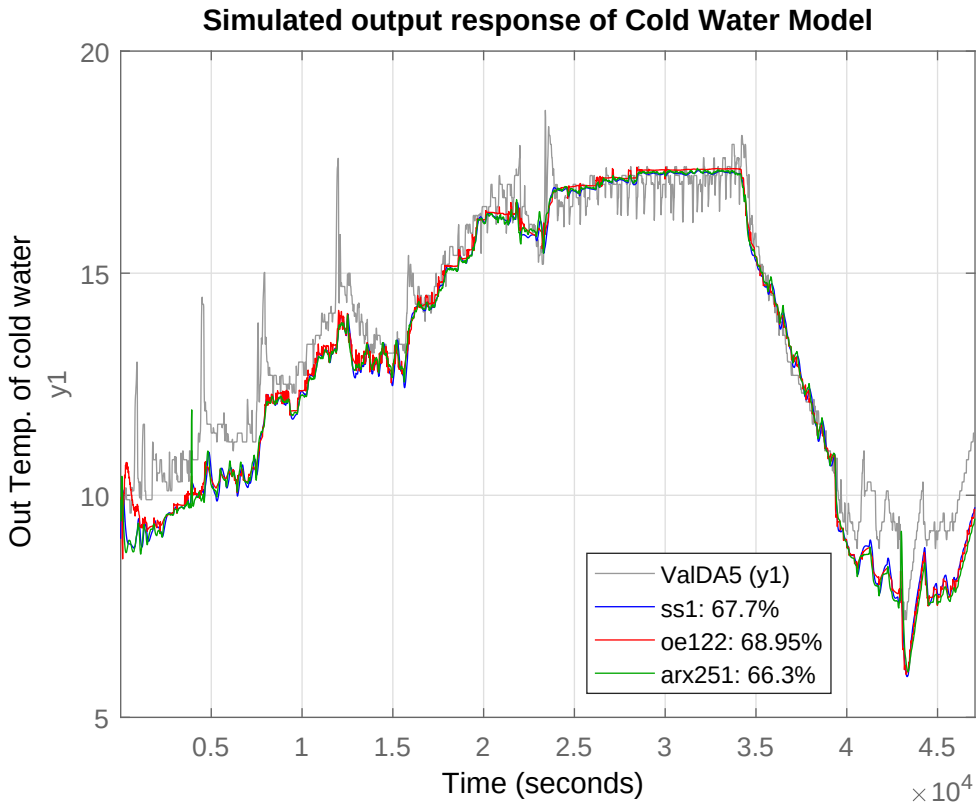

Figure 3.20: Simulated response comparison of different models for cold water out temperature

3.4.4 Electric power output model

The chiller consumes electricity during its operation in both hot water and gas mode. For modelling the electric power of the chiller instead of using the identification techniques, it could be expressed as a function of hot water power, refrigeration power and gas consumption during its operation. The simplest way is to make the relationship linear.

$$E_{power} = m\left(|\dot{Q}_{ref}| + |\dot{Q}_{gas}| + |\dot{Q}_{hw}|\right) + c \tag{3.18}$$

where, E_{power} is an electric power consumption of the chiller during its operations. The $\dot{Q}_{ref}$, $\dot{Q}_{gas}$ and $\dot{Q}_{hw}$ are the refrigeration power of the chiller, power from gas consumed and power provided by hot water to the chiller, respectively. Parameter m is the slope of a linear fitting and c is an offset. Note that the relationship given by equation 3.18 is provided by RSE and the values of fitting variables m and c were not precisely known. However, minimizing electric power of the chiller is one of the objectives and it can be achieved by minimizing the sum of $\dot{Q}_{ref}, \dot{Q}_{gas}$ and $\dot{Q}_{hw}$. Hence, hence sum of power P_{sum} can be expressed by,

$$P_{sum} = \dot{Q}_{ref} + \dot{Q}_{gas} + \dot{Q}_{hw} \tag{3.19}$$

The model based on equation 3.19 was developed. The refrigeration power, gas power and hot water power can be calculated using the following equations.

$$\begin{aligned} \dot{Q}_{ref} &= q_c \cdot c_l \cdot (T_{cw}^{in} - T_{cw}^{out}) \\ \dot{Q}_{gas} &= q_g \cdot PCI \\ \dot{Q}_{hw} &= q_t \cdot c_l \cdot (T_{hw}^{in} - T_{hw}^{out}) \end{aligned} \tag{3.20}$$

where, q_c, q_g and q_t are the cold water flow, gas flow and hot water flow; T_{cw}^{in} and T_{cw}^{out} are the cold water input and output temperature of the chiller; T_{hw}^{in} and T_{hw}^{out} are the hot water input and output temperature of the chiller respectively. PCI is a gross heat of combustion of a natural gas and it is reported as $36\,MJ/Nm3$ for a $1\,m^3$.

3.5 Pump model

The pumps used in the system are variable speed type and can be modelled as a linear gain. P_{ctrl} is the binary signal to ON/OFF the pump whereas F_{pin} is the input flow to the pump that can be manipulated from $0 - 100\%$.

$$F_{pout} = F_{pin} \cdot P_{ctrl} \tag{3.21}$$

The relationship between the pump flow and its electric power consumption for hot water pump can be given by,

$$P_{pump} = \frac{150}{3600} \cdot q_t \tag{3.22}$$

The objective of optimal controller will also consider to minimize the electric power consumed by the hot water pump during its operation.

3.6 User Model

The power consumption from the user had to be modelled to complete the simulator of the solar cooling plant. As shown in figure 3.21, the input flow to the user after point A is controlled by a PID controller acting on a valve CV302 as per the user requirement. Hence, it was reasonable to identify the model of output temperature T^B of a user as a function of the input temperature T^A and the power demand by user. Notice that the cold water flow after point A is not considered as the input to this model because the measurement of this flow is unavailable.

The power demand by the user is defined by the equation which is a function of the radiation and environment temperature. This relationship was provided by RSE and was the exact model used in the plant for defining the power demand [W] from user and can be written as,

$$Q_{usr} = I(t) \cdot 8 + \{[max(T_a(t), 22)] - 22\} \cdot 1000 \tag{3.23}$$

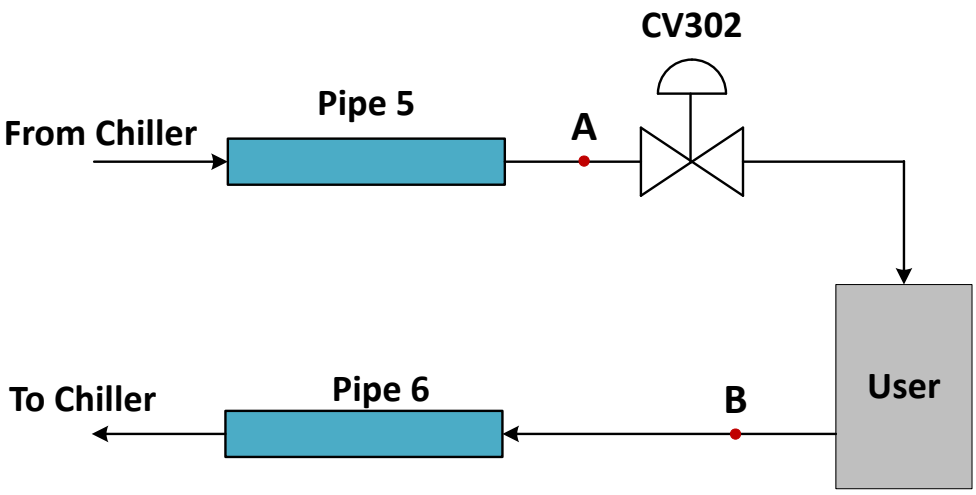

Figure 3.21: User model explanation

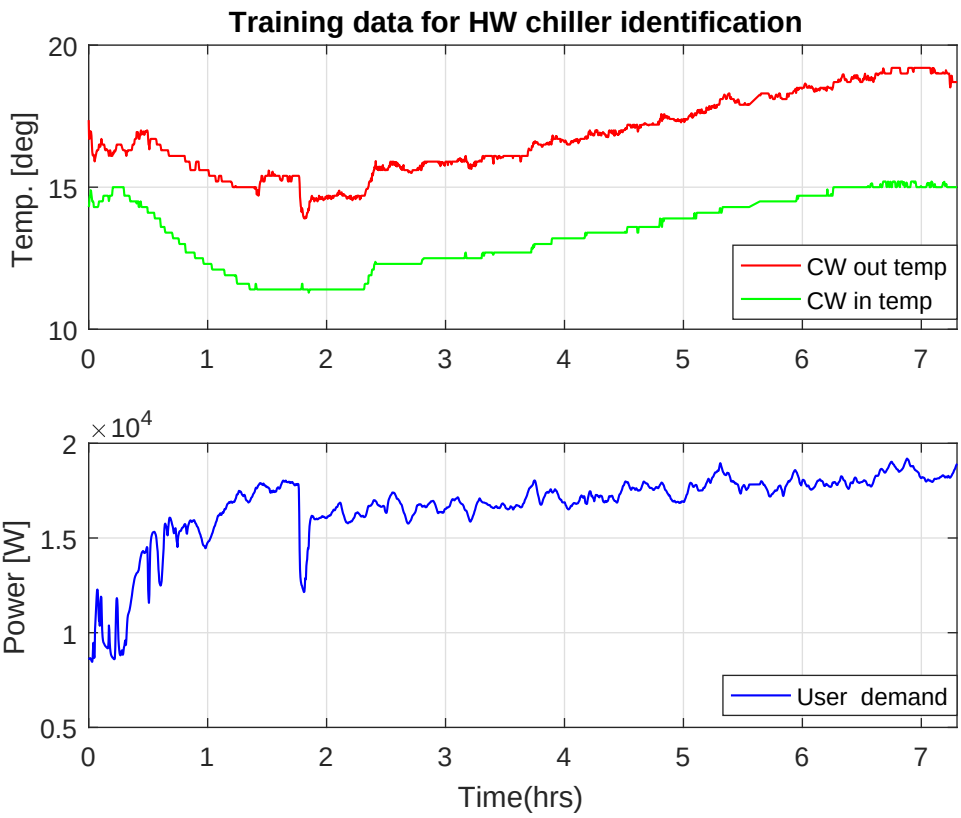

Figure 3.22: User training data set

The training data set for the identification of the User model can be seen in figure 3.22. The training data set consists of the input cold water temperature and user power demand that serve as inputs to the model. The output cold water temperature of the User present in this data set is regarded to be the output of the model.

Figure 3.23 shows the validation of the identified models. The identified model are the *Discret-time state space* (ssUsr) and *Discret-time transfer function* (tfUsr) with fitting of 91 % and 84 % respectively. The obvious choice was the state space

model as it is a two state model with better fitting. The model is governed by equation 3.17 and the matrices for this model can be given by,

$$A_u = \begin{bmatrix} 0.9353 & 0.2722 \\ 0.0517 & 0.1274 \end{bmatrix}; B_u = \begin{bmatrix} 0.03665 & 1.186e-05 \\ -0.09991 & -3.316e-05 \end{bmatrix}$$

$$C_u = \begin{bmatrix} 8.28 & 0.0102 \end{bmatrix}; D_u = \begin{bmatrix} 0 & 0 \end{bmatrix}$$

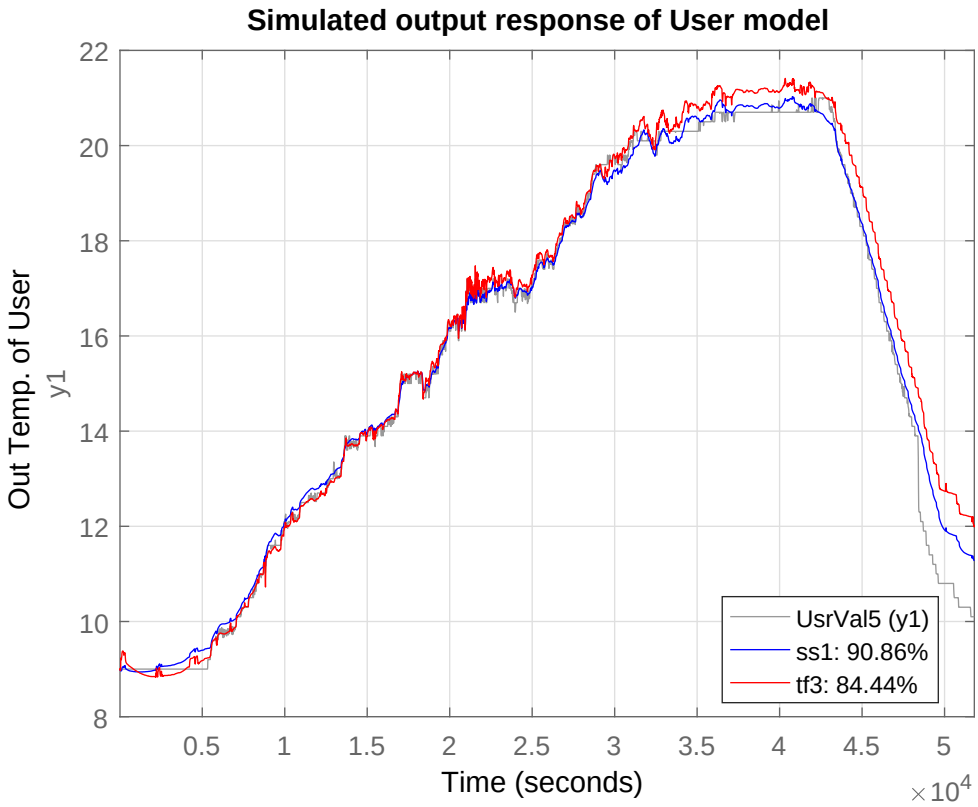

Figure 3.23: User training data

3.7 Simulator of the Solar cooling plant

After the development and implementation of individual components of the solar cooling plant, they were coupled together to build a simulator for the whole plant. Figure 3.24 represents this simulator and the connection between the individual components of the plant. The *Solar collector* exposed to the solar radiation is fed with water by *pipe 3*. The output hot water either goes to *Hot storage* or *pipe 2* depending on the actuation of bypass valve CV002 through *pipe 1*. CV002 is an ON/OFF valve and if it's ON then, it sends hot water to *Hot storage* otherwise passes it to *pipe 2*. The hot water from *pipe 2* further goes to *Chiller* which uses this hot fluid to produce the refrigeration and outputs the hot water with lower temperature than input hot water temperature. This hot water is then fed back again to solar collector through *pipe 3* and the process repeats.

The cold water that is an input to the *Chiller* from *pipe 6* is cooled utilizing the hot water and sent to *Cold storage* or *pipe 5* through *pipe 4* depending on the actuation of valve CV301 which works similar to CV002. The cold water is then utilized by the *User* that consumes the refrigeration power from cold water and returns the cold water to *Chiller* again for cooling through *pipe 6*.

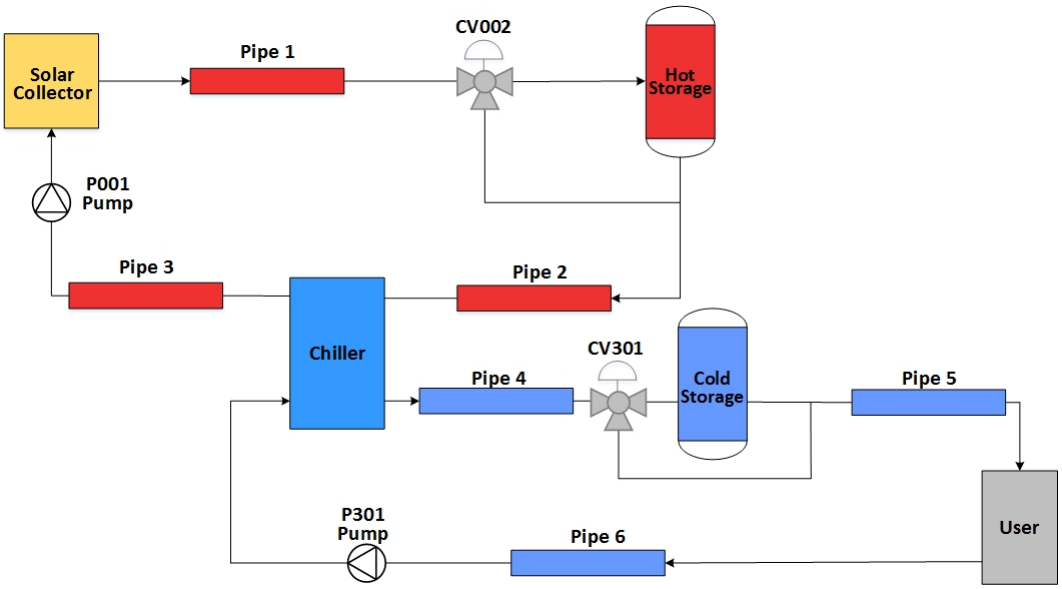

Figure 3.24: Solar Cooling system simulator schematic implemented in simulink

3.7.1 Simulation results

The big simulator built in Simulink is represented as an input-output sub-system. The sub-system created in Simulink for the solar plant looks similar to figure 3.25. To validate the model, the data from the plant was used to impose the inputs to the simulator and the output obtained from it was compared to real data. For instance, 1st July of 2016 was a sunny day since the solar radiation was mostly higher than $850\,W/m^2$ as shown in figure 3.26. The user demand and the environment temperature rise during the day, whereas the radiation starts increasing in the morning

and stays constant till the operation period of plant. Note that the hot and cold storages were bypassed during the operation of the plant for the whole day. The plant operated on gas in the morning while, the hot water in the hot water circuit was being heated. After the hot water input to the chiller reached above $165°C$, the chiller was switched to the hot water mode until the end of the day.

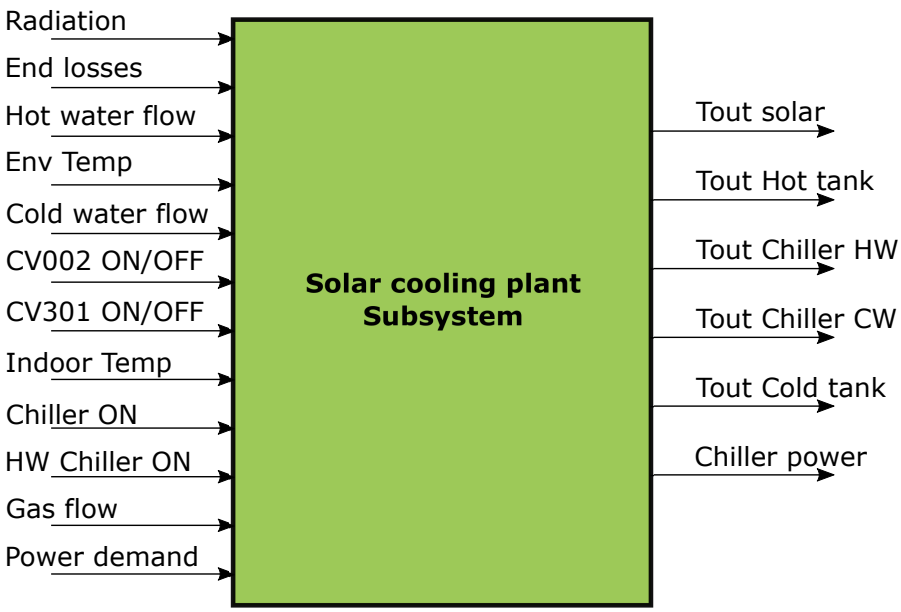

Figure 3.25: Solar Cooling system subsystem in simulink

Figure 3.27 shows the hot water input-output temperature of the solar collector from the simulator and the real data. As it is possible to see for first 2.5 hours, when the hot water is being heated, the estimation by the simulator goes really high. This is because, in the real plant even when the hot water is being heated it passes through chiller and loses some of the heat to chiller. The existing model of chiller is not modelled on such operating condition data; hence it doesn't take care of such loss which results in increment of the temerature of the hot water. As the operation of optimal controller would focus on steady state operation, it was not required to build a model that considers this loss. As far as the steady state part is concerned, the model produces similar trend to real data.

The hot water temperature input-output temperature of chiller from the simulator and real data can be seen in figure 3.28. As explained for solar collector validation plot 3.27, the chiller output also shows the rise at the 2.5 hours, whereas for steady state it follows the trend of real data.

The cold water validation is represented in figure 3.29. As per the plot, the model follows the trend of real data. The fitting may not seem satisfactory but the difference between the input-output temperature of the real data and model seems to be almost the same. It means that the energy balance over some period would be the same.

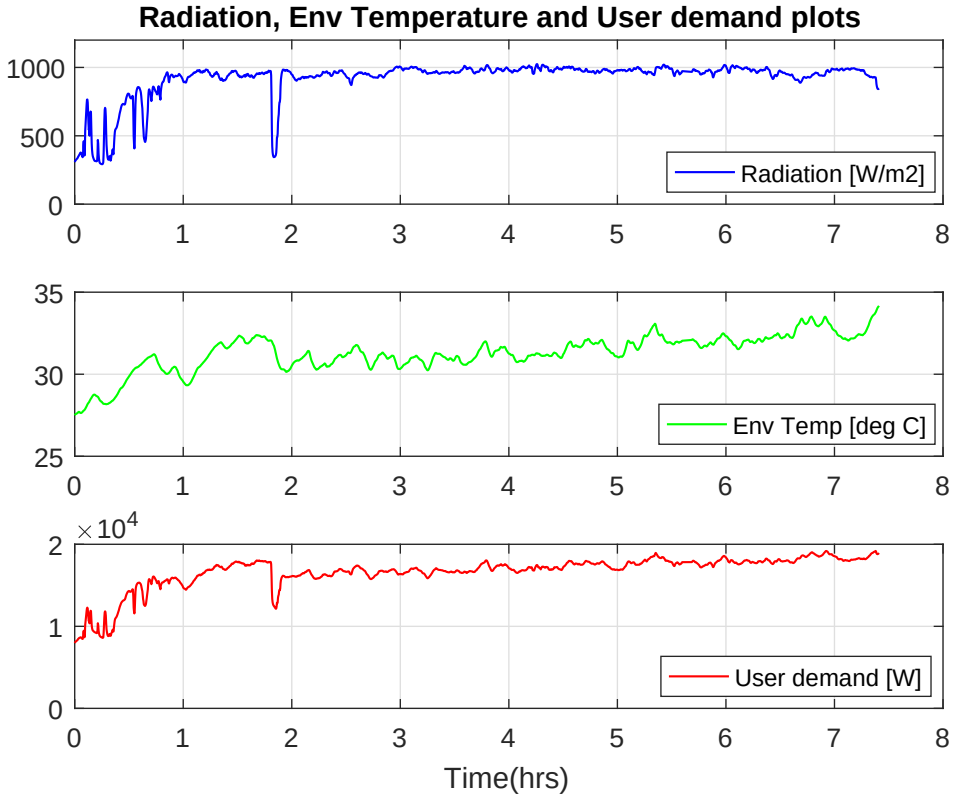

Figure 3.26: Solar collector validation (In Solar Plant Simulator)

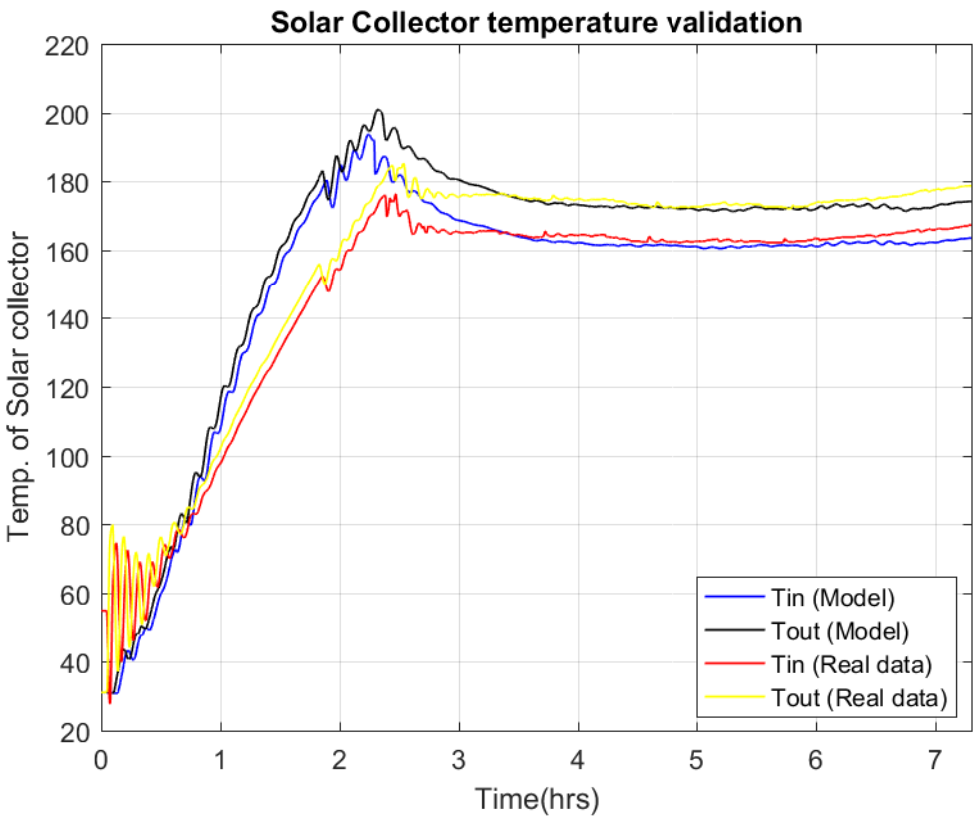

Figure 3.27: Solar collector validation (In Solar Plant Simulator)

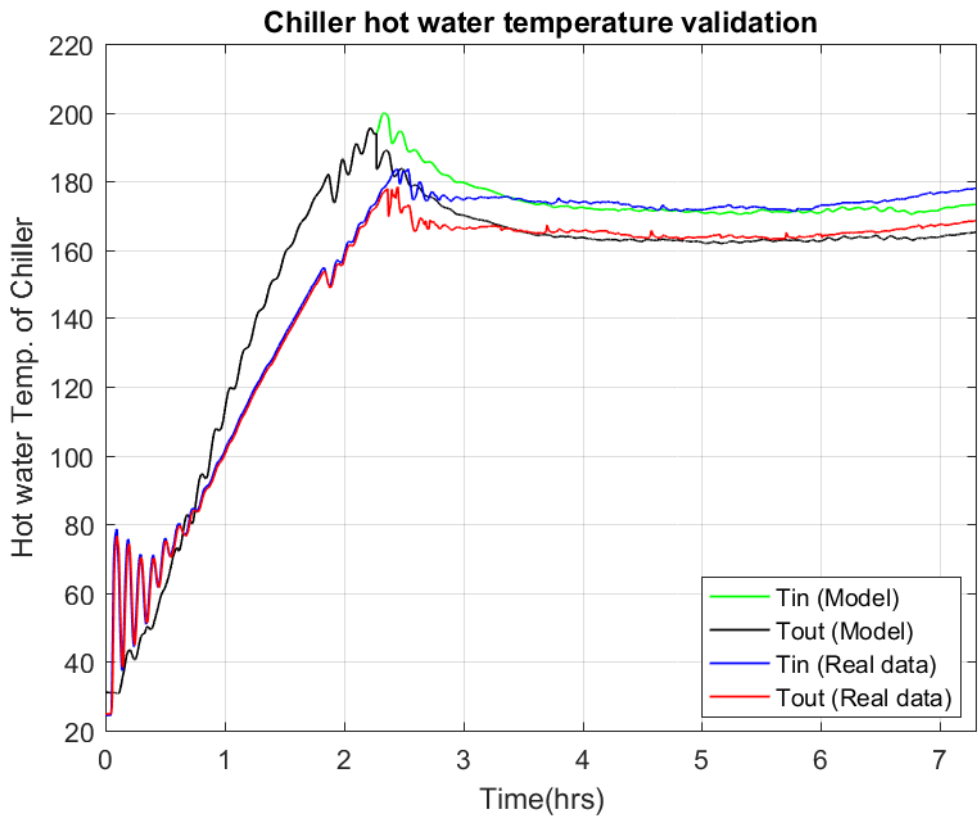

Figure 3.28: Chiller hot water temperature validation (In Solar Plant Simulator)

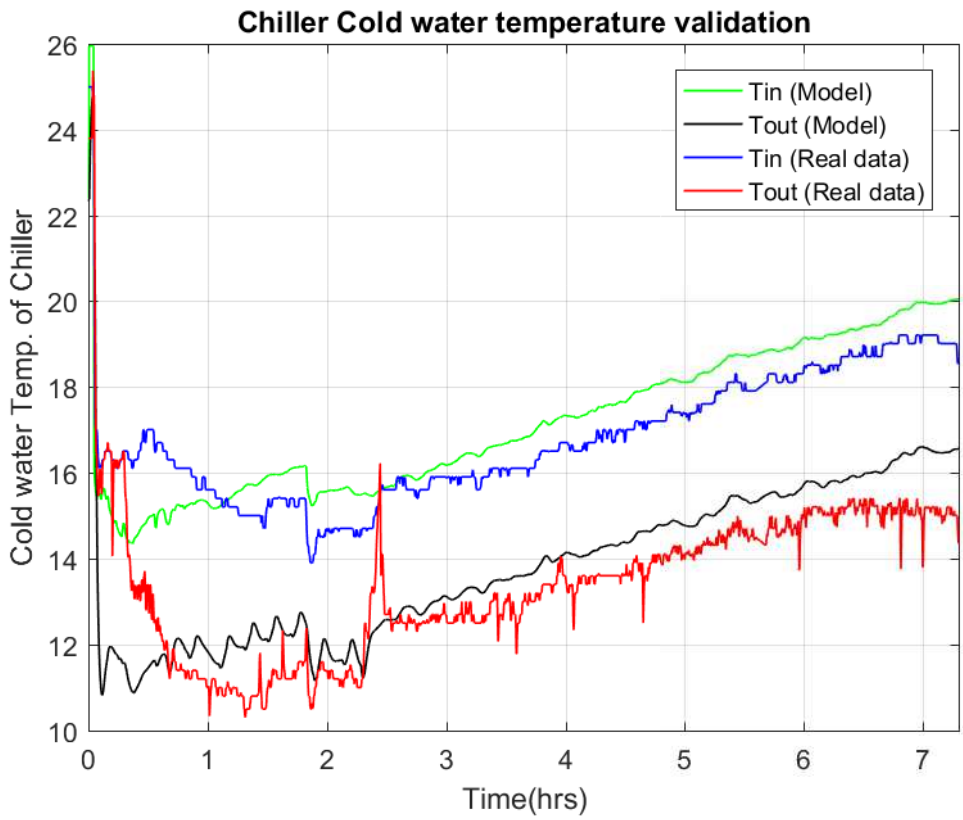

Figure 3.29: Chiller cold water temperature validation (In Solar Plant Simulator)

The power sum P_{sum} model validation can be seen in first plot of figure 3.30. The readings from the plant are quite oscillating. The power sum model is a simple linear model hence, it might not be able to reproduce all the oscillations but tracks the real data satisfactorily. As the electric power had to be optimized over some period, the instantaneous prediction didn't have to be accurate but the energy consumption over some period should match real data. In the second plot of figure 3.30 it can be seen that the total energy of a simulator is almost equivalent to real data.

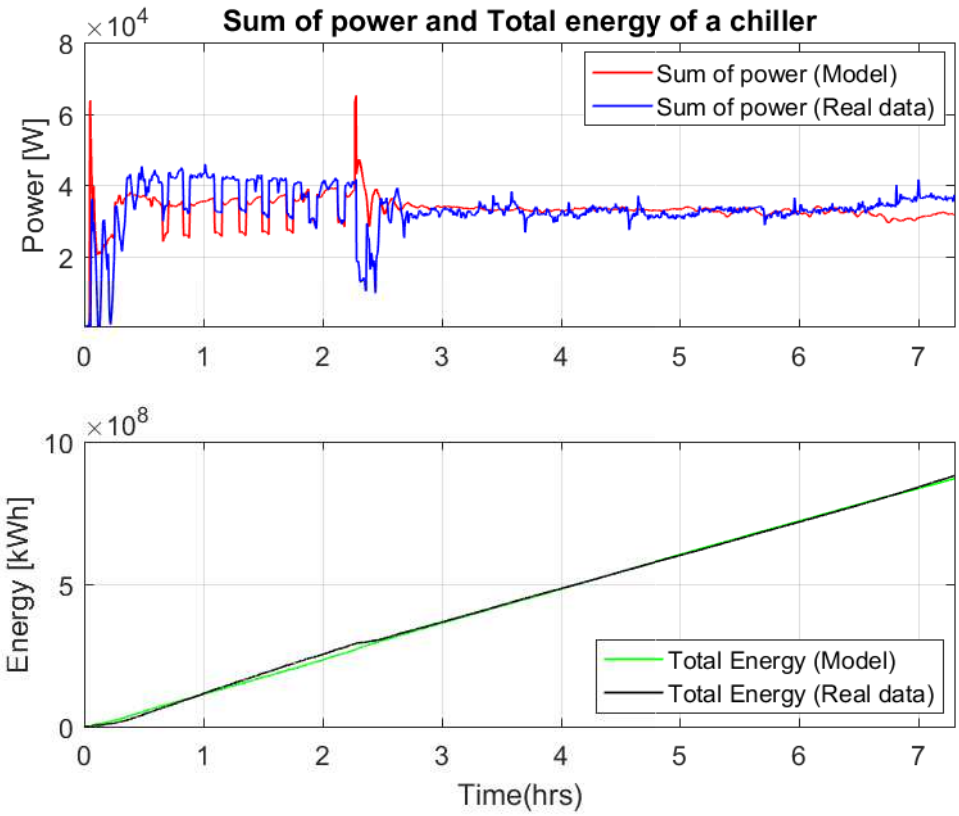

Figure 3.30: Electric power of a chiller validation (In Solar Plant Simulator)

3.8 Summary

In this chapter, the models for the equipment of the plant are developed, implemented and validated. From these models the simulator of a Solar cooling plant had been built and tested against the data gathered from real plant. The behaviour of the model is satisfactory, although some additional efforts could be put in for its further evaluation to make it more similar to the real system. In any case, the models developed in this chapter will be used in upcoming chapters to design the optimal control for the Solar cooling plant.

Chapter 4

Optimal Control in a fixed configuration of the plant

This chapter describes one of the control architecture adopted for the optimal control of the plant. Since last few decades, it has been typical to a use two layered architecture for process industry, when the cost related to the economic objective function must be minimized. The economic cost can be related to energy efficiency, time required for the process, etc. Two different case studies will be developed to check this strategy, the *fixed system configuration* and *changing configuration* (Hybrid model). The current chapter demonstrates the developement of the control for *fixed system configuration.*

4.1 Fixed configuration of the plant

In the fixed configuration of the plant, the hot storage and cold storage are excluded from the hot water and cold water circuits respectively. The hot water from the solar collector goes to the chiller and is fed back to the collector after it has been used by the chiller. The hot water flow acts as a manipulated variable for the control system to optimize the electric power consumption by the plant by reducing the electric power consumption by the chiller and the pump. In the same way, the cold water goes from the chiller to the user and after usage, it is sent back to the chiller for cooling again. In this configuration, the chiller is supposed to work always in hot water mode. Figure 4.1 shows the sketch of this configuration.

4.2 Control architecture

The control architecture that has been adopted for the plant is depicted in figure 4.2. It is a two-layer architecture which optimally controls the plant through a *fixed system configuration.* The Real Time Optimizer (RTO) acts as an upper layer which defines the optimal operating conditions for the plant, considering the disturbances forecast; then a faster MPC is used to maintain these optimal operating conditions. The MPC is based on the linearized reduced order model of the plant.

The practice of implementing real-time optimization (RTO) using a rigorous steady-state model, in conjunction with model predictive control (MPC), dates back to the

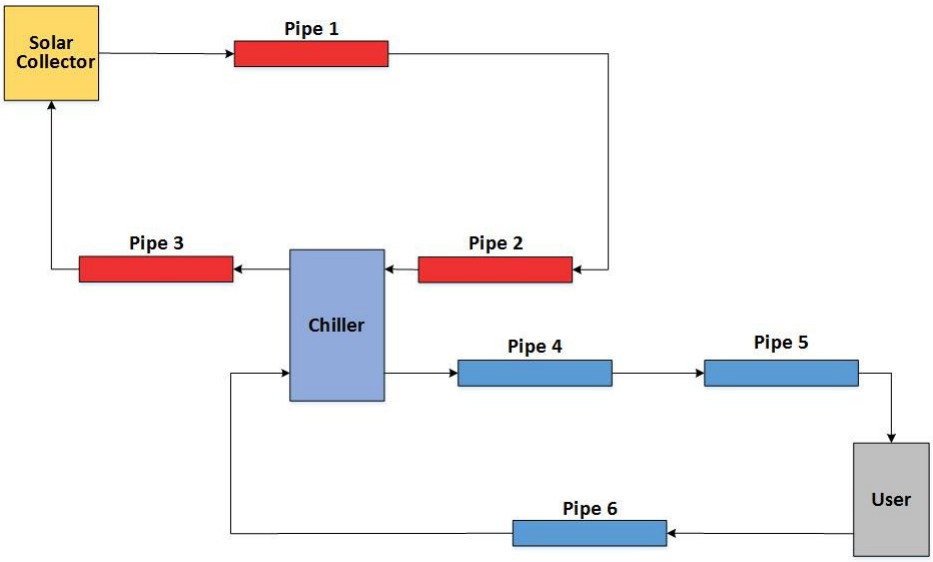

Figure 4.1: Simulink simulator for solar collector

late 1980s [18]. Since then, numerous projects have been implemented in refinery and chemical plants, and RTO has received significant attention in the industrial and academic literature. RTO deals with methods of maximizing an economic objective related to the operation of a continuous process. Economic optimization studies for oil refining and chemicals production systems have proven to be very beneficial and the resulting tools and algorithms have been accepted by the industry [19].

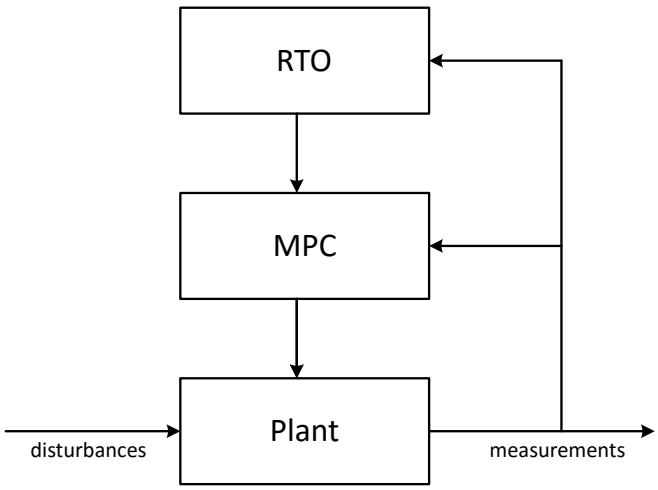

Figure 4.2: Control structure for the fixed configuration of the plant

Most RTO systems are based on rigorous non-linear steady state models of the process system, combined with data reconciliation or parameter estimation to update key-parameters, such as feed compositions and efficiencies. Rigorous modeling implies the use of multi-component mass and energy balances, vapor–liquid equilibrium expressions, and reaction kinetics; however, some amount of empirical approaches may be required to describe some effects that are not easily modeled, such as hydraulic effects or reaction kinetics. Typically, the RTO application optimizes the process operating conditions and updates the set-points to local MPCs, which are based on linear dynamic models.

An advantage of the two-layer implementation over a single one is that it can better respond to disturbances and maintain the feasibility between RTO executions. The typical RTO formulation based on linear models can be given as [18],

$$\begin{aligned} \min_{y^{TG} u^{TG}} & C_y^T\, y^{TG} + C_u^T\, u^{TG} \\ y^{TG} &= G_{ss}\, u^{TG} + b \\ y^{min} \leq & \; y^{TG} \leq y^{max} \end{aligned} \tag{4.1}$$

where, C_y and C_u are the costs associated with the outputs and inputs (controller manipulated variables), respectively; y^{TG} and u^{TG} are the optimal targets for the outputs and inputs, respectively; superscripts min and max refer to the constraint limits for the inputs and outputs; G_{ss} is the steady-state gain matrix obtained from the MPC dynamic model; and b is the steady-state model bias term, which is updated based on current output measurements and predictions from the dynamic model. Constraint priorities are handled either through the addition of soft penalty terms or by solving a sequence of Linear Programs. Minimum and maximum limits are set equal to create setpoints, which then become constraints in equation 4.1. Relatively low weights or priorities are used on these setpoints to avoid potential conflict with higher priority specifications and constraints.

4.3 Static model of the plant

The RTO works on the static models, hence it was required to develop these models from the dynamic model of a system obtained in chapter 3. This section addresses the development of the static models for each equipment of the plant which will then constitute to build a static model of the whole plant.

4.3.1 Static model of a solar collector

The dynamic model of the solar collector is governed by the equation 3.5 derived in section 3.1. Letting,

$$\tau_m = \frac{\rho_m c_m A_m}{D_i \pi H_t}, \beta_1 = \frac{\eta_0 G \eta_{end}}{D_i \pi H_t}, \beta_2 = \frac{H_1}{D_i \pi H_t}, \tau_{s_1} = \frac{\rho_f c_f A_f}{D_i \pi H_t}, \tau_{s_2} = \frac{\rho_f c_f}{D_i \pi H_t}$$

in equation 3.5, it can be reformulated as,

$$\begin{cases} \tau_m \dfrac{\partial T_m}{\partial t}(t,x) = \beta_1 I(t) - \beta_2 (T_m(t,x) - T_a(t)) - (T_m(t,x) - T_f(t,x)) \\ \tau_{s_1} \dfrac{\partial T_f}{\partial t}(t,x) + \tau_{s_2} q(t) \dfrac{\partial T_f}{\partial x}(t,x) = T_m(t,x) - T_f(t,x) \end{cases} \tag{4.2}$$

In the steady state, for constant inputs and disturbances $\bar{T}_{f_0}, \bar{q}, \bar{I}, \bar{T}_a$, setting all the derivatives to zero, $\frac{\partial(\cdot)}{\partial t} = 0$ and letting $\frac{\partial T_f}{\partial x} = \frac{T_f - T_{f_0}}{\partial x}$ the previous equation becomes,

$$\begin{cases} \beta_1 \bar{I} - \beta_2 (\bar{T}_m - \bar{T}_a) - \bar{T}_m + \bar{T}_f = 0 \\ \tau_{s_2}\, \bar{q}\, \dfrac{1}{\partial x} (\bar{T}_f - \bar{T}_{f_0}) = \bar{T}_m - \bar{T}_f \end{cases} \tag{4.3}$$

Further,

$$\begin{cases} (1+\beta_2)\,\bar{T}_m = \beta_1 \bar{I} + \beta_2 \bar{T}_a + \bar{T}_f \\ \dfrac{\tau_{s_2}\bar{q}}{\partial x}\,\bar{T}_f = \dfrac{\tau_{s_2}\bar{q}}{\partial x}\,\bar{T}_{f_0} + \bar{T}_m \end{cases} \tag{4.4}$$

Finally, substituting the value of $\bar{T}_m$ from the first equation of 4.4 in the second equation and rearranging the terms we get,

$$\left[\frac{\tau_{s_2}\bar{q}}{\partial x} + 1 - \frac{1}{1+\beta_2}\right]\bar{T}_f = \frac{\tau_{s_2}\bar{q}}{\partial x}\,\bar{T}_{f_0} + \frac{\beta_1}{1+\beta_2}\bar{I} + \frac{\beta_2}{1+\beta_2}\bar{T}_a \tag{4.5}$$

Alternatively it can be written as,

$$\bar{T}_f = \gamma_{s_1}(\bar{q})\,\bar{T}_{f_0} + \gamma_{s_2}(\bar{q})\,\bar{I} + \gamma_{s_3}(\bar{q})\,\bar{T}_a \tag{4.6}$$

where,

$$\gamma_{s_1}(\bar{q}) = \frac{\frac{\tau_{s_2}\bar{q}}{\partial x}}{\left[\frac{\tau_{s_2}\bar{q}}{\partial x} + 1 - \frac{1}{1+\beta_2}\right]}, \gamma_{s_2}(\bar{q}) = \frac{\frac{\beta_1}{1+\beta_2}}{\left[\frac{\tau_{s_2}\bar{q}}{\partial x} + 1 - \frac{1}{1+\beta_2}\right]}, \gamma_{s_3}(\bar{q}) = \frac{\frac{\beta_2}{1+\beta_2}}{\left[\frac{\tau_{s_2}\bar{q}}{\partial x} + 1 - \frac{1}{1+\beta_2}\right]}$$

It is clear from equation 4.6 that, $\gamma_{s_1}, \gamma_{s_2}$ and γ_{s_3} depend on $\bar{q}$ and the higher the flow of the fluid, the lower the gain from $\bar{I}, \bar{T}_a$ and $\bar{T}_s$. This equation represents the relationship for the output of solar collector as a single element with all the constant inputs and disturbances. The solar collector is modelled as a distributed parameter system, hence it can be expressed by the set of equations,

$$\begin{cases} \bar{T}_{f_1} = \gamma_{s_1}(\bar{q})\,\bar{T}_{f_0} + \gamma_{s_2}(\bar{q})\,\bar{I} + \gamma_{s_3}(\bar{q})\,\bar{T}_a \\ \bar{T}_{f_2} = \gamma_{s_1}(\bar{q})\,\bar{T}_{f_1} + \gamma_{s_2}(\bar{q})\,\bar{I} + \gamma_{s_3}(\bar{q})\,\bar{T}_a \\ \vdots \\ \bar{T}_{f_N} = \gamma_{s_1}(\bar{q})\,\bar{T}_{f_{N-1}} + \gamma_{s_2}(\bar{q})\,\bar{I} + \gamma_{s_3}(\bar{q})\,\bar{T}_a \end{cases} \tag{4.7}$$

For instance, $\bar{T}_{f_1}$ is the output temperature of the first element of the collector and it has input temperature $\bar{T}_{f_0}$. The $\bar{T}_{f_1}$ then serves as the input temperature to next piece and the process repeats for all the pieces. The $\bar{T}_{f_N}$ is regarded as the output temperature of the solar collector.

4.3.2 Static model of a tank

The dynamic model of a tank is described by equation 3.13. This equation can be used to derive the following static model of a tank.

$$c_f\,\bar{q}\,(\bar{T}_{in} - \bar{T}_t) - H_{tank}\,A_{ext}\,(\bar{T}_t - \bar{T}_a) = 0 \tag{4.8}$$

After rearranging the terms we get the static equation for the tank output temperature,

$$\bar{T}_t = \left[\frac{c_f\bar{q}}{c_f\bar{q} + H_{tank}A_{ext}}\right]\bar{T}_{in} + \left[\frac{H_{tank}A_{ext}}{c_f\bar{q} + H_{tank}A_{ext}}\right]\bar{T}_a \tag{4.9}$$

The equation can also be written as,

$$\bar{T}_t = \gamma_{t_1}(\bar{q})\,\bar{T}_{in} + \gamma_{t_2}(\bar{q})\,\bar{T}_a \tag{4.10}$$

This equation represents the output temerature of the tank in steady state. The same static model of the tank can be used for hot and cold storages with appropriate parameter concerning the dimension and heat loss coefficient.

4.3.3 Static model of a pipe

The pipe dynamic model given by equation 3.15 can be exploited to derive the static model of the pipe. At steady state the equation becomes,

$$\rho_f c_f \bar{q}\,\frac{\bar{T}_{pf} - \bar{T}_{pf_0}}{\partial x} + \pi D_{ip} H_p (\bar{T}_{pf} - \bar{T}_a) = 0 \tag{4.11}$$

let,

$$\beta_p = \frac{\rho_f c_f \bar{q}}{\pi D_{ip} H_p\,\partial x}$$

The equation 4.11 becomes,

$$(1+\beta_p)\,\bar{T}_{pf} - \beta_p\,\bar{T}_{pf_0} - \bar{T}_a = 0 \tag{4.12}$$

Further,

$$\bar{T}_{pf} = \frac{\beta_p}{(1+\beta_p)}\,\bar{T}_{pf_0} + \frac{1}{(1+\beta_p)}\,\bar{T}_a \tag{4.13}$$

The equation can be expressed in the form of $\gamma_{p_1}(\bar{q})$ and $\gamma_{p_2}(\bar{q})$,

$$\bar{T}_{pf} = \gamma_{p_1}(\bar{q})\,\bar{T}_{pf_0} + \gamma_{p_2}(\bar{q})\,\bar{T}_a \tag{4.14}$$

where,

$$\gamma_{p_1}(\bar{q}) = \frac{\beta_p}{(1+\beta_p)}; \qquad \gamma_{p_2}(\bar{q}) = \frac{1}{(1+\beta_p)}$$

Similar to the model of solar collector, the pipe model can also be expressed as the distributed parameter system.

$$\begin{cases} \bar{T}_{pf_1} = \gamma_{p_1}(\bar{q})\,\bar{T}_{pf_0} + \gamma_{p_2}(\bar{q})\,\bar{T}_a \\ \bar{T}_{pf_2} = \gamma_{p_1}(\bar{q})\,\bar{T}_{pf_1} + \gamma_{p_2}(\bar{q})\,\bar{T}_a \\ \vdots \\ \bar{T}_{pf} = \gamma_{p_N}(\bar{q})\,\bar{T}_{pf_{N-1}} + \gamma_{p_2}(\bar{q})\,\bar{T}_a \end{cases} \tag{4.15}$$

Note that, for the cold water circuit pipes and cold storage tank, the environment temperature T_a is considered to be equal to the indoor temperature T_{indor} as they are located in the building to be conditioned. The same model is applied for the hot water and cold water pipes with corresponding dimensional parameters and heat loss coefficient.

4.3.4 Static models of a chiller

The models for the hot water output temperature, cold water output temperature and Power sum of the chiller are obtained from model identification as explained in section 3.4.1. So the static model for these outputs will simply be equal to the sum of the static gains multiplied by the respective inputs.

$$\begin{cases} \bar{T}_{hw}^{out} = G_{hw_1}\,\bar{T}_{hw}^{in} + G_{hw_2}\,\bar{T}_a + G_{hw_3}\,\bar{q}_t + G_{hw_4}\,\bar{T}_{cw}^{in} + G_{hw_5}\,\bar{q}_c; \\ \bar{T}_{cw}^{out} = G_{cw_1}\,\bar{T}_{cw}^{in} + G_{cw_2}\,\bar{T}_a + G_{cw_3}\,\bar{q}_c + G_{cw_4}\,\bar{T}_{hw}^{in} + G_{cw_5}\,\bar{q}_t + G_{cw_6}\,\bar{q}_g; \\ \bar{P}_{sum} = \dot{Q}_{ref}(\bar{q}_c) + \dot{Q}_{gas}(\bar{q}_g) + \dot{Q}_{hw}(\bar{q}_t) \end{cases} \tag{4.16}$$

where, T_{hw}^{out} and T_{cw}^{out} are the hot and cold water output temperature of the chiller; T_{hw}^{in} and T_{cw}^{in} are the hot and cold water input temperatures to the chiller; q_t,q_c and q_g are the hot water flow, cold water flow and gas flow respectively. T_a is an environment temperature. The static gains and their values can be found in following table

Table 4.1: Gains of chiller models

Symbol	Description	Value
G_{hw_1}	Static gain from hot water input temperature	0.9052
G_{hw_2}	Static gain from environment temperature	0.2628
G_{hw_3}	Static gain from hot water flow	1.62×10^4
G_{hw_4}	Static gain from cold water input temperature	-0.0521
G_{hw_5}	Static gain from cold water flow	-8.71×10^3
G_{cw_1}	Static gain from cold water input temperature	0.8849
G_{cw_2}	Static gain from environment temperature	0.0390
G_{cw_3}	Static gain from cold water flow	-1.40×10^3
G_{cw_4}	Static gain from hot water input temperature	-0.0038
G_{cw_5}	Static gain from hot water flow	-147.63
G_{cw_6}	Static gain from gas flow	-0.3971

4.3.5 Static model of the pump

The static model for the electric power consumption of the hot water pump can be simply written with reference to equation 3.22,

$$\bar{P}_{pump} = \frac{150}{3600} \cdot \bar{q}_t \tag{4.17}$$

4.3.6 Static model of the user

The static model for the user is built from the identified model mentioned in section 3.6. The output temperature of the user model is simply the sum of multiplication gain from the input temperature to the user and the power demand of the user.

$$\bar{T}_{usr}^{out} = G_t\,\bar{T}_{usr}^{in} + G_p\,\bar{P}_{usr} \tag{4.18}$$

where, $G_t = 0.8661$ and $G_p = 3 \times 10^{-4}$ are the static gains from the input temperature T_{usr}^{in} and user demand P_{usr} respectively. T_{usr}^{out} is an output temperature of the user.

4.4 Implementation of the RTO

The static model built in previous section 4.3 had been used to formulate the RTO problem. As mentioned before the hot storage and cold storage tanks were not considered for this scheme. To build the RTO in MATLAB, an inbuild nonlinear programming solver `fmincon` was used. The solver finds the minimum of a problem specified by,

$$\min_x f(x) \text{ such that } \begin{cases} c(x) \leq 0 \\ c_{eq}(x) = 0 \\ A\,x \leq b \\ A_{eq}\,x = b_{eq} \\ lb \leq x \leq ub \end{cases} \tag{4.19}$$

where, b and b_{eq} are vectors, A and A_{eq} are matrices, $c(x)$ and $c_{eq}(x)$ are functions that return vectors, and $f(x)$ is a function that returns a scalar. $f(x)$, $c(x)$, and $c_{eq}(x)$ can be nonlinear functions. x, lb, and ub can be passed as vectors or matrices [20]. The `fmincon` finds the minimum of a problem given an initial solution $x0$ and subject to the linear equalities $A_{eq} * x = b_{eq}$, linear inequalities $A * x \leq b$, nonlinear inequalities $c(x)$ or equalities $c_{eq}(x)$, so that the solution is always in the range $lb \leq x \leq ub$. The function `nonlcon` is used to define the nonlinear constraints for the problem.

```
x = fmincon(fun,x0,A,b,Aeq,beq,lb,ub,nonlcon)
```

The initial state $x0$ is found by solving static linear equations of the whole system defined by equations 4.7, 4.15, 4.16, 4.17, 4.18. Keeping all the inputs and disturbances to the system at the constant values $\bar{q}_t, \bar{q}_c, \bar{q}_g, \bar{I}, \bar{T}_a$ and $\bar{T}_{indor}$, the system can be formulated as a system of linear equation,

$$A_{static} * x_0 = b_{static} \tag{4.20}$$

and can be solved simply as an algebraic linear problem to obtain x_0.

4.4.1 Cost function for the RTO

For implementation of the RTO, the considered cost function is given by,

$$\begin{aligned} \min_x w_1\,x(i)^2 + w_2\,x(j)^2 + w_3\,x(k)^2 \\ c_{eq}(x) = 0 \\ A_{eq}\,x = b_{eq} \\ lb \leq x \leq ub \end{aligned} \tag{4.21}$$

where, $x \in R^n$ is a vector of inputs, states and disturbances of the system. $x(i)$ is the power sum of chiller P_{sum} at position $i \leq n$, $x(j)$ is electric consumption of pump P_{pump} at position $j \leq n$ and $x(k)$ is the difference between the cold water output temperature and setpoint for the cold water temperature $(T_{cw}^{out} - T_{cw}^{set})$ of the chiller at position $k \leq n$ in x such that, $i \neq j \neq k$. $w1$, $w2$ and $w3$ are the weights on $x(i)$, $x(j)$ and $x(k)$.

Constraints

C_{eq} defines the nonlinear equality constraints of the system. These constrains are required to define the nonlinear static equations of the system. For example the equation 4.7 defining the static model of solar collector has the nonlinearity due to the dependency on hot water flow (q_t) in the equation. The model of the hot water pipes and power sum model of the chiller show a similar dependency on q_t. These equations represent the nonlinear equalities of the system.

$A_{eq}\,x = b_{eq}$ defines the equality constraints of the system. The equations defining the static models of the cold water pipes, hot water output and cold water output temperature of the chiller, pump electric power, user and the values of the disturbances are considered as the linear equalities of the system.

The upper and lower bounds on the hot water flow and the hot water output temperature of the solar collector are bounded through appropriate upper and lower bounds.

4.4.2 Validation of RTO

The RTO developed using the cost function and the constraint 4.21 was solved using `fmincon`, by providing appropriate initial conditions $x0$ to the function. The values of the input, disturbances and weights on the decision variable were set as follows,

Table 4.2: Inputs, disturbances and weights given to the RTO

Symbol	Description	Value	Unit
q_t	Hot water flow	5.25×10^4	m^3/s
I	Radiation	970	W/m^2
T_a	Environment temperature	32	$°C$
T_{indor}	Indoor temperature	28	$°C$
Q_{usr}	User demand	1.6	kW
w_1	Normalized weight for $x(i)$	$1000/(3.5 \cdot 10^4)^2$	-
w_2	Normalized weight for $x(j)$	$100/(300)^2$	-
w_3	Normalized weight for $x(k)$	$10/(4)^2$	-

The setpoint was set to $T_{cw}^{set} = 13$ and the bounds were defined for the input flow $3.34 \times 10^4 \leq q_t \leq 5.56 \times 10^{-4}$ and the solar output temperature $T_{sol}^{out} \leq 180$. Using these values and after solving the optimization problem, the RTO gave the optimal value of the input $q_{t_{opt}} = 3.335 \times 10^{-4}\, m^3/s$, that minimizes the terms in the cost function 4.21, respecting the bounds on q_t and T_{sol}^{out}. The values given by RTO was then validated with the simulator of the plant (excluding hot and cold storage) fed with the same values of disturbances but the optimal flow $q_{t_{opt}}$ as input.

The following graphs show the comparison of the values calculated by the RTO and output given by the plant simulator fed with constant disturbances defined in Table 4.2 and $q_{t_{opt}}$. It can be seen from the figures 4.3 and 4.4 the values calculated by the RTO are almost the same as the one given by the simulator. It also worth mentioning that, with the constant inputs to the system, the plant reaches the steady state in 2.5 - 3 hours.

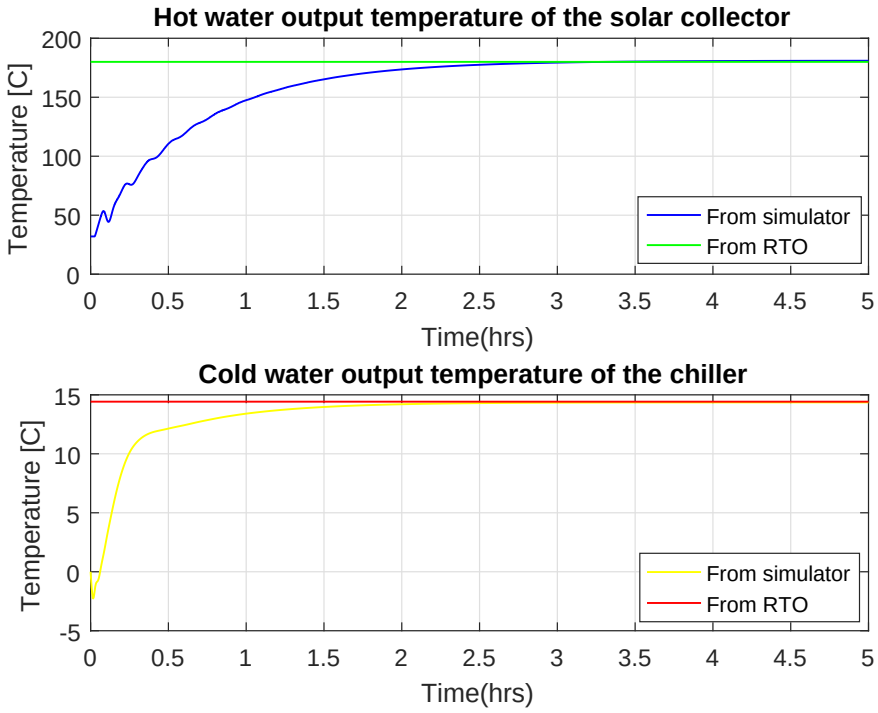

Figure 4.3: Validation of the hot water output temperature of the collector and the cold water output temperature of the chiller calculated by the RTO and the simulator of the plant

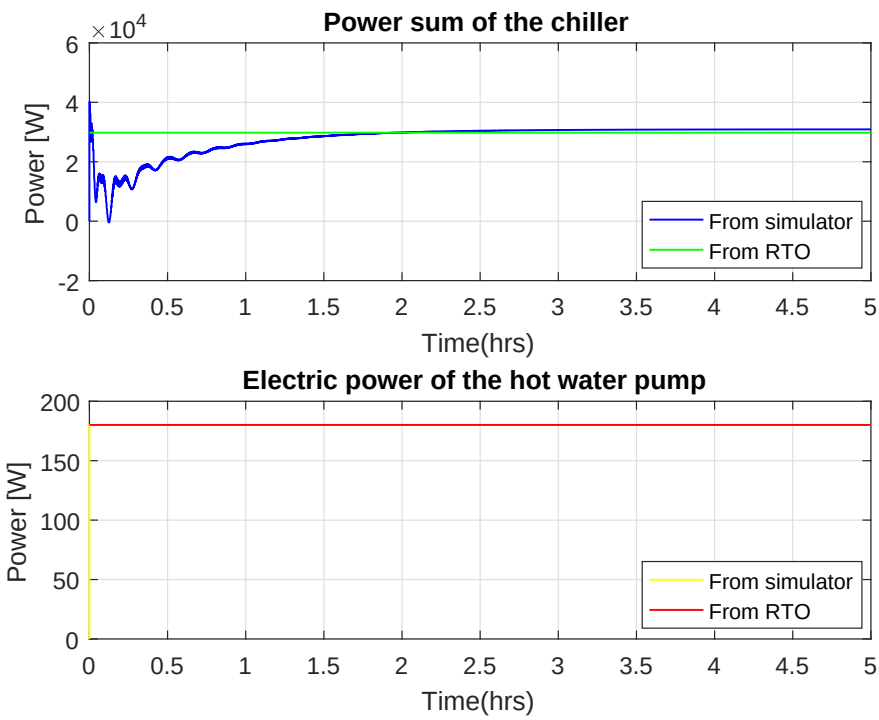

Figure 4.4: Validation of the power sum of the chiller and electric power of the pump calculated by RTO with the simulator of the plant

4.4.3 Simulation of RTO

The RTO was then tested with the profile of the disturbances for 8 hours with the sampling time of an hour. The RTO runs every hour taking into account the current input and disturbances, it calculates the optimal value of the input for the next hour. The profile of the disturbances provided to the RTO can be seen in figure 4.5. Note that every hour the intial value of the input to the RTO is considered to be equal to the optimal value of the input calculated by RTO in the previous hour.

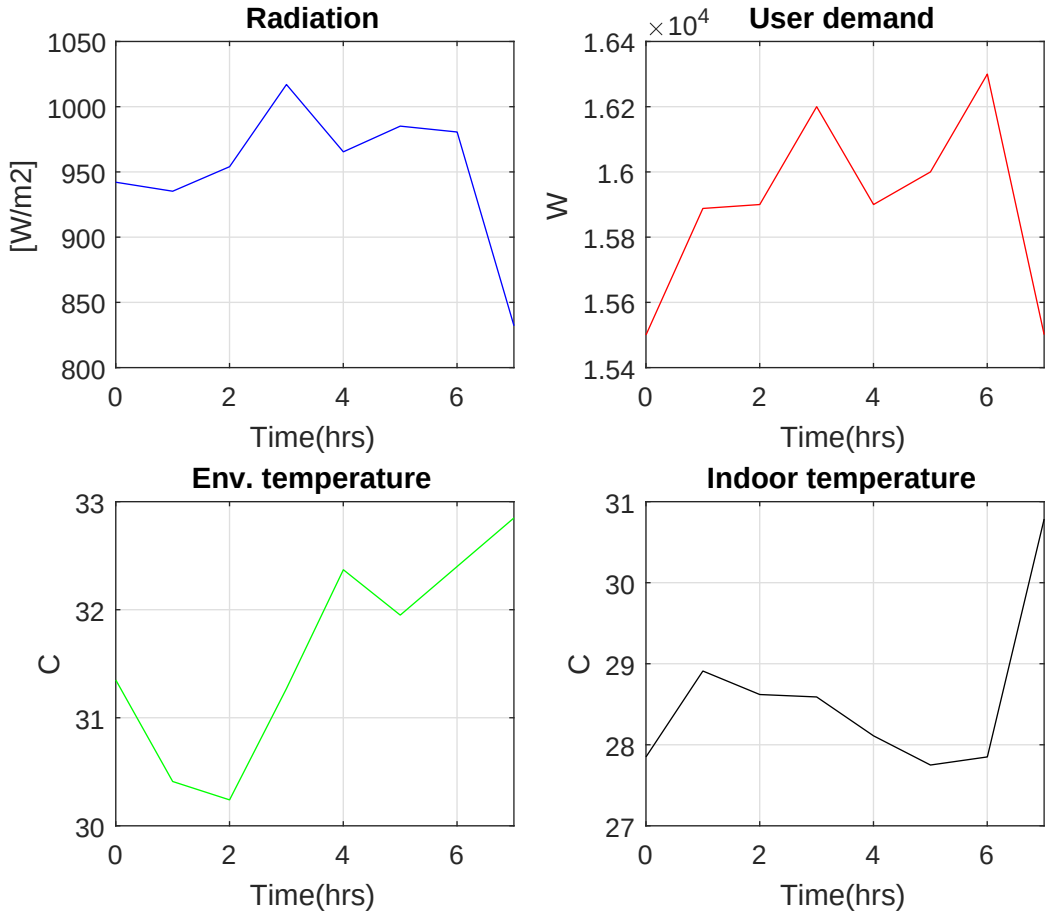

Figure 4.5: Input disturbances to the RTO for eight hour simulation

The result of this simulation can be seen in the figure 4.6 and 4.7. The RTO calculates an optimal value of the hot water flow according to the values of the disturbances in order to minimize the power sum of chiller, the electric power of pump and the difference between the setpoint and cold water output temperature every hour. It also respects the bounds on the hot water flow and hot water output temperature of the solar collector. Hence, it can be concluded that the RTO works well.

However, in practice the disturbances don't stay constant during an hour but have some dynamics. Hence, the plant needs a low level fast controller that maintains the setpoint provided by the RTO for every hour to compensate the effect of the dynamics of disturbances. This brings a need for the development of a low level fast MPC controller which will be discussed in detail in the next section of this chapter.

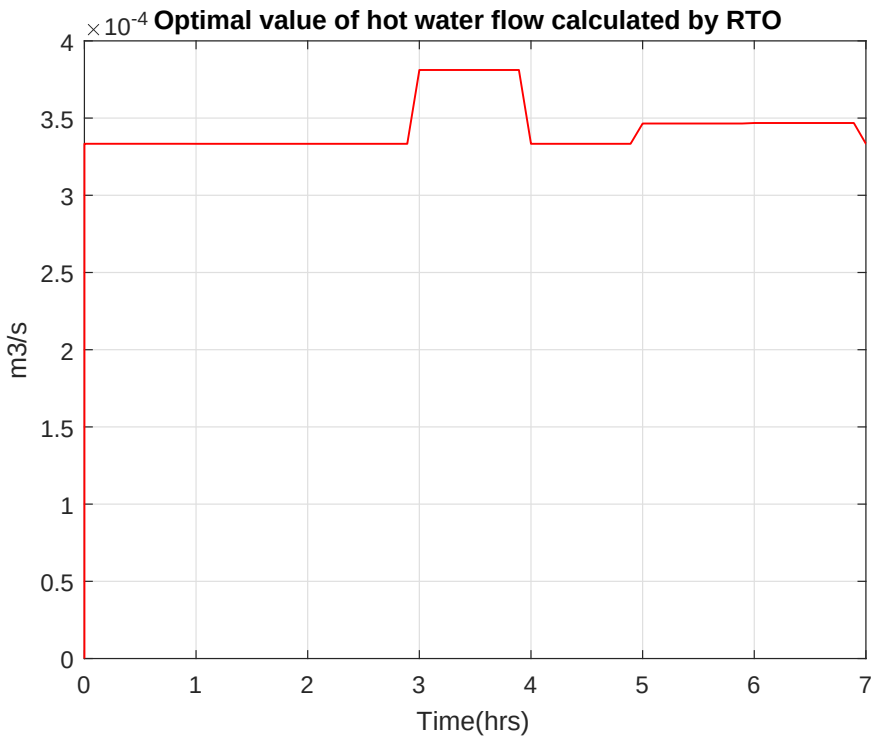

Figure 4.6: Optimal value of $q_{t_{opt}}$ calculated by RTO in 8 hours simulation

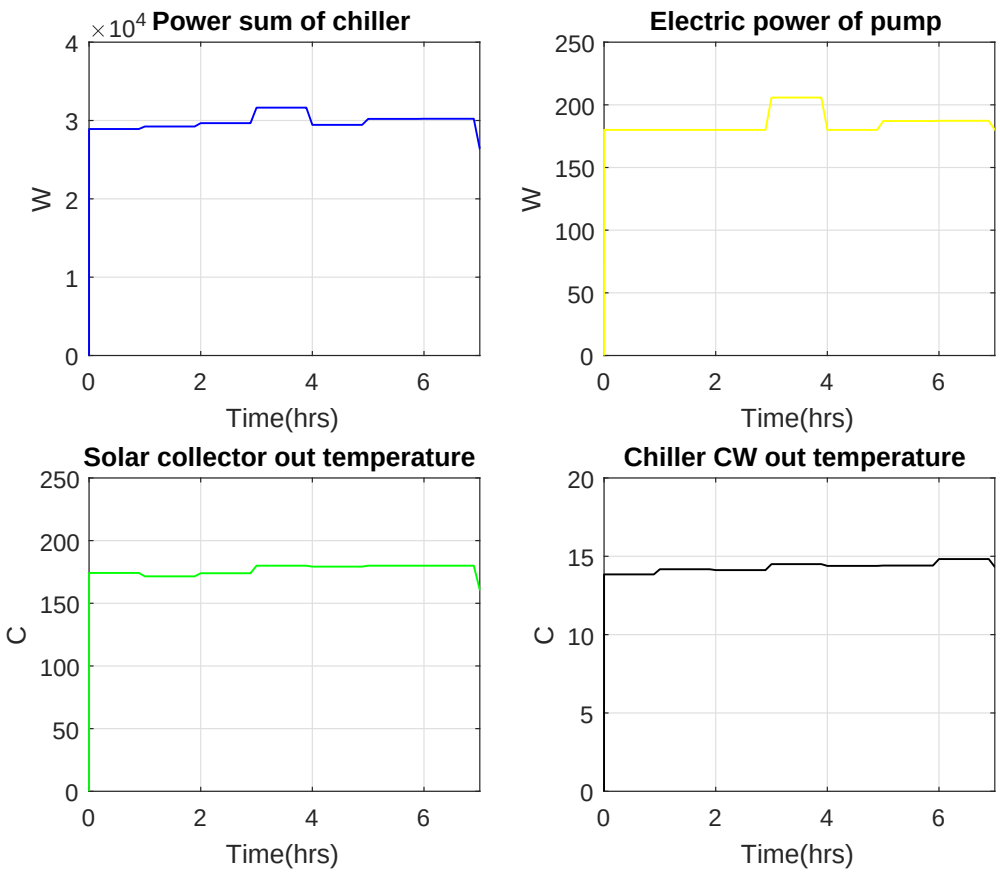

Figure 4.7: Output values from the 8 hours simulation of the RTO

4.5 Model Predictive Control design

Model Predictive Control (MPC), has been widely adopted in industry as an effective means to deal with multivariable constrained control problems since last few decades [21]. The advantages of MPC are: it handles multivariable control problems naturally, it can take account of actuator limitations and it allows operation closer to constraints, which frequently leads to more profitable operation. The main ingredients of an MPC algorithm are [22]:

- A process model, usually in discrete-time.
- Input, output and state constraints.
- A cost function J defined, at any time instant k, over a finite horizon $[k, k+N]$.
- An optimization algorithm computing the future optimal control sequence.
- The so-called Receding Horizon (RH) principle: At any time instant k, based on the available process information, solve the optimization problem with respect to the future control sequences $[u(k), ..., u(k+N-1)]$ and apply only its first element $u^0(k)$. Then, at the next time instant k+1, a new optimization problem is solved, based on the process information available at time k+1, along the prediction horizon $[k+1, k+N]$. Figure 4.8 gives an idea about this strategy.

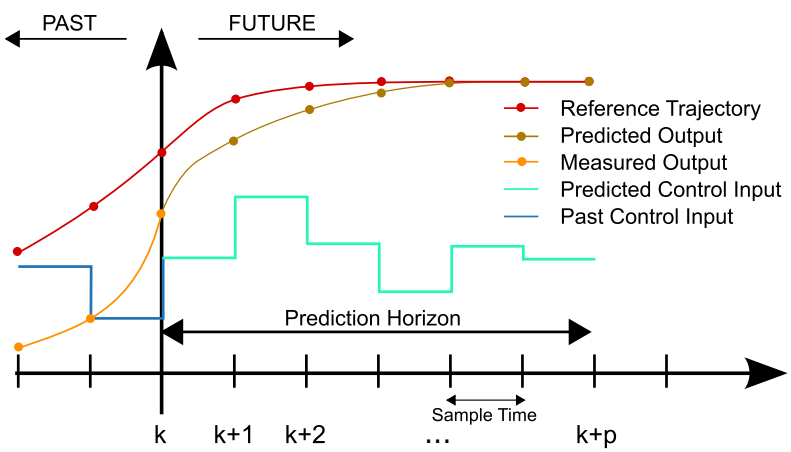

Figure 4.8: Receding horizon principle in MPC scheme (Source:[23])

4.5.1 MPC development for the solar cooling plant

The schematic for the implementation of an MPC can been seen in figure 4.9. The MPC controller is built with explicit integral action [22]. The advantage of this strategy is that, it guarantees tracking of reference signal with zero steady state error. The goal of this strategy is to track the reference y_{RTO} computed by the RTO procedure by manipulating the input u with zero steady state error e.

The variation on the input and output with respect to their nominal value computed with RTO one can be given by,

$$\delta u = u - u_{RTO} \qquad \delta y = y - y_{RTO}; \tag{4.22}$$

Consider the system enlarged with an integral action,

$$\begin{aligned} \delta x(k+1) &= A\,\delta x(k) + B\,\delta u(k) \\ v(k+1) &= v(k) + e(k+1) \end{aligned} \tag{4.23}$$

where $e(k) = y^0_{RTO} - y(k)$. Equivalently,

$$\begin{aligned} \delta x(k+1) &= A\,\delta x(k) + B\,\delta u(k) \\ v(k+1) &= v(k) + y^0_{RTO} - C\,\delta x(k+1) \\ &= v(k) + y^0_{RTO} - C\,A\,\delta x(k) - C\,B\,\delta u(k) \end{aligned} \tag{4.24}$$

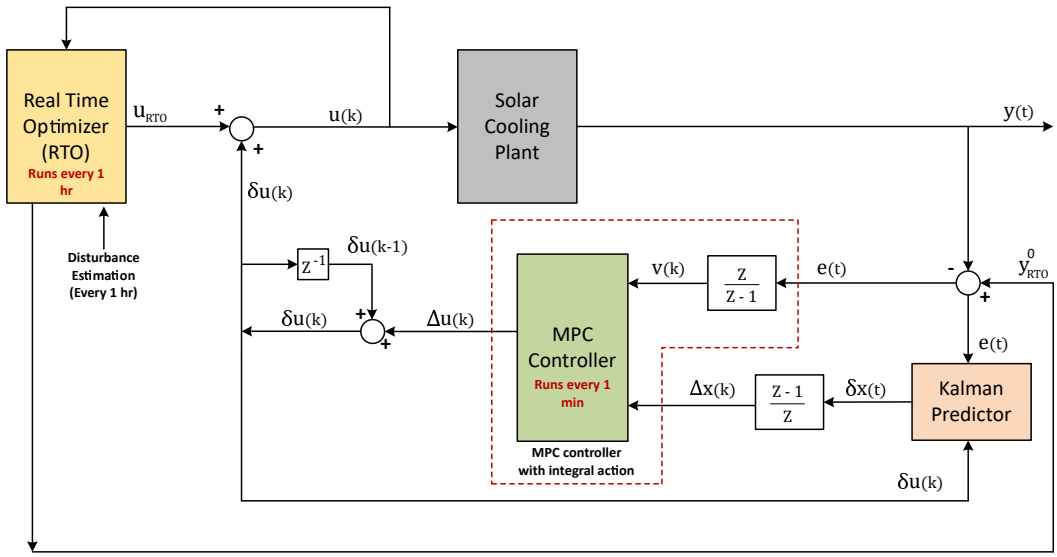

Figure 4.9: MPC scheme with RTO

Now defining the delta model of above expressions by subtracting their value at the previous time instants from the current one,

$$\begin{aligned} &\Delta x(k) = \delta x(k) - \delta x(k-1); \qquad \Delta u(k) = \delta u(k) - \delta u(k-1); \\ &\Delta y(k) = \delta y(k) - \delta y(k-1) \end{aligned} \tag{4.25}$$

Recalling the $v(k+1) - v(k) = e(k+1)$, the enlarged system can be written as,

$$\begin{bmatrix} \Delta x(k+1) \\ e(k+1) \end{bmatrix} = \begin{bmatrix} A & 0 \\ -C\,A & I \end{bmatrix} \begin{bmatrix} \Delta x(k) \\ e(k) \end{bmatrix} + \begin{bmatrix} B \\ -CB \end{bmatrix} \Delta u(k) \tag{4.26}$$

For this enlarged system, usually called in *velocity form*, the following performance index can be considered,

$$\begin{aligned} \min_{\Delta u(k+i), i=0,\ldots,N-1} J(\Delta x(k), \Delta u(\cdot), k) = &\sum_{i=0}^{N-1} \Big(\parallel e(k+i) \parallel_Q^2 + \parallel \Delta u(k+i) \parallel_R^2 \Big) \\ &+ \parallel e(k+N) \parallel_S^2 \end{aligned} \tag{4.27}$$

subject to constraints on the future state and control variable and increments. This formulation guarantees that $J = 0$ when $e(k+i) = 0$, i.e. $y(k+i) = y^0_{RTO}$, and $\Delta u(k+1) = 0$, i.e. u is constant.

Note that $x(k+i)$ and $u(k+i)$ can be easily written as functions of $x(k+i-1)$, $\Delta x(k+i)$, $u(k+i-1)$ and $\Delta u(k+i)$. Once the future optimal sequence $\Delta u^0(k+i), i = 0, ..., N-1$ of the control increments in computed, and according to the receding horizon approach, the following control variable is effectively used.

$$u(k) = u(k-1) + \Delta u^0(k) \tag{4.28}$$

The features of this strategy are :

- This approach does not require to estimate any disturbance d and/or to compute the corresponding steady state $(\bar{x}, \bar{u})$ at any new variation of the reference signal.
- Constraints on Δu can be very helpful to describe the physical restrictions on the rate of variation of the control variables.
- Additional terms weighting the future state increments can be easily included into the performance index to be minimized.

Kalman predictor

As it can be seen from figure 4.9, the implemented scheme uses a continuous time Kalman predictor to estimate the δx provided the value of δu and δy. An observer was needed as not all the δx were measurable and had to be estimated. For the system in continuous time,

$$\begin{aligned} \delta\dot{x}(t) &= A\,\delta x(t) + B\,\delta u(t) + v_x(t) \\ \delta y(t) &= C\delta x(t) + v_y(t) \end{aligned} \tag{4.29}$$

the steady state Kalman predictor in continous time can be given as,

$$\begin{aligned} \delta\dot{\hat{x}}(t) &= A\,\delta\hat{x}(t) + B\,\delta u(t) + \bar{L}[\delta y(t) - C\,\hat{x}(t)] \\ &= (A - \bar{L}C)\,\delta\hat{x}(t) + B\,\delta u(t) + \bar{L}\,\delta y(t) \end{aligned} \tag{4.30}$$

with

$$\bar{L} = \bar{\tilde{P}}\,C'\,\tilde{R}^{-1} \tag{4.31}$$

where, $\bar{\tilde{P}}$ is the unique positive definite solution of the stationary Riccati equation [22]. Obviously, the necessary condition are that, the pair (A, B_q) is reachable and the pair (A,C) is observable. Here, B_q is such that $\widetilde{Q}_k = B_q\,B_q'$ and $\widetilde{Q}_k \geq 0$ is a noise covariance matrix.

4.6 Implementation

As shown in figure 4.9, the RTO runs every hour given the estimation of disturbances every hour and the input value u from the system. The MPC runs every minute and is built on the reduced order linearized system around the equilibrium point $\bar{x}$, computed with RTO. The next hour, the new value of input is calculated by RTO which is then fed to system along with the disturbances and the system is linearized again around the new equilibrium point. In the developed Simulink environment, the linearization was performed using the `Time-Based Linearization` block in Simulink.

The linearized model has a high order and it is advisable to use model order reduction techniques to compute a simpler approximate observer and regulator [22]. First the balanced realization for stable portion of the system was determined using `balreal` function in MATLAB. Then, the minimal order system is found by eliminating the uncontrollable and unobservable part of the linearized state space model. This is done using the `minreal` function in MATLAB. The reduced order linearized system is characterized by the following equation,

$$\begin{aligned} \dot{x}_r(t) &= A_r\, x_r(t) + B_r\, u(t) \\ y(t) &= C_r\, x_r(t) + D_r\, u(t) \end{aligned} \tag{4.32}$$

Using values of the matrices A_r, B_r and C_r in equation 4.26, it can be written as,

$$\begin{bmatrix} \Delta x_r(k+1) \\ e(k+1) \end{bmatrix} = \begin{bmatrix} A_r & 0 \\ -C_r\, A_r & I \end{bmatrix} \begin{bmatrix} \Delta x_r(k) \\ e(k) \end{bmatrix} + \begin{bmatrix} B_r \\ -C_r\, B_r \end{bmatrix} \Delta u(k) \tag{4.33}$$

Alternatively this system can be written in the compact form,

$$X(k+1) = A\, X(k) + B\, \Delta u(k) \tag{4.34}$$

Since the linearization is valid only in the neighborhood of the equilibrium, the prediction given by the model is less precise as the time horizon increases. However, for small horizons the prediction of system future evolution is quite reasonable. Starting with this model the prediction is performed through a simple recursive procedure. Recalling the Lagrange equation for discrete time system,

$$X(k+i) = A^i X(k) \; + \sum_{j=0}^{i-1} A^{i-j-1} B\, \Delta u(k+j)$$

for $i \in (1,\ ...,\ N)$.
and letting

$$\widetilde{X}(k) = \begin{bmatrix} x(k+1) \\ x(k+2) \\ \vdots \\ x(k+N-1) \\ x(k+N) \end{bmatrix}, \quad \widetilde{A} = \begin{bmatrix} A \\ A^2 \\ \vdots \\ A^{N-1} \\ A^N \end{bmatrix}, \quad \Delta U(k) = \begin{bmatrix} \Delta u(k) \\ \Delta u(k+1) \\ \vdots \\ \Delta u(k+N-2) \\ \Delta u(k+N-1) \end{bmatrix},$$

$$\widetilde{B} = \begin{bmatrix} B & 0 & 0 & \cdots & 0 & 0 \\ AB & B & 0 & \cdots & 0 & 0 \\ \cdots & \cdots & \cdots & \cdots & \cdots & \cdots \\ A^{N-2}B & A^{N-3}B & A^{N-4}B & \cdots & B & 0 \\ A^{N-1}B & A^{N-2}B & A^{N-3}B & \cdots & AB & B \end{bmatrix}$$

one obtains,

$$\widetilde{X}(k) = \widetilde{A}\,\widetilde{X}(k) + \widetilde{B}\,\Delta U(k) \tag{4.35}$$

Moreover, defining the weighting matrices with N blocks on the diagonal,

$$\widetilde{Q} = \begin{bmatrix} Q & 0 & \cdots & 0 & 0 \\ 0 & Q & \cdots & 0 & 0 \\ \vdots & \vdots & \ddots & \vdots & \vdots \\ 0 & 0 & \cdots & Q & 0 \\ 0 & 0 & \cdots & 0 & S \end{bmatrix} \quad , \widetilde{R} = \begin{bmatrix} R & 0 & \cdots & 0 & 0 \\ 0 & R & \cdots & 0 & 0 \\ \vdots & \vdots & \ddots & \vdots & \vdots \\ 0 & 0 & \cdots & R & 0 \\ 0 & 0 & \cdots & 0 & R \end{bmatrix} \tag{4.36}$$

The performance index to be minimized can be written as,

$$\min_{\Delta u(k)} J(\Delta x(k), \Delta u(k), k) = \widetilde{X}'(k)\,\widetilde{Q}\,\widetilde{X}(k) + \Delta U'(k)\,\widetilde{R}\,\Delta U(k) \tag{4.37}$$

Contraints used for MPC formulation

For the MPC formulation the constraints on the future inputs increment were put. The minimum and maximum bound on the increment were calculated as

$$\begin{aligned} \Delta u_{max} &= u_{max} - u(k) = u_{max} - u_{RTO} - \delta u(k) \\ \Delta u_{min} &= u_{min} - u(k) = u_{min} - u_{RTO} - \delta u(k) \end{aligned} \tag{4.38}$$

where, u_{max} and u_{min} are the upper and lower bound of the input variable. The constraint on the input increment hence can be defined for the horizon N as,

$$\begin{aligned} \Delta u_{min} &\leq \Delta u(k) \leq \Delta u_{max} \\ \Delta u_{min} &\leq \Delta u(k) + \Delta u(k+1) \leq \Delta u_{max} \\ &\vdots \\ \Delta u_{min} &\leq \sum_{i=0}^{N-1} \Delta u(k+i) \leq \Delta u_{max} \end{aligned} \tag{4.39}$$

The optimization problem defined by equation 4.37 can be solved using the prediction model given by equation 4.35, the values of $\widetilde{Q}$ and $\widetilde{R}$ matrices and constraints defined in the equation 4.39.

Solver for MPC

The YALMIP toolbox is one of the known toolboxes in solving such optimization problems. The toolbox runs with MATLAB and has several solvers that can be chosen according to the structure of the problem and requirements. For this work the CPLEX solver developed by IBM was used to solve the optimization problem. The development of the optimization problem was done as mentioned in [24].

4.6.1 Simulations

The simulation of MPC was performed for an hour for which, the optimal setpoints were taken from RTO simulation results for the 8 hour simulation described in section 4.4.3. The chosen hour duration was between $3-4$ with the optimal input value $q_{opt} = 3.81 \times 10^{-4}$. The system was linearized in continuous time around the nominal state $\bar{x}$, feeding this optimal input and constant disturbances $\bar{d}$ during this hour of RTO operation. The obtained linearized system had 165 states, hence the model reduction technique was applied to obtain the reduce order system of order three. The reduced order system can be characterized by following matrices.

$$A_r = \begin{bmatrix} -6.4503 & -1.8598 & 3.3318 \\ -1.8761 & -0.9234 & 0.3857 \\ 3.3701 & 0.3417 & -6.2767 \end{bmatrix}; B_r = \begin{bmatrix} 16154.56 \\ 3851.11 \\ -14910.91 \end{bmatrix} \tag{4.40}$$

$$C_r = \begin{bmatrix} 16129.86 & 3839.69 & -14887 \end{bmatrix}; \quad D_r = \begin{bmatrix} 0 \end{bmatrix}$$

The continuous time Kalman filter was built based on these matrices using the `lqr` function of MATLAB. The gain vector returned by this function is given by,

$$L = \begin{bmatrix} 7.27 \\ 1.60 \\ -6.67 \end{bmatrix} \tag{4.41}$$

The matrices A_r, B_r, C_r and D_r describe the continuous time system and had to be discretized for the MPC formulation. The value of u_{min} and u_{max} for the constraint were 2.78×10^{-4} and 5.56×10^{-4} respectively. The weights on the error $Q = 1$ and on the input increment $R = 0.001$ were chosen. The prediction horizon of $N = 5$ was used that corresponds to 5 minute time duration.

The MPC was then formulated using YALMIP based on the discretized matrices obtained from continuous time reduced order system 4.40, the cost function 4.37 and constraints 4.39.

The MPC was fed with the disturbances for an hour of its operation sampled at every $60\,s$. The profile of all the input disturbances can be seen in figure 4.10. Note that the disturbances are kept constant for almost 2.4 hours, as the MPC starts working after that. The disturbances profile is then provided to the model with the sampling time of $60\,s$ for an hour.

Figure 4.11 shows the output error results. For first 2.4 hours, the error on the output after transient settles and stays constant. This error is due to the modelling uncertainty in the RTO as it is built on the simple steady state model. After 2.4 hours, the Kalman predictor start working and provides the δx to MPC. The MPC starts working at the same time and tries to bring the output error to zero by manipulating the input. The output error doesn't quite become zero but oscillates around zero, as the Kalman filter is built on the approximate reduced order

model and the MPC uses the estimated states given by Kalman filter and is based approximate model. The MPC formulated with explicit integral action doesn't use the information of disturbances which change every 60 s and it is also one of the reason for non-zero output error. It can also be noticed that the MPC with integral action can remove the biased error due to modelling uncertainty in the RTO.

The input hot water flow to the system changes from the setpoint of the RTO during the operation of MPC as it can be seen in figure 4.12. The MPC to reduces the flow in order to bring the output error to zero. This is quite reasonable because the Power sum (output) of the chiller is directly proportional to the input hot water flow and reducing the flow will in turn result in the lower Power sum. During the operation, MPC respects the bounds on the input specified in the constraints.

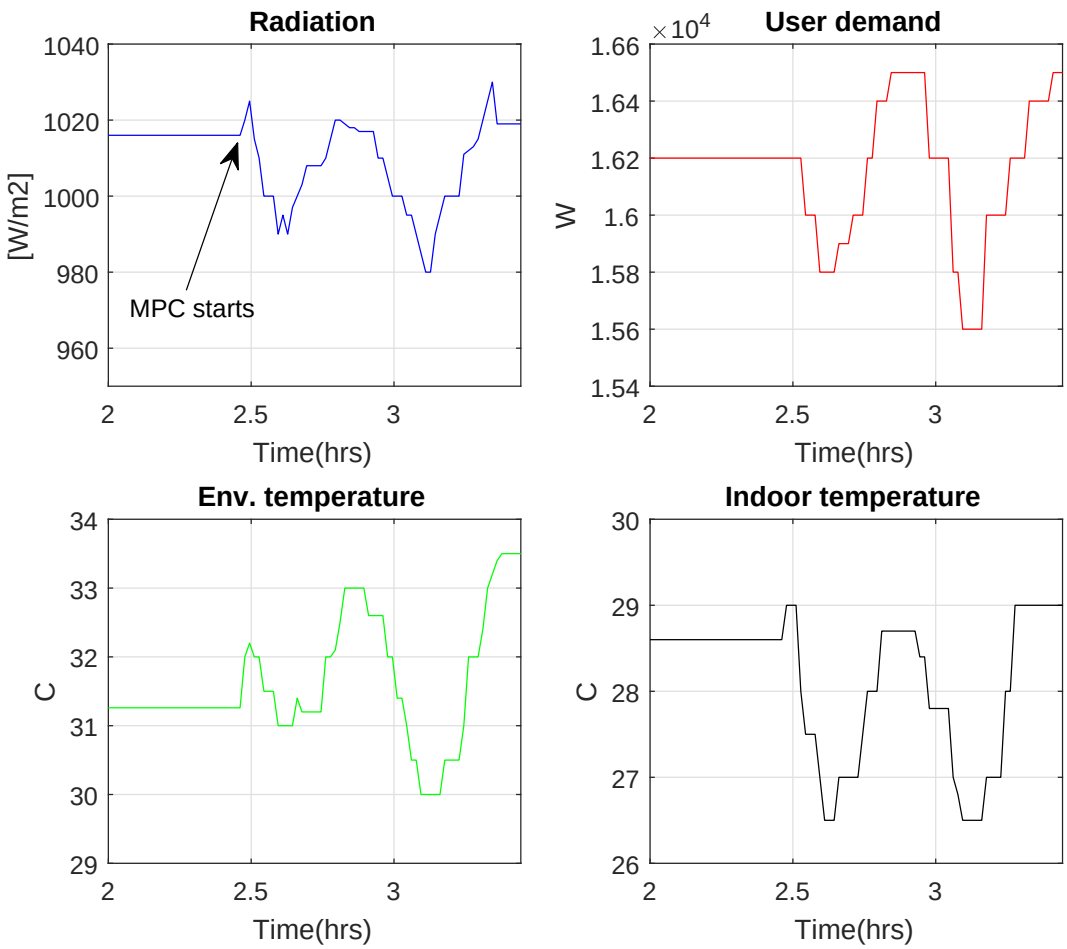

Figure 4.10: Input disturbances to the MPC during its operation

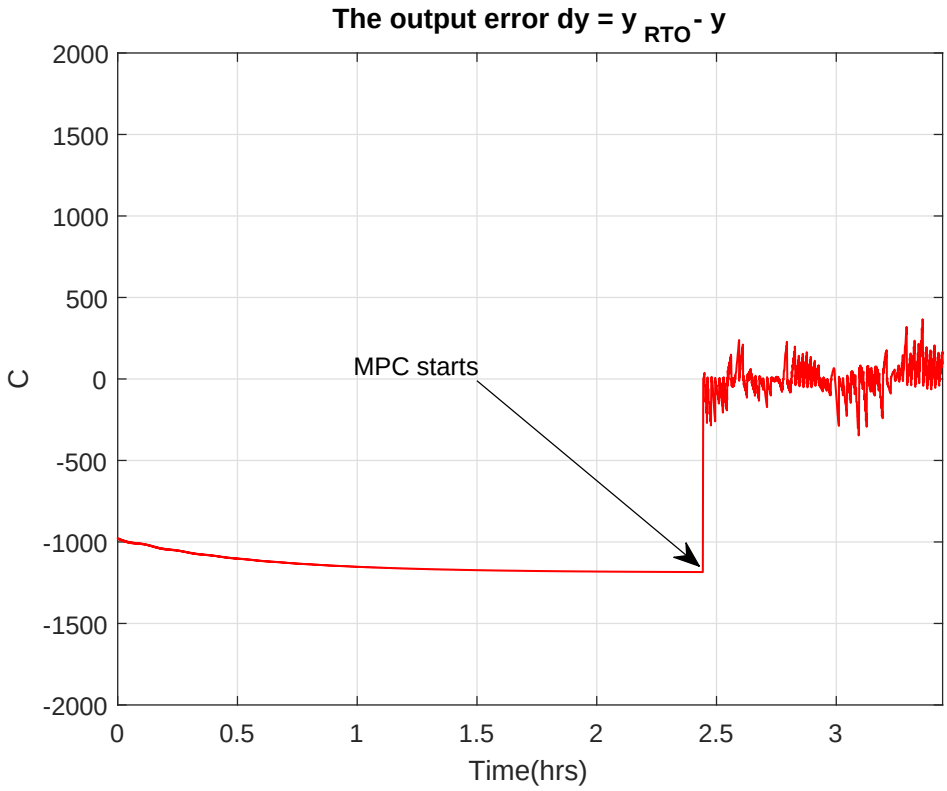

Figure 4.11: Hot water flow during the operation of MPC

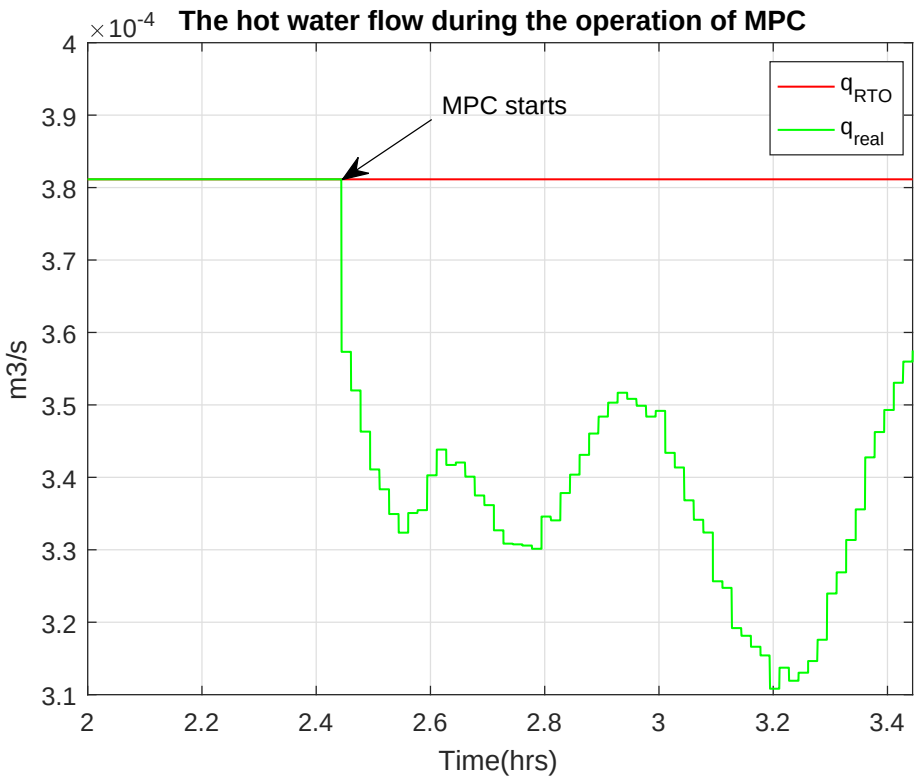

Figure 4.12: Hot water flow during the operation of MPC

4.7 Summary

In this chapter, the two-layered architecture for the fixed configuration of a plant was introduced. The RTO which serves as an upper layer in this architecture was built with the steady state model of the plant. After validation of RTO against the simulator of the plant, the satisfactory operation of RTO is observed. The MPC formulated with an explicit integral action based on the reduced order linearized model does quite well to track the output setpoint provided by the RTO.

Chapter 5

Optimal control in a Hybrid configuration of the plant

In Chapter 4, a two layer architecture for the optimal control of the solar cooling plant was introduced. This architecture can be extended to cope up with the Hybrid configuration of the plant and exploits both the continuous and binary variables of the plant in order to have more degrees of freedom to choose the optimal operating conditions. This chapter describes the hybrid model of the plant and defines the control strategy useful to compute the optimal control of plant.

5.1 Hybrid configuration of the plant

The hybrid configuration of the plant can be seen in the figure 5.1. There are three on/off valves CV002, CV003 and CV301 included in this configuration represented by binary variables δ_1, δ_2 and δ_3. The hybrid model exploits the possibility to modify the state of these valves to change the configuration of the plant by including or excluding some of the equipment of the plant. For instance, switching the valve CV002 ($\delta_1 = 1$ (on) or 0 (off)) allows to include or exclude the hot storage in the hot water circuit. In the same way CV003 (δ_2) and CV301 (δ_3) allows to include/exclude the chiller and the cold storage in the hot water and cold water circuit. This strategy of including storages and valves has additional benefits over the fixed configuration. For instance, it is possible store the heat in the hot storage to save the energy from the solar radiation when the user demand is less and can be kept for later use. In addition, it can produce more cold water operating on using hot water and cool down the cold storage to satisfy the demand from user during the time when there is no solar radiation.

As this model is a combination of the continuous and binary variables, it is called hybrid model. The advantage of this kind of the model is that it gives more degrees of freedom to the higher level optimizer to choose the best configuration of the plant given the estimation of the disturbances to optimize the overall energy efficiency.

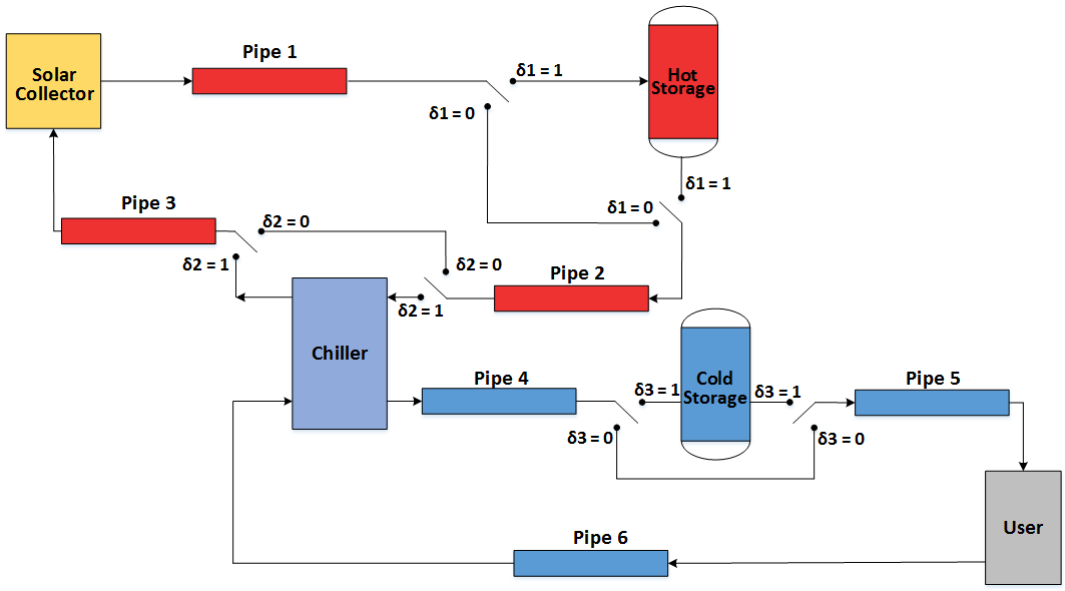

Figure 5.1: Hybrid configuration of the solar cooling plant

5.2 Control architecture

The control architecture stays the same as mentioned in the last chapter except the higher layer is a MPC based on hybrid model that gives optimal setpoint u_i (continuous) to a low level MPC controller to follow. Moreover, the higher level MPC manipulates directly the boolean variables of the plant to define the optimal configuration of the plant using the prediction of disturbances. In the case of the solar cooling plant these variables are nothing but the on/off valves. The configuration of the plant is kept constant until the higher level MPC runs next time and defines a new configuration of the plant.

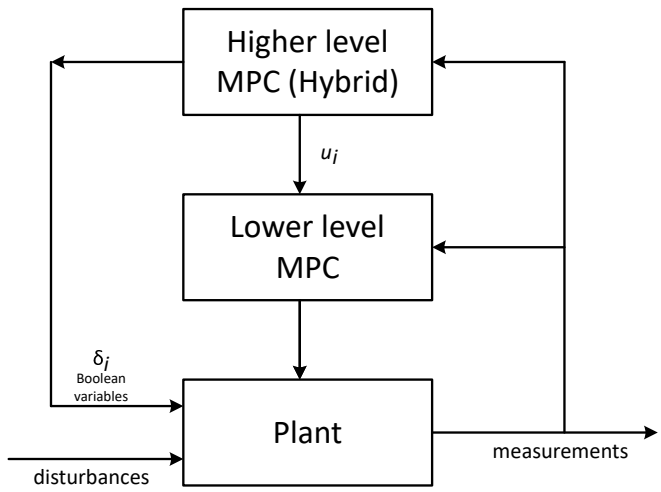

Figure 5.2: Control structure for the hybrid configuration of the plant

The lower level fast MPC based on the linearized model of the plant is used to maintain these optimal operating conditions.

5.3 Hybrid model

With growing number of dynamical systems integrated with logical/discrete decision components, the study of the dynamic system with continuous and discrete variable has gained increasing attention. The investigation of hybrid systems is creating a new and fascinating discipline bridging control engineering, mathematics, and computer science [25]. Several researcher have presented new techniques to solve some of the subclasses of this new class of new problems [26].

This type of system can be formulated as the mixed logical dynamical (MLD) described by linear dynamic equations subject to linear mixed-integer inequalities, i.e. inequalities involving both the continuous and binary variables. The general form of the MLD can be described through following linear relations [27].

$$\begin{aligned} x(t+1) &= A_t\, x(t) + B_{1t}\, u(t) + B_{2t}\, \delta(t) + B_{3t}\, z(t) \\ y(t) &= C_t\, x(t) + D_{1t}\, u(t) + D_{2t}\, \delta(t) + D_{3t}\, z(t) \\ E_{2t}\delta(t) + E_{3t}\, z(t) &\leq E_{1t}\, u(t) + E_{4t}\, x(t) + E_{5t} \end{aligned} \tag{5.1}$$

where $t \in \mathbb{Z}$,

$$x = \begin{bmatrix} x_c \\ x_l \end{bmatrix},\ x_c \in \mathbb{R}^{n_c},\ x_l \in \{0,1\}^{n_l},\ n \triangleq n_c + n_l$$

is the state of the system, whose components are distinguished between continuous x_c and 0-1 x_l;

$$y = \begin{bmatrix} y_c \\ y_l \end{bmatrix},\ y_c \in \mathbb{R}^{p_c},\ y_l \in \{0,1\}^{p_l},\ p \triangleq p_c + p_l$$

is the output vector;

$$u = \begin{bmatrix} u_c \\ u_l \end{bmatrix},\ u_c \in \mathbb{R}^{m_c},\ u_l \in \{0,1\}^{m_l},\ u \triangleq u_c + u_l$$

is the command input, collecting both continuous commands u_c and binary (on/off) commands u_l (discrete command, i.e. assuming value within a finite set of reals, can be modeled as 0-1 commands); $\delta \in \{0,1\}^{r_l}$ and $z \in \mathbb{R}^{r_c}$ represent respectively auxiliary logical and continuous variables. $A_t, B_{1t}, B_{2t}, B_{3t}, C_t, D_{1t}, D_{2t}, D_{3t}, E_{1t}, E_{2t}, E_{3t}$, E_{4t} and E_{5t} are the matrices of suitable dimensions [28], [29].

5.4 Development of the hybrid model

To define the hybrid model, it is recommended to build a simple but reasonable model of each component of the system in order to keep the final order of the overall system as minimum possible. Otherwise with high order model, the problem becomes complex and it takes more computation time to get the solution of the optimization problem to be recursively solved by the MPC algorithm. The steady state models developed in section 4.3 were used to develop the hybrid model of the solar collector, pipes, chiller and user. While for the storage tank more detailed dynamic models was needed to define the functionality similar to the real plant.

5.4.1 Dependency on hot water flow

As the dynamic and static model of the equipment in the hot water circuit including chiller have dependency on hot water flow q_t, the system becomes nonlinear. To address this problem, the hot water flow was defined such that it can only take predefined values from finite set given by

$$q_{t_i} \in \{q_{t_1}, q_{t_2}, \cdots, q_{t_m}\} \tag{5.2}$$

and each value of flow in the set is associated to a boolean variable defined as $\{\delta_{q_1}, \delta_{q_2}, \cdots \delta_{q_m}\}$ with the constraint

$$\sum_{i=1}^{m} \delta_{q_i} = 1 \tag{5.3}$$

So, at any time instance, the function of q_{t_i}, can take a finite value such that $f(q_{t_i}) \in \{f(q_{t_1}), f(q_{t_2}), \cdots, f(q_{t_m})\}$. Then, if S is the solution of a function $f(q_{t_i})$, it can be written as,

$$S = \sum_{i=1}^{m} f(q_{t_i})\, \delta_{q_i} \tag{5.4}$$

This ensures that the q_t can take only one value at a time from defined set 5.2. The function of q_t can be called a piece wise linear function. This solves the nonlinearity problem due to dependency on q_t in the hybrid model formulation. Note that as a feature of hybrid model i.e. handling continuous and boolean variables together, this strategy can be easily implemented.

5.4.2 Hybrid model for the solar collector

The static model of the solar collector is described in section 4.3.1. As mentioned before, it is better to have simple but reasonable model for all the equipment. So, the solar collector was considered to be a single element with input and output temperature characterized by equation 4.6 (instead of distributed parameter system). In the discrete time the same equation can be written as,

$$T_f(k+1) = \gamma_{s_1}\big(q_t(k)\big)\, T_{f_0}(k) + \gamma_{s_2}\big(q_t(k)\big)\, I(k) + \gamma_{s_3}\big(q_t(k)\big)\, T_a(k) \tag{5.5}$$

From 5.4.1, the dependency on q_t can be addressed in this equation analogous to the equation 5.4. So the equation for the output temperature the T_f of the solar collector in discrete time, as function of hot water flow and input, is given by

$$\begin{aligned} T_f(k+1) = &\left[\sum_{i=1}^{m} \gamma_{s_{1,i}}\big(q_{t_i}(k)\big)\delta_{q_i}\right] T_{f_0}(k) + \\ &\left[\sum_{i=1}^{m} \gamma_{s_{2,i}}\big(q_{t_i}(k)\big)\delta_{q_i}\right] I(k) + \\ &\left[\sum_{i=1}^{m} \gamma_{s_{3,i}}\big(q_{t_i}(k)\big)\delta_{q_i}\right] T_a(k) \end{aligned} \tag{5.6}$$

5.4.3 Hybrid model for the storage tank

For the hot storage, the static model is not sufficient to account dynamics when there is no hot water input flow and the tank cools down due to the heat losses to the environment. Hence a first order model was chosen to derive the hybrid model of the hot storage.

Starting from equation 3.13 and letting $\alpha_t = \frac{H_{tank} A_{ext}}{c_f\, M_f}$, the output temperature of the tank can be expressed by

$$\frac{\partial T_t(t)}{\partial t} = -\frac{q_t(t)}{M_f}\, T_t(t) + \frac{q_t(t)}{M_f}\, T_{in}(t) - \alpha_t\, T_t(t) + \alpha_t\, T_a(t) \tag{5.7}$$

Rearranging the terms, the equation becomes

$$\frac{\partial T_t(t)}{\partial t} = -\left(\frac{q_t(t)}{M_f} + \alpha_t\right) T_t(t) + \frac{q_t(t)}{M_f}\, T_{in}(t) + \alpha_t\, T_a(t) \tag{5.8}$$

Setting, $\gamma_t = -\left(\frac{q_t(t)}{M_f} + \alpha_t\right)$ yields

$$\frac{\partial T_t(t)}{\partial t} = \gamma_t\, T_t(t) + \frac{q_t(t)}{M_f}\, T_{in}(t) + \alpha_t\, T_a(t) \tag{5.9}$$

This problem can be solved using Lagrange formula given by [30],

$$x(t) = e^{A(t-t_0)}\, x_{t_0} + \int_{t_0}^{t} e^{A(t-\tau)} B u(\tau) d\tau \tag{5.10}$$

where, x_{t_0} is initial state, $u(t)$ is an input and $t \geq t_0$. Applying this formula with $\Delta t = t - t_0$ and after deduction, the solution for the equation 5.9 can be written as,

$$T_t(t) = e^{\gamma_t\, \Delta t}\, T_{t_0}(t_0) + (e^{\gamma_t\, \Delta t} - 1)\, \frac{q_t}{M_f\, \gamma_t}\, T_{in}(t_0) + (e^{\gamma_t\, \Delta t} - 1)\, \frac{\alpha_t}{\gamma_t}\, T_a(t_0) \tag{5.11}$$

In discrete time, letting $t = kT + T$ and $t_0 = kT$ it becomes

$$T_t(k+1) = e^{\gamma_t\, \Delta t}\, T_{t_0}(k) + (e^{\gamma_t\, \Delta t} - 1)\, \frac{q_t}{M_f\, \gamma_t}\, T_{in}(k) + (e^{\gamma_t\, \Delta t} - 1)\, \frac{\alpha_t}{\gamma_t}\, T_a(k) \tag{5.12}$$

Here, T_{t_0} is an initial value of the output temperature of the tank. Note that Δt must be chosen such that the solution given by this equation is reasonable and validates with real data.

Remembering the formulation for the finite values of the hot water flow, the parameter γ_t and flow q_t must be included as expressed below in the previous equation.

$$\gamma_t = \sum_{i=1}^{m} \gamma_{t_i}\big(q_i(k)\big)\delta_{q_i};\;\; q_t = \sum_{i=1}^{m} q_i(k)\delta_{q_i} \tag{5.13}$$

This model is valid only when there is input flow i.e. the tank is included in the hot

water circuit ($\delta_1 = 1$). But when the tank is bypassed, the cooling of the tank is governed by the equation 5.7 after setting $q_t(t) = 0$.

$$\frac{\partial T_t(t)}{\partial t} = -\alpha_t\, T_t(t) + \alpha_t\, T_a(t) \tag{5.14}$$

The solution to this equation can be obtained again by applying Lagrange formula and expressed in discrete time,

$$T_t^{Nf}(k+1) = e^{\alpha_t\,\Delta t}\, T_{t_0}^{Nf}(k) + (e^{\alpha_t\,\Delta t} - 1)\, T_a(k) \tag{5.15}$$

where, T^{Nf} represents the no flow temperature of the tank. So the overall model of the tank output temperature can be written as

$$T_{t_{all}}(k+1) = T_t(k+1)\,\delta_1 + T_t^{Nf}(k+1)(1-\delta_1) \tag{5.16}$$

Note that in case of the cold storage tank the equation 5.16 is valid and as the cold water flow q_c is constant , the formulation for γ_t and flow q_t is not required as mentioned in equation 5.13.

5.4.4 Hybrid model for the pipes

Similar to the solar collector hybrid model, the pipe can be modelled as a single element model with input and output temperature instead of the distributed parameter model. Starting with the equation 4.14 and taking account of the formulation for hot water flow in 5.4, the model of the pipe can be written as,

$$T_{pf}^{hw}(k+1) = \left[\sum_{i=1}^{m} \gamma_{p_{1,i}}^{hw}\big(q_i(k)\big)\delta_{q_i}\right] T_{pf_0}^{hw}(k) + \left[\sum_{i=1}^{m} \gamma_{p_{2,i}}^{hw}\big(q_i(k)\big)\delta_{q_i}\right] T_a(k) \tag{5.17}$$

For cold water pipe the flow q_c is constant hence the equation can be simply written as

$$T_{pf}^{cw}(k+1) = \gamma_{p_1}^{cw}(q_c(k))\, T_{pf_0}^{cw}(k) + \gamma_{p_2}^{cw}(q_c(k))\, T_a(k) \tag{5.18}$$

5.4.5 Hybrid model for the chiller

From the static model of the chiller described by the equation 4.16, the discrete time hybrid model can be obtained by considering the finite value of the hot water flow.

$$\begin{aligned} T_{hw}^{out}(k+1) &= G_{hw_1}\, T_{hw}^{in}(k) + G_{hw_2}\, T_a(k) + G_{hw_3} \sum_{i=1}^{m} q_i(k)\delta_{q_i} \\ &\quad + G_{hw_4}\, T_{cw}^{in}(k) + G_{hw_5}\, q_c(k); \\ T_{cw}^{out}(k+1) &= G_{cw_1}\, T_{cw}^{in}(k) + G_{cw_2}\, T_a(k) + G_{cw_3}\, q_c + G_{cw_4}\, T_{hw}^{in}(k) \\ &\quad + G_{cw_5} \sum_{i=1}^{m} q_i(k)\delta_{q_i} + G_{cw_6}\, q_g(k)\, \delta_{gas}; \end{aligned} \tag{5.19}$$

$$P_{sum}(k) = \dot{Q}_{ref}(q_c(k)) + \dot{Q}_{gas}(q_g(k))\, \delta_{gas} + \sum_{i=1}^{m} \dot{Q}_{hw}(q_i(k))\delta_{q_i}$$

As showed in figure 3.15, the chiller has a controller that regulates the gas flow in case when there is no hot water available and the user demand exists. It is considered that the gas flow is controlled by the proportional controller inside the chiller that acts on the error of the cold water output temperature. It may not be the exact representation for the functionality of the chiller in the existing plant but this assumption was made in order to complete the model of the chiller considering both the mode of operation i.e. *hot water mode* and *gas mode*. Note that boolean variable δ_{gas} is introduced to the equation of T_{cw}^{out} and P_{sum} to switch between gas ($\delta_{gas} = 1$) and hot water ($\delta_{gas} = 0$) mode. The switching occurs from gas to hot water mode when the T_{hw}^{in} is less than or equal some threshold temperature, generally $165°C$.

This error for the cold water output temperature can be expressed as,

$$e_{cw} = T_{cold} - T_{CW}^{out} \tag{5.20}$$

where, T_{cold} is the setpoint for the cold water temperature of chiller. The proportional controller was tuned to with a gain of $k_g = -2$ in order to control the cold water output temperature of the chiller by controlling the gas flow in the range of 0-3 Nm^3/hr. So the gas flow can be expressed by the following equation

$$q_g = k_g * (T_{cold} - T_{CW}^{out}) \tag{5.21}$$

This eqation is considered as output of the hybrid model so that it can be included in the cost function for optimization. This expression can be incorporated in the equation 5.19 for T_{cw}^{out} and P_{sum} to complete the hybrid model for the chiller.

5.4.6 Model of the user

For the user, a static model can be used to get the discrete time model. The output temperature of the user doesn't depend on the hot water flow q_t, hence the model of the user is not hybrid but can be used in the formulation of the hybrid model of the whole plant.

$$T_{usr}^{out}(k) = G_t\, T_{usr}^{in}(k) + G_p\, P_{usr}(k) \tag{5.22}$$

where, the gains have the same value mentioned in 4.3.6.

5.4.7 Mulitiplication of continous and boolean variables

The hybrid model described in the above sections might involve the multiplication of continuous and boolean variables or two boolean variables. This multiplication can be handled using *mixed-integer linear inequalities* [27]. The multiplication of the continuous $f(x)$ and boolean δ variable can be expressed by the following linear inequality that uses the continuous auxiliary variable y. The expression $y = \delta f(x)$ is equivalent to

$$\begin{aligned} &y \leq M\,\delta, \\ &y \geq m\,\delta, \\ &y \leq f(x) - m\,(1-\delta), \\ &y \geq f(x) - M\,(1-\delta). \end{aligned} \tag{5.23}$$

where, M and m are the maximum and minimum of the function $f(x)$. From this inequalities, it can be easily realized that when the $\delta = 1$ then $y = f(x)$ and when $\delta = 1$ then $y = 0$.

Similarly, the multiplication of two boolean variables δ_1 and δ_2 can be expressed by following linear inequalities with the help of a boolean auxiliary variable δ_3. $delta_3 = \delta_1\,\delta_2$ is equivalent to

$$\begin{aligned} -\delta_1 + \delta_3 &\leq 0 \\ -\delta_2 + \delta_3 &\leq 0 \\ \delta_1 + \delta_2 - \delta_3 &\leq 0 \end{aligned} \tag{5.24}$$

5.5 The optimization problem

The optimization problem of the higher layer MPC can be expressed as the finite-horizon open loop optimal control problem using the hybrid model developed previously.

$$\begin{aligned} \min_{u(k+i), i=0,\ldots,N-1} J(x(k), u(\cdot), k) = \sum_{i=0}^{N-1} \Big(\parallel y(k+i) - y^0(k+i) \parallel_Q^2 + \parallel u(k+i) \parallel_R^2 \Big) \\ + \parallel y(k+N) - y^0(k+N) \parallel_S^2 \end{aligned} \tag{5.25}$$

subject to constraints,

$$\begin{aligned} &x(k+1) = A_t\, x(k) + B_{1t}\, u(k) + B_{2t}\, \delta(k) + B_{3t}\, z(k) \\ &y(k) = C_t\, x(k) + D_{1t}\, u(k) + D_{2t}\, \delta(k) + D_{3t}\, z(k) \\ &E_{2t}\delta(k) + E_{3t}\, z(k) \leq E_{1t}\, u(k) + E_{4t}\, x(k) + E_{5t} \\ &y_m \leq y(k) \leq y_M \end{aligned} \tag{5.26}$$

where, u is the vector of inputs of the plant comprised of the hot water flow q_t and boolean input variables δ_1, δ_2 and δ_3 representing the on/off valves. The output variable y is a vector of continuous variable that is composed of the power sum P_{sum} of the chiller and gas flow consumption q_{gas} by the chiller.

First three expressions of the previous set of equations are defined from the MLD model. This MLD model considers the dynamics of the plant and all the constraints defined during its development. This constraints are related to the equation 5.3 which ensures the pre-defined set of input variable hot water flow such that $q_t \in \{q_{t_1}, q_{t_2}, ..., q_{t_m}\}$. The value of this set is defined in the MLD model that constraints to take specific value of the hot water flow from this set only, at any given time during optimization. The constraints related to multiplication of the continuous and boolean or two boolean variables specified by equations 5.23 and 5.24 are also part of MLD model.

The last expressions of equation 5.26 is specific to the bounds on the hot water output temperature of the solar collector that must be defined.

5.6 Implementation

Hybrid model

The hybrid model was implemented using the HYSDEL toolbox which allows to model the hybrid system in MATLAB using the customized programming language [29]. To build the model for the hot water, five states were defined from 60% to 100% of the maximum value of the hot water flow, with an increase of 10% such that $q_{t_i} = \{3.34 \times 10^{-4}, 3.89 \times 10^{-4}, 4.44 \times 10^{-4}, 5 \times 10^{-4}, 5.56 \times 10^{-4}\}$.

This HYSDEL toolbox upon definition and compilation of the model, gives the matrices of the hybrid system defined in section 5.3. These matrices can be used to build a higher level MPC.

Higher layer MPC

An implementation of the hybrid MPC was done as shown in figure 5.3. Ideally, the states of the plant should be estimated using an observer for the use of hybrid MPC but for this simulation it was considered that all the states are measurable from the plant. Hence, in this scheme, the higher layer hybrid MPC runs every hour by reading the states x from the plant simulator and using the prediction of disturbances d. The disturbances are solar radiation, environment temperature, chiller cold water temperature setpoint, indoor temperature and user demand. Note that the prediction of these disturbances were provided with 1 hour sampling time. Every hour when the hybrid MPC runs, it gives the optimal value of the hot water flow q_t and valve commands δ_1, δ_2 and δ_3 to the plant simulator. It also gives the status for the gas or the hot water mode of the chiller with the help of the boolean parameter δ_{gas}.

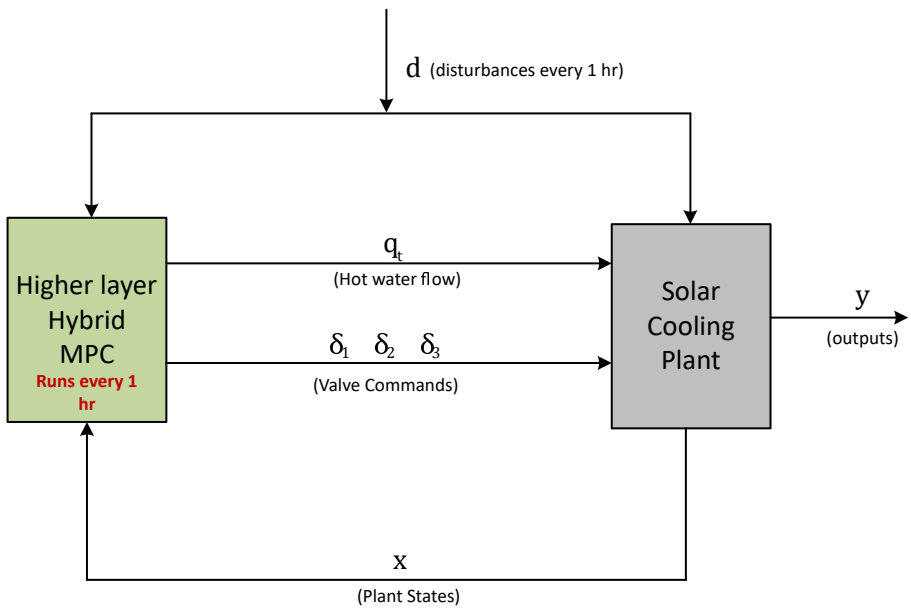

Figure 5.3: Higher layer hybrid MPC implementation with plant simulator

Prediction model

The prediction model for the optimization problem can obtained from equation 5.1 of the MLD model. The procedure to obtain the prediction model is similar to the one mentioned in section 4.6 of Chapter 4. Referring to equation 4.35, the prediction model for the MLD model can be written as,

$$\widetilde{X}(k) = \widetilde{A}\,\widetilde{X}(k) + \widetilde{B}_{1t}\,U(k) + \widetilde{B}_{2t}\,\delta(k) + \widetilde{B}_{3t}\,Z(k) \tag{5.27}$$

where,

$$\widetilde{X}(k) = \begin{bmatrix} x(k) \\ x(k+1) \\ x(k+2) \\ \vdots \\ x(k+N-1) \\ x(k+N) \end{bmatrix}, \quad \widetilde{A} = \begin{bmatrix} I \\ A \\ A^2 \\ \vdots \\ A^{N-1} \\ A^N \end{bmatrix}, \quad U(k) = \begin{bmatrix} u(k) \\ u(k+1) \\ \vdots \\ u(k+N-2) \\ u(k+N-1) \end{bmatrix},$$

$$\widetilde{B_{it}} = \begin{bmatrix} 0 & 0 & 0 & \cdots & 0 & 0 \\ B & 0 & 0 & \cdots & 0 & 0 \\ AB & B & 0 & \cdots & 0 & 0 \\ \cdots & \cdots & \cdots & \cdots & \cdots & \cdots \\ A^{N-2}B & A^{N-3}B & A^{N-4}B & \cdots & B & 0 \\ A^{N-1}B & A^{N-2}B & A^{N-3}B & \cdots & AB & B \end{bmatrix}$$

Note that the structure of $\widetilde{B}_{1t}, \widetilde{B}_{2t}$ and $\widetilde{B}_{3t}$ is represented by the matrix $\widetilde{B}_{it}$. Similarly, the output prediction model can be written as,

$$\widetilde{Y}(k) = \widetilde{C}_t\,\widetilde{X}(k) + \widetilde{D}_{1t}\,U(k) + \widetilde{D}_{2t}\,\delta(k) + \widetilde{D}_{3t}\,Z(k) \tag{5.28}$$

where,

$$\widetilde{C} = \begin{bmatrix} C & 0 & \cdots & 0 & 0 \\ 0 & C & \cdots & 0 & 0 \\ \vdots & \vdots & \ddots & \vdots & \vdots \\ 0 & 0 & \cdots & C & 0 \\ 0 & 0 & \cdots & 0 & C \end{bmatrix} \quad , \widetilde{D_{it}} = \begin{bmatrix} D & 0 & \cdots & 0 & 0 \\ 0 & D & \cdots & 0 & 0 \\ \vdots & \vdots & \ddots & \vdots & \vdots \\ 0 & 0 & \cdots & D & 0 \\ 0 & 0 & \cdots & 0 & D \end{bmatrix} \tag{5.29}$$

The structure of $\widetilde{D}_{1t}, \widetilde{D}_{1t}$ and $\widetilde{D}_{3t}$ is represented by matrix $\widetilde{D}_{it}$. Now the cost function to be minimized can be written using prediction model for the optimization problem and it becomes

$$\min_{u(k)} J(x(k), u(k), k) = \widetilde{Y}'(k)\,\widetilde{Q}\,\widetilde{Y}(k) + U'(k)\,\widetilde{R}\,U(k) \tag{5.30}$$

where , $\widetilde{Q}$ and $\widetilde{R}$ are the weighting matrices with N blocks on the diagonal as similar to equation 4.36.

Constraints

The constraints generated from the MLD formulation were directly considered in the optimization problem. For the simulation, it was considered that the chiller stays always on during the simulation time, so that $\delta_2 = 1$ has been assumed. The solar output temperature was constraint to be $T_{sol}^{out} \leq 180$.

5.7 Simulations

The simulation of the Higher layer MPC was performed by defining the optimization problem as explained in the previous two sections. YALMIP was used again with CPLEX solver for simulation purpose. The prediction horizon of $N = 3$ was considered corresponding to three hours duration. The profile of the disturbances for this simulation can be found in figure 5.4 that are provided with the sampling time of 1 hour. The cold water set point is kept constant $T_{set}^{CW} = 12$ for all the simulation hours (not showed in following figure), which is one of the disturbances.

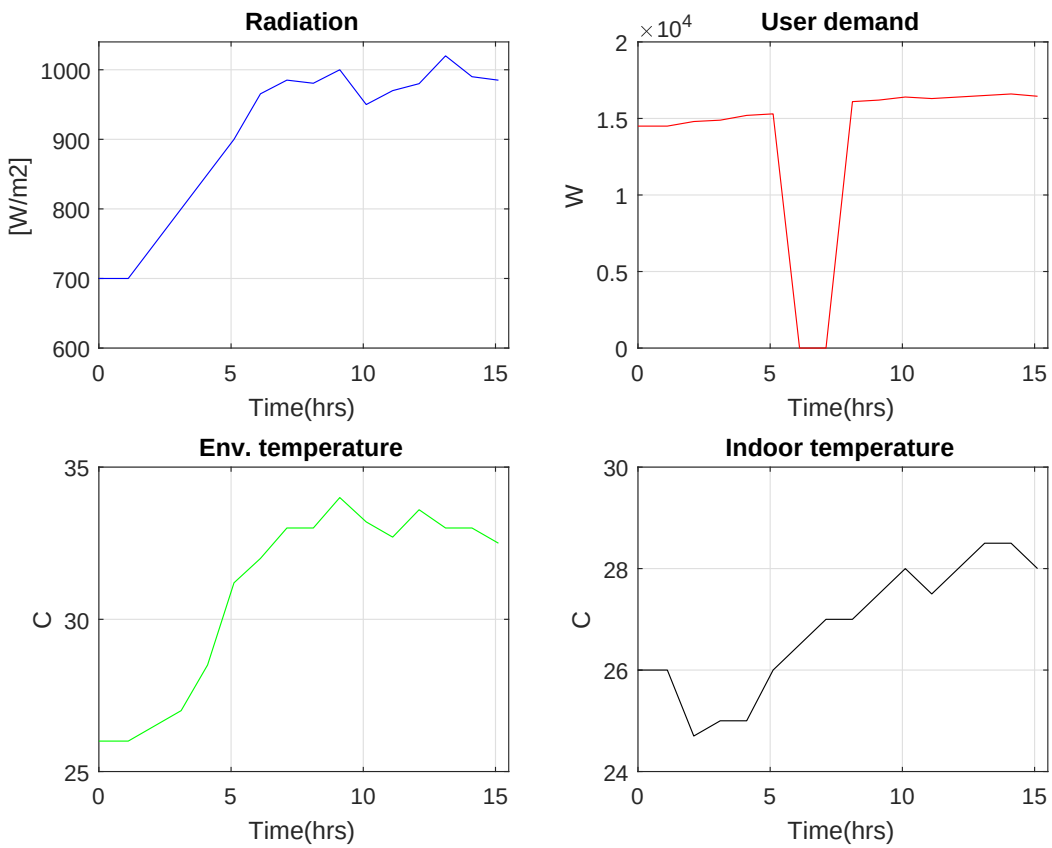

Figure 5.4: The

The optimal setpoint for the hot water flow q_{opt} can be seen in figure 5.5. For the first hour, the plant is fed with constant hot water flow $q_t = 5.25 \times 10{-}4\, m^3/s$. After that hour, the hybrid MPC starts working every hour and calculates the optimal hot water flow setpoint q_{opt} that is fed to the plant simulator. The plant evolves over the time and gives the updated states to the hybrid MPC every time the MPC runs.

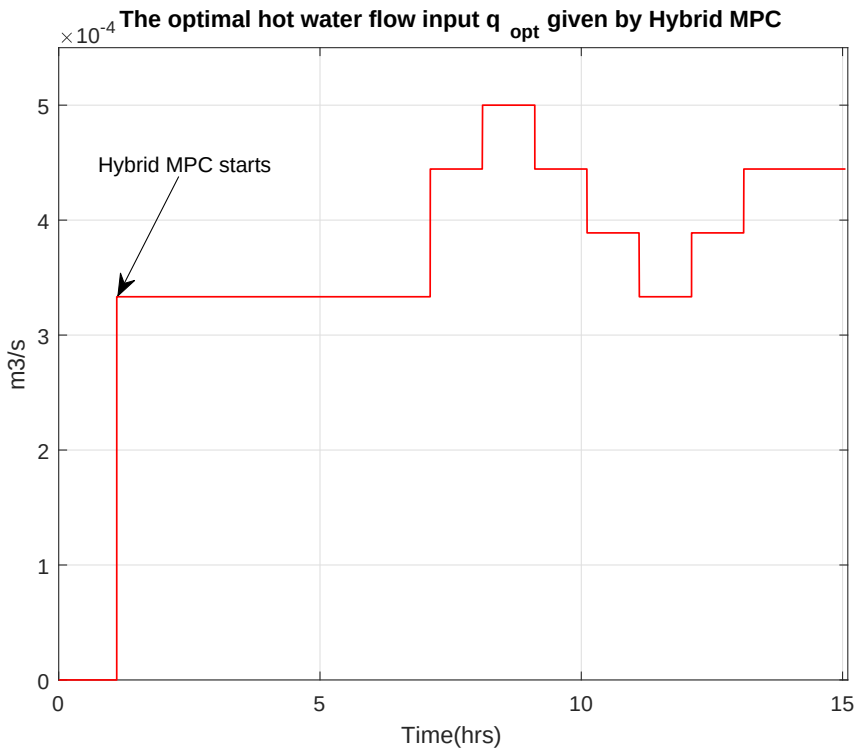

Figure 5.5: The hot water optimal setpoint q_{opt} calculated by hybrid MPC every hour after it starts working

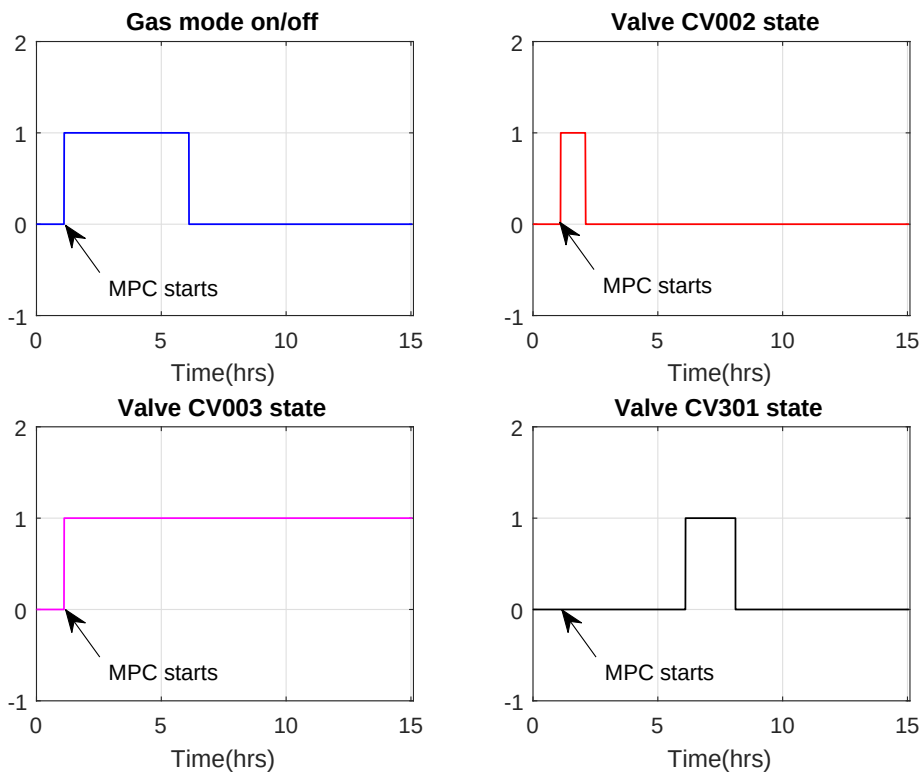

Figure 5.6: The graphs representing the gas mode on/off state δ_{gas} (upper left), valve CV002 state δ_1 (upper right), valve CV003 state δ_2 (lower left) and valve CV301 state δ_3 (lower right)

Figure 5.6 shows the states for the gas on/off mode and valves. At the beginning, when the MPC starts, it turns on the chiller in gas mode because the radiation is low and the hot water can't suffice the user demand. The gas mode is kept on till the 6th hour (upper left figure).

It also decides to turn on the CV002 valve for the first hour as the chiller works on gas mode and the hot storage could be heated meanwhile to store the heat (upper right figure). But, when the MPC runs for the next hour, it decides to turns off the valve CV002 to send the hot water to the chiller.

The valve CV003 is always on as it is supposed to route the hot water to chiller during the whole simulation time. This was defined in the constraints of the optimization problem.

The valve CV301 is turned on at the 6th hour of simulation time as the user demand during next two hours is zero (refer figure 5.4) and it tries to cool down the cold storage tank. Once the user demand increases, at the 8th hour, valve CV301 is turned off to send the cold water to the user for consumption.

From the above simulation results, it can be inferred that the hybrid MPC is able to calculate the optimal value of hot water flow every hour taking account of the disturbances and states from the plant simulator. It is also able to define the states for the chiller modes (hot water and gas) and the valves to define a configuration of the plant every hour.

However, the disturbances don't stay constant for 1 hour duration and have some dynamics. To account for these dynamics and follow the optimal setpoint of hot water flow q_{opt}, the lower layer fast linear MPC is required. This linear MPC should be built on the linearized system around the operating point every hour as discussed in Chapter 4.

5.8 Summary

This chapter presented the idea of a two layer architecture defined for the hybrid configuration of the plant. It also described the development of the MLD models for all the equipment of the plant and defined the optimization problem for higher level MPC. The higher layer hybrid MPC implementation and simulation results showed that the MPC is able to find the optimal setpoint of hot water flow for the plant and define its configuration.

Chapter 6

Conclusion

This thesis has presented the modelling and simulation of a Solar cooling plant and proposed a two layer control architecture for the plant in two different configuration. This chapter summarizes the main contributions and discusses some remaining challenges and future work directions.

Modelling and simulation

The models of the solar collector, hot water pipes, cold water pipes, hot storage and cold storages have proven to be good after validations and simulations. There is still a possibility to improve these models by better calculating or estimating the heat loss and heat transfer coefficients for these models. However, they are good enough for the control design.

The model of the chiller, which is a complex part of the system, showed some challenges due to presence of an unknown controller within it. Anyhow it was successfully modelled using the model identification techniques which proved effective when the internal function of the system need not be known and it can be considered as a black-box. Due to unavailability of the information on the linear parameters of the electric power consumption of the chiller, the model for its Power sum was developed that suffices the need.

The electric power model of the pump is quite straightforward and has been obtained from its specifications. The User model based on the identification techniques shows good results upon validation.

The overall simulator of the plant built from all these component models shows satisfactory results. These models were adequate to design the predictive control of the system.

Predictive control

The two layer architecture for the control of the system was thoughtfully realized and developed for the system in both the *Fixed configuration* and *Hybrid configuration* operation mode.

For the *Fixed configuration* mode, RTO design was accomplished through the static model of the system. This RTO model validates with the data from the simulator of the plant and is able to calculate the optimal setpoint for the lower layer MPC, given the forecast of the disturbances. The 8 hours simulation performed using this RTO guarantees its operation with changing disturbances.

The lower level fast linear MPC with explicit integral action is designed using the reduced order linearized model around the operating point. This MPC uses the state error estimation given by a Kalman predictor that is also based on the same reduced order system and tries to minimize the output error to zero. Even though the MPC is designed to make the output error zero, the output error shows some oscillation around zero because, the MPC uses the Kalman predictor based on reduced order model and it doesn't directly use the information of the disturbance. This two layer architecture allows the successful optimal setpoint tracking of the plant, given the forecast of the disturbances.

For the *Hybrid configuration*, the theoretical development for the higher level MPC was demonstrated using the *mixed logical dynamical* system formulation. This formulation allows to incorporate the continuous and boolean variables of the system to define the optimal configuration given the prediction of the disturbances. The hybrid MPC is implemented and tested to check its functionality for 15 hour simulation time. The result of this simulation indicates that the MPC is able to calculate the optimal input to the plant and defines its configuration by deciding the states of the valves and chiller operation modes.

Future work

For the modelling and simulation part, the future work could be to refine the existing model to improve the results. Especially, through the systematic experimentation it might be useful to gather the data from chiller to identify the controller inside. It could also be interesting to model the chiller by first principle equation although it will be cumbersome and its usability in the control design should be further investigated.

Other MPC techniques could be studied for the design of the lower layer MPC in *Fixed configuration* mode to achieve better results. For the two layer control architecture of *Hybrid configuration* mode, the lower level MPC should be implemented. This MPC could be similar to the one developed for the Fixed configuration mode to begin with. The energy saving analysis for these two strategies then could be compared to analyze the energy performance of the plant.

Finally, these control strategies could be applied on the real Solar cooling plant to check the operation and performance of the plant for both the strategies. Of course, additional and necessary work will be required for this activity.

Bibliography

[1] Augello L., Armanasco F., Rossetti A. *"Progetto di un impianto sperimentale di solar cooling con collettori termici a concentrazione"*. RSE, 2013.

[2] Armanasco F., Caracciolo E., Rossetti A. *"Impianto sperimentale di solar cooling all'interno della test facility aziendale di RSE."*. RSE, 2015.

[3] Paci E. *"Sperimentazione di Impianti di Solar Cooling a Media Temperatura"*. Master Thesis, University of Milan. 2015.

[4] Goldman Energy Pty Ltd. *"How does an absorption chiller work?"*. Retrieved on March 2017 http://goldman.com.au/energy/company-news/how-does-an-absorption-chiller-work/

[5] Rossetti A., Armanasco F. *"Performance evaluation of a medium-temperature solar cooling plant"*. Elsevier: Energy Procedia, 2015

[6] Riederer P., Keilholz W., Ducreux V.. *"A method to automatically export and use TRANSYS models within Simulink and vice versa"*. Eleventh International IBPSA Conference, 1628-1633, July 27-30, 2009.

[7] Camacho E.F., Rubio F.R., Berenguel M., Valenzuela L. *"A survey on control schemes for distributed solar collector fields. Part I: Modeling and basic control approaches"*. Elsevier:Solar Energy 81, 1240–1251, Feb 7, 2007.

[8] Xu L., Wang Z.F., Yuan G.F., Sun F.H., Zhang X.L. *"Thermal performance of parabolic trough solar collectors under the condition of dramatically varying DNI"*. International Conference on Concentrating Solar Power and Chemical Energy Systems SolarPACES 2014, Energy Procedia 69, 218–225, 2015.

[9] Cau G. & Cocco D. *"Comparison of medium-size concentrating solar power plants based on parabolic trough and linear Fresnel collectors"*. Energy Procedia 45 , 101-110, 2014.

[10] Fischer S. & al. *"Experience from tests on concentrating and tracking collectors"*. European Solar Thermal Industry Federation (ESTIF), QAiST, 2012.

[11] Chong K.K. & Wong C.W. *"General Formula for On-Axis Sun-Tracking System. In Solar collectors and Panels, Theory and Applications "*. Intech., 2010.

[12] Atlante della radiazione solare. ENEA. Retrieved from http://www.solaritaly.enea.it/

[13] Bittanti S., De Marco A., Giannatempo M., Prandoni V. *"A Dynamic Model of an Absorption Chiller for Air Conditioning "*. International Conference on Renewable Energies and Power Quality Granada (Spain), Mar 23-25, 2010.

[14] Vasilescu C., Hera D., Infante Ferreira C. *"Model for double-effect absorption refrigeration cycle"*. Termotecnica, 43-48, Feb, 2011.

[15] Forssell U., Ljung L. *"Closed-loop identification revisited"*. Automatica 35, 1215-1241, 1999.

[16] Rimantas Pupeikis *"On System Identification Using the Closed-Loop Observations"*. Informatica Vol. 12, No. 3, 439–454, 2001.

[17] Sanfelice Bazanella A., Gevers M., Miskovic L. *"Closed-loop identification of MIMO systems: a new look at identifiability and experiment design"*. European Journal of Control Vol. 16, 228–239, 2010.

[18] Mark L. Darbya, Michael Nikolaoub, James Jonesc, Doug Nicholsond. *"RTO: An overview and assessment of current practice"*. Journal of Process Control 21, 874–884, 2011.

[19] De Souzaa G., Odloaka D., C. Zaninb A. *"Real time optimization (RTO) with model predictive control (MPC)"*. Computers and Chemical Engineering 34, 1999–2006, 2010.

[20] The MathWorks Inc. *"Global Optimization Toolbox: User's Guide (r2016b)"*. Retrieved on January 2017 from https://www.mathworks.com/help/

[21] Bemporad A., Morari M. *"Robust model predictive control: A survey. In: Garulli A., Tesi A. (eds) Robustness in identification and control"*. Lecture Notes in Control and Information Sciences, vol 245. Springer, London, 1999.

[22] Magni L., Scattolini R. *"Advanced and multivariable control"*. Pitagora editrice Bologna, 2014.

[23] Behrendt M. *"MPC scheme basic."* https://creativecommons.org/licenses/by-sa/3.0/deed.en (CC BY-SA 3.0)

[24] Löfberg J. *"YALMIP: A toolbox for modelling and optimization in MATLAB"*. IEEE International Symposium on Computer Aided control system design,Taipei,Taiwan, 2004.

[25] Antsaklis, P.J. *"A brief introduction to the theory and applications of hybrid systems."*. Proc. IEEE 88(7),879–886 ,2000.

[26] Silva, Miguel Pedro and Ayala Botto, Miguel and Pina, Luis and Bemporad, Alberto and Sa da Costa, José *"Robust optimal control of linear hybrid systems: An MLD approach."*. CONTROLO 2004 - Sixth Portuguese Conference on Automatic Control, 2004.

[27] Bemporad A., Morari M. *"Control of systems integrating logic, dynamics, and constraints"*. Automatica 35, 407-427, 1999.

[28] Danilo Torrisi F., Bemporad A. *"HYSDEL—A Tool for Generating Computational Hybrid Models for Analysis and Synthesis Problems"*. IEEE Transactions On Control Systems Technology, vol. 12, no. 2,235-239, 2004.

[29] Kvasnica M., Herceg M.,Morari M.,Gaulocher S., Poland J. *"HYSDEL 3.0 – Manual"*. Retrieved January 2017 from http://control.ee.ethz.ch/ cohysys/hysdel/download.php

[30] P. Bolzern, R. Scattolini, N. Schiavoni. *"Fondamenti di Controlli Automatici"*. McGraw-Hill Press, 2008